Mechanism of Interaction of Human Parotid Secretory Protein - Derived Antimicrobial Peptides: A Biophysical Insight

Vinod Balhara

A Thesis
In the Department
Of
Chemistry and Biochemistry

Presented in Partial Fulfillment of the Requirements
For the Degree of
Doctor of Philosophy (Chemistry) at
Concordia University
Montreal, Quebec, Canada

July 31, 2014

CONCORDIA UNIVERSITY
SCHOOL OF GRADUATE STUDIES

This is to certify that the thesis prepared

By: Vinod Balhara

Entitled: Mechanism of Interaction of Human Parotid Secretory Protein Derived Antimicrobial Peptides: A Biophysical Insight

and submitted in partial fulfillment of the requirements for the degree of

Doctor of Philosophy (Chemistry)

complies with the regulations of the University and meets the accepted standards with respect to originality and quality.

Signed by the final examining committee:

_____ Chair
Dr. A. Chapman

_____ External Examiner
Dr. I. Marcotte

_____ External to Program
Dr. C. Brett

_____ Examiner
Dr. L. Kalman

_____ Examiner
Dr. P. Joyce

_____ Thesis Supervisor
Dr. C. Dewolf

Approved by: _____
Dr. H. Muchall , Graduate Program Director

July 31, 2014 _____
Interim Dean J. Locke,
Faculty of Arts and Science

Abstract

Mechanism of Interaction of Human Parotid Secretory Protein Derived Antimicrobial Peptides: A Biophysical Insight

Vinod Balhara, Ph.D.
Concordia University, 2014

Despite the success in conventional antibiotic development, antibiotic resistance and development of superbugs has become a global public health problem with much deeper impact on our society and economy. Naturally occurring antimicrobial peptides (AMPs) are an organism's built-in defense that combat microbial infections in healthy individuals. AMPs and their synthetic analogs have attracted attention worldwide as potential therapeutics against multi-drug resistant bacterial strains. Human parotid secretory protein (hPSP) is a major salivary protein expressed in the oral cavity of humans. GL13K, GL13NH2 and GL13D/N are short thirteen amino acid long cationic AMPs derived from the hPSP and found to exhibit antimicrobial and/or anti-inflammatory effects. It is essential to identify the membrane and peptide properties that allow GL13 peptides identify and target bacterial membranes over eukaryotic membranes, to reveal the mechanistic details for the mechanism of action of GL13 peptides.

Liposomes and supported lipid bilayers comprised of 1, 2-dioleoylphosphatidylcholine and 1, 2-dioleoylphosphatidylglycerol were used as models for eukaryotic and bacterial membranes respectively to study the effect of electrostatic forces. Membranes containing cholesterol were used to study the effect of membrane packing density. A research methodology was adopted in which we first investigated the peptide binding and secondary structure transformation upon interaction with membrane using isothermal titration calorimetry and circular dichroism. Later we identified the impact of this interaction on the membrane integrity, whether it causes

membrane fusion and/or membrane lysis using carboxyfluorescein leakage assays, dynamic light scattering, dual polarization interferometry and atomic force microscopy.

The activity and selectivity of GL13 peptides are due to a fine balance between their cationic and amphipathic nature. Increased amphipathicity or structuring of the peptide is found to be associated with a loss of specificity. Cholesterol was found to significantly attenuate the membrane lytic activity and enhance the selectivity towards bacterial model membranes. GL13K and GL13NH2 were found to act by the carpet mechanism where GL13K caused localized micellization accompanied by the loss of lipid molecules and GL13NH2 acted mainly by causing transient destabilization of the membrane without loss of lipid molecules from the membrane. GL13D/N seemed to act by a combination of various mechanisms such as the carpet and toroidal pore mechanisms. GL13K is proposed to be the best candidate for therapeutic applications as antimicrobial.

Acknowledgements

First, I would like to thank my supervisor Dr. Christine DeWolf for imbibing confidence in me and providing me this opportunity to do my doctoral research in her group. You had always been a great source of motivation and provided an invaluable support and guidance during past several years that I spent at Concordia University.

I am thankful to my committee members Dr. Laszlo Kalman and Dr. Paul Joyce for monitoring my progress. Your questions, comments and suggestions have always been invaluable and helped me progress in right direction. Many more thanks to Dr. Kalman for my questions and discussions in his spare time and allowing me to work in his lab in particular with DPI.

I would like to offer my special thanks to Dr. Jack Kornblatt and Dr. Judith Kornblatt. I have no words to explain what you have done and how much it means to me in my life.

I would like to thank Dr. Rolf Schmidt for all his great advice about improving my writing and presentation skills and providing all the trainings.

Our collaborator Dr. S.-U. Gorr is thanked for providing various peptides that I worked with in my project.

Thanks to all members of my examining committee.

I am thankful to all my present and previous lab members (Justin, Mokate, Ahmed, Arison, Sahar, Erum, Nithya, Sahana, Ivan, Hala, Melissa, Kevin) for all helpful discussions and keeping a great environment in the lab.

I would like to thank everyone in the department of Chemistry and Biochemistry for being great colleagues and friends for making my stay at Concordia fun and memorable. Thanks CBGSA for the fun Friday evenings.

I would like to offer lots of thanks to my sweet wife Nandini. Thanks for your encouragements and love. You made my life so colourful and full of honey. Special thanks and love for my son Madhavendra Singh Balhara for not giving me too hard time while writing my thesis. Your cute smile has always been a great motivation and source of energy for me.

I am very much appreciated and deeply moved by maa (Sumitra), papa (Satya Narain), my brothers (Pradeep, Sandeep and Sanjeev) and my sister (Pinki) for encouraging me to become a good researcher and human being.

Special thanks to my friend Nitin Gaur for the kindness and great help in my studies and life. You have a very important role in some of my achievements in my life.

Finally, I would like to thank all my friends in Montreal in particular Dharmendra, Jassi, Teji and Bhushan and also lovely nephew (Rohit) and niece (Shreya). Thanks to everyone who has helped me reaching here.

I would like to dedicate my thesis and whatever I have ever accomplished in my life to my uncle (Zile Singh Balhara) and mother like aunt (Darshana). I know mummy you would have been very happy and proud seeing me achieve what you always wished and dreamed for me, if you had a chance to be with us. May god rest you in peace where ever you are. Miss you a lot.

TABLE OF CONTENTS

Abbreviations

AMR	Antimicrobial resistance
AFM	Atomic force microscopy
ANSORP	Asian network for surveillance of resistant pathogens
ATP	Adenotyrosine phosphate
BPI	Bactericidal/permeability-increasing
CD	Circular dichroism
CETP	Cholesteryl ester transport protein
DLS	Dynamic light scattering
DOPC	1, 2-dioleoylphosphatidylcholine
DOPG	1, 2-dioleoylphosphatidylglycerol
DPI	Dual polarization interferometry
EARSS	European Antimicrobial Surveillance System
EU	European Union
FDA	Food and Drug Administration
FRET	Fluorescence resonance energy transfer
GIXD	Grazing incidence x-ray diffraction

HPLC	High performance liquid chromatography
ICARE	Intensive Care Antimicrobial Resistance Epidemiology
ITC	Isothermal titration calorimetry
IDSA	Infectious Diseases Society of America
LB	Langmuir-Blodgett
LUV	Large unilamellar vesicles
MDR	Multi drug resistant
MIC	Minimum inhibitory concentrations
MRSA	Methicillin resistant Staphylococcus aureus
NNIS	National Nosocomial Infection Surveillance
PSP	Parotid secretory protein
R.I.	Refractive index
SCOPE	Surveillance and Control of Pathogens of Epidemiological
SLB	Supported lipid bilayers
TE	Transverse electric
TM	Transverse magnetic

List of Figures

List of Tables

1 INTRODUCTION

1.1 MOTIVATION

Over last few decades bacterial resistance to antibiotics has become a major health, social and economic problem [1, 2]. One of the biggest scientific and therapeutic challenges is the development of multi drug resistant (MDR) strains of Gram-positive and Gram-negative bacterial strains [1-5]. The Infectious Diseases Society of America (IDSA) recently has identified six high priority pathogens (*Enterococcus faecium, Staphylococcus aureus, Klebsiella pneumonia, Acinetobacter baumannii, Pseudomonas aeruginosa, and Enterobacter species*) known as "ESKAPE" pathogens [6, 7]. "ESKAPE" pathogens have been found to be the top priority pathogens in all demographics and age groups [1, 2, 5, 8]. Bacterial biofilm forming bacteria are also increasing at an alarming rate, bacteria forming biofilms are several fold more resistant (10-1000 fold) to antibiotics as compared to their planktonic bacterial counterparts such as the biofilms of *Pseudomonas aeruginosa* that causes cystic fibrosis [9-11].

MDR bacteria have generated increased morbidity and mortality rates. This has a much deeper impact on our society and economy. Infections caused by these bacterial strains are the third leading cause of deaths in developed nations. Studies have shown that hospital acquired bacterial infections kill hundreds of thousands of Americans annually and cost between USD $21 to $34 billion annually to the US health care system [7]. According to these studies, antibiotic resistant infections in the US resulted in increased hospital stays by 23.8 % leading to 29.3% increased hospital costs by. Pneumonia causing bacteria which are resistant to antibiotics kill over 1.8 million children annually [2].

Even though bacterial resistance to conventional antibiotics is increasing, the development of new antibiotic therapeutics has come to a halt. According to a recent report published by IDSA only two antibiotics, Telavancin and Ceftaroline fosamil, were approved during the period 2008-2012 as compared to fourteen approvals during 1988-1992 (see Figure 1-1) [6]. The decrease in the antibiotic pipeline combined with increasing bacterial resistance could lead to a post antibiotic era. The World Health Organization celebrated 2011 World Health Day with the theme "Antimicrobial resistance: no action today, no cure tomorrow" to increase and promote the awareness among medical professionals and policy makers for proper use of antibiotics and also to promote regulations for increased funding for antibiotic development research projects. Increased awareness about the issue has particularly gained momentum in the developed Western and European nations over the past decade. The European Union and North American countries are funding many bacterial infection surveillance studies and public funded research projects for antibiotic discovery [1, 6]. There is an urgent need to develop new antimicrobials with novel mechanisms of action, against which bacteria have fewer chances of developing resistance.

Antimicrobial peptides (AMPs) seem to be potent candidates as antibiotics. AMPs are part of the innate immune system in most plants and animals. Various bacteria and fungi, despite encountering these AMPs for millions of years, have not been able to develop resistance against them [12, 13]. The majority of AMPs do not act *via* a stereospecific protein receptor mediated mechanism but rather target the fundamental difference in composition of the membranes between the host and the pathogens [13, 14]. However, the exact mechanism of bacterial killing by these peptides is not yet fully understood and is highly debated. Common consensus is that these peptides distinguish between host and pathogen mainly based on the difference in membrane composition. AMP activity is often associated with electrostatic-based membrane discrimination

between bacterial and eukaryotic membranes but also comprises a contribution from membrane packing/fluidity [15]. The antibacterial activity of AMPs is generally due to membrane perforation, although some AMPs even target intracellular targets in bacteria to exert antibacterial activity. Bacteria are less likely to develop resistance against AMPs by redesigning their membrane since changing membrane composition, the organization of lipids or both is not easy to adopt and might compromise important membrane barrier functions. This has attracted many researchers to think of exploiting these AMPs and their synthetic analogs as novel antibiotics [16, 17]. A potent antimicrobial or antibiotic should have selective toxicity and a fast killing action, targeting a broad antibacterial spectrum and limited chances of resistance development [18].

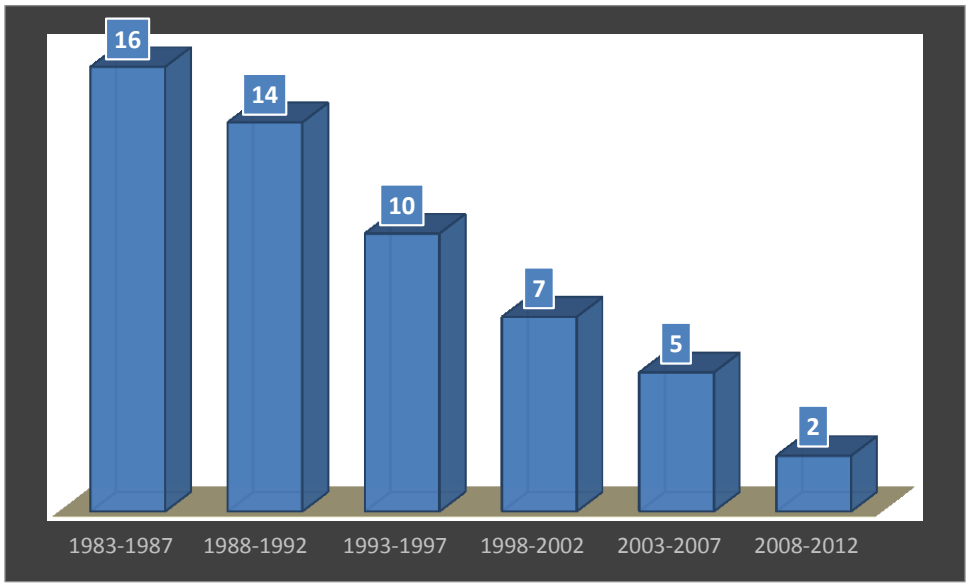

Figure 1-1 Antibiotic therapeutic approval statistics.

Antibiotic therapeutics approved by United States Food and Drug Administration over past three decades. Data taken from the report published by Boucher Helen *et. al.* [6]

1.2 BACKGROUND

The discovery of antibiotics improved human health and life time tremendously. Antibiotics are estimated to have been existing in the biosphere for billions of years. It has been estimated that the antibiotics erythromycin and streptomycin may have evolved 800 and 600 million years ago [19]. Our knowledge of the clinical use of antibiotics dates back in history to times when ancient Indians, Chinese and Egyptians used honey, bread molds, animal urine and saliva for curing some infections [20-22]. The scientific community became extensively interested in antibiotics only after the proposal of Germ Theory by Louis Pasteur in mid-nineteenth century; after which it accepted that the infections are caused by external microorganisms. He also demonstrated that certain microorganisms are able to exert antagonistic action against other organisms [23]. Later Rudolf Emmerich and Oscar Loew were two of the first scientists to observe and prove the clinical use of a microorganism's secretions to combat infections. They observed, isolated and purified a blue pigment called Pyocyanase from *Bacillus pyocyaneus* (now known as *Pseudomonas aeruginosa*) which was effective against some of the deadly infections of that time for example diphtheria [24, 25]. It was during this year when term "antibiosis" was coined by Vuillemin meaning a process by which one form of life can be killed by another. Later this term was made more specific to "antibiotic" by Selman Waksman (discoverer of streptomycin) meaning a chemical substance produced and secreted by one organism that is destructive or harmful to another.

Sir Alexander Fleming's discovery of penicillin (also known as the miracle drug of 20th century) in 1928 heralded the beginning of the antibiotic era [26]. This revolutionised medical science making it possible to treat some of the deadliest and most highly infectious diseases. However, penicillin's use as an antibiotic to the highest level to protect human race only occurred in the

1940's when Howard Florey and Ernst Chain were able to isolate and develop processes for penicillin's mass scale production [27]. In 1945 these three scientists Flemming, Florey and Chain shared the Nobel Prize in Physiology and Medicine during 1945 for the discovery of the penicillin. Since then a large number of potent antimicrobials have been discovered for clinical use to combat infections caused by microorganisms. Many antibiotics have been used indiscriminately to combat various infections and this increased use of antibiotics imposed a selection pressure on various organisms leading to antibiotic resistance. Clinical resistance against antibiotics can appear within a few months or up to several years after a new antibiotic is introduced [28]. Although it is highly accepted that antimicrobial resistance (AMR) spread increased due to overuse or misuse of antibiotics, there are also reports that bacterial resistance existed even prior to human use of antibiotics. During evolution process bacteria have developed resistance against the antibiotic chemicals produced and secreted by other competing species [29]. Resistance against penicillin was first observed in *Staphylococcus aureus* and *Escherichia coli* only four years after its clinical use began in 1942 [30]. Ever since then a large number of antibiotic resistant strains have been identified and discussed in detail in these references [1, 6, 8, 19, 30]. Antibiotic therapies have been efficient in treating various infections due to the availability of a wide variety of antibiotics that act by different mechanisms.

The biggest setback to antibiotic therapy occurred due to the development of MDR strains which are capable of withstanding even against combinatorial therapies. MDR strains are growing rapidly and they are difficult and expensive to treat, in some cases making it almost impossible to treat infections. MDR strains are also known as superbugs, where the term superbugs is usually used for the bacterial strains with increased morbidity and mortality by virtue of resistance against multiple drugs intended for their cure. It has been suggested that we are

heading towards a pre-antibiotic era, while some call it post-antibiotics era. Recent medical advances such as cancer treatments, HIV cures and transplantation have a high dependence on the availability of effective antimicrobials. With a deeper insight into both a historical and a genetic perspective of bacterial resistance to current antibiotics, scientific experts and several international health organizations such as WHO, IDSA and the European Antimicrobial Surveillance System (EARSS) have made recommendations on how to combat bacterial infections in the future. Here is a list of few important initiatives or recommendations made:

1. **Bacterial resistance surveillance:** Proper surveillance systems are necessary to provide information about the trends in the spreading of infectious diseases, resistance mechanisms and drug use. In 1999 the European Union (EU) started a very efficient and detailed surveillance program (known as EARSS) for various top priority pathogens. EARSS suggested three types of surveillances necessary for proper control of bacterial resistance and infections namely pathogen surveillance, host surveillance and population surveillance [1]:
   A large number of surveillance programs have been conducted and are ongoing across the world namely the Surveillance and Control of Pathogens of Epidemiological Importance (SCOPE) program, the Intensive Care Antimicrobial Resistance Epidemiology (ICARE), Asian Network for Surveillance of Resistant Pathogens (ANSORP), the National Nosocomial Infection Surveillance (NNIS) System and the Alexander Project [31]. These measures can directly influence infection control in the community and hospitals [1, 31]. Since the implementation of the surveillance program, the bacterial spread and virulence of some Methicillin resistant *Staphylococcus aureus* (MRSA) strains has decreased in many EU countries. However, an increase in resistance of *E. coli* and *K. pneumoniae* to even 3rd

generation cephalosporins, fluoroquinolones and aminoglycosides has been observed[1]. This information was then further used to design therapy plans and antibiotic research.

2. **Regulations for proper use of antimicrobials**: Although bacterial resistance is inevitable, the proper and efficient use of antibiotics can result in enhancing the time for which an antibiotic can be used efficiently. The judicious use can have significant and lasting improvement in the treatment of infectious diseases. For instance, Davies *et. al.* [19] suggested that the availability of penicillin as an over-the-counter drug during 1950's could have a significant contribution towards penicillin resistant bacterial strains. Similarly, underuse due to indecisive use, lower dose, and lower standard antibiotics can have deterrent effects on the efficacy of the antibiotics. This is a major problem in developing nations where people have easy access to antibiotics without prescription and to substandard antibiotics [2]. Overuse of antibiotics in animal husbandry and agriculture to promote food production is also a significant contributor to AMR resistance [2, 29]. It has been established that the total amount of antibiotics used in animal husbandry accounts for over 50 % of the total use of antibiotics [2]. This excessive use of antibiotics allows bacteria present in animal stock and food crops to develop resistance against them. These resistant bacteria can be transferred to humans and can be difficult to cure due to their resistance to commonly used antibiotics, posing a threat to human species.
3. **Initiatives to develop new antimicrobial agents:** Surveillance of antimicrobial agent use and AMR development are important to develop better regulations and interventions by regulatory bodies. This is a good prevention process but we cannot rely on them as a solution to stop AMR. There is an urgent need to develop new antimicrobial agents with novel mechanisms of action. Over the past few decades the antimicrobial pool has been continuously decreasing, an

end result of the loss of interest by the pharmaceutical industry, as antimicrobials research is no longer considered a profitable segment. Recognizing this problem of reduced antimicrobial development and increased AMR, several governments have initiated public funded initiatives to promote antimicrobial research [6]. The EU has initiated a public-private collaboration funding of 223.7 million Euros to increase antibiotic development. In 2012, the US Food and Drug Administration (FDA) appointed an antibacterial task force and enacted new initiatives intended for promoting antibacterial development.

Antibiotics developed in the 20th century were products of bacterial origin or there synthetic analogs [32]. The identification of more potent antimicrobials from these sources has significantly decreased over the past few decades. More recently, the increasing knowledge of bacterial genomes is opening up the potential to use some of the already known bacterial species to identify new natural antimicrobial products that bacteria are able to synthesize, for example *Streptomyces coelicolor* which was studied for over 50 years, was known to have about 5-6 products with antimicrobial effect but its genome sequencing revealed potential gene clusters for about twenty products [33]. Exploration of biological diversity has revealed new antimicrobials with broad chemical diversity [19].

An important class of antimicrobials that has attracted attention over the past few decades is AMPs. AMPs have been suggested as and proven to be potent antibiotic candidates. AMPs exhibit a broad range of activity varying from a bactericidal to an immune-modulatory effects. Most of the antimicrobial peptides studied have a minimum inhibitory concentration in the low micromolar range. They are mainly cationic and amphipathic in nature. A potent antimicrobial or antibiotic should have selective toxicity and a fast killing action, target a broad antibacterial spectrum and be less prone to AMR. An extensive database of over 2000 known and potential

natural AMPs or their synthetic analogs (antibacterial, antiviral, antifungal and antitumor) has been established.

1.3 ANTIMICROBIAL PEPTIDES

AMPs as antimicrobials are considered a hot and new topic but AMPs were known and discovered at the same time as penicillin. Nicin discovered in 1928 was one of the first AMPs and is widely used in food preservation even today. Gramicidin was discovered and isolated by René Dubos in 1939 from culture supernatant of the soil bacterium *Bacillus brevis* [34]. However, AMP research gained momentum and exposure as potent antimicrobials during the last three decades. As result of extensive research on AMPs as potential antimicrobial, some of these AMPs entered several levels of clinical trials for various applications in humans. During the 1980's Boman and colleagues were first to identify cationic AMPs cecropins A and B from the giant silk moth *Hyalophora cecropia* [35], this was followed by the discovery of melittin from bee venom. Michael Zasloff discovered and isolated magainin 1 and 2 from the African frog *Xenopus laevis* and developed it as a therapeutic product [13]. Magainin was one of the first peptides to pass clinical trials for use in humans as an antimicrobial. However its approval was denied by FDA as it failed to show added advantages over existing antibiotics. Most of the AMPs discovered during this period were from insects. The activity of these AMPs against several disease causing microbial pathogens motivated scientists to explore the new classes of potent AMPs. AMPs exhibit a wide range of biological activity against bacteria, fungi, viruses and even cancer cells [36].

Like other animals and insects, humans have been able to evolve and resist against the microbial pressure due to their adaptive innate immune system of which AMPs form an important

constituent. Endogenous AMPs of human origin rather than those of other insects or organisms can be potent candidates as antimicrobials due to reduced host cell toxicity of these agents. Defensins were some of the first antimicrobial peptides to be isolated from a variety of mammalian species. Histatins, cathelicidin, α- and β- defensins are well characterized AMPs identified and isolated from human skin or epithelial cells [34, 36]. These peptides exhibit different secondary structures and mechanisms of action. Defensins form a β-sheet structure due to the presence of various cysteine residues forming disulphide bridges. A total of four α- defensins and six β- defensins have been isolated from humans and they all exhibit conserved β-sheet structure [36]. Cathelicidins are synthesized as prepropeptides. Their structure is comprised of a signal peptide at the N-terminal end, a conserved proregion in the middle, and a C-terminal part containing the antimicrobial peptide. Cathelicidins are processed in two steps. First, the signal peptide is cleaved off and the resulting propeptide AMP is activated and stored in target cells. Only one cathelicidin LL-37 has been identified and is expressed in leukocytes and epithelial cells of skin, gastrointestinal and respiratory tract [36]. LL-37 is the active part of the antimicrobial protein, human cationic antimicrobial protein-18. Histidine rich histatins are peptides expressed in saliva by submandibular glands. Cathelicidin and histatins have a random coil structure in buffer and adapt an α-helical structure in the membrane bound state, i.e. upon interaction with bacterial cell surface [36].

The oral cavity is a major port of entry for bacterial infections in humans and harbors over 700 species of bacteria. Most of these bacteria are non-pathogenic in healthy individuals but can cause severe diseases in immuno-compromised patients of cancer, AIDS or several other diseased states. Oral epithelial cells, neutrophils and salivary glands secrete a large number of AMPs into the oral cavity which kill pathological bacteria and other microorganisms to maintain

healthy bacterial flora and prevent us from unwanted pathogenicity of some of the virulent bacteria or other microorganisms. Human parotid secretory protein (PSP) is part oral cavity AMPs which were identified and fully characterized by Gorr et. al.[37, 38]. This group was the first to demonstrate that human hPSP is expressed in keratinocytes of human parotid glands [37] and show that hPSP expression is up regulated by bacteria and humoral factors such as cytokines and sex hormones[37]. Antibacterial and anti-inflammatory activity suggested that hPSP has an important role in the innate defense at gingival epithelial cells like other human AMPs such as β-defensins -2 and -3. Aiming to exploit and benefit from these properties of hPSP Gorr *et. al.* identified and designed several AMP sequences which will be discussed in terms of their sequence, structure and function in section 1.4.

1.3.1 AMPs classification and important properties

AMPs are diverse in their structure and function. A large number of AMPs are known with a wide range of functions, structures and origins. No single classification scheme has been defined that is applicable to all AMPs and different classification systems based on AMPs origin, biological function, mechanism of action, charge and structure can be found in the literature [16, 39, 40]. Secondary structure based classification is the most commonly used and is based on the secondary structure adapted by the AMPs upon interaction with membranes or hydrophobic environments similar to membranes. Accordingly, both synthetic and natural AMPs have been classified into the four main secondary structure classes: α - helical, β - sheet, loop and extended peptides [16, 39-43] with the first two being the most common. AMPs can vary in the extent of secondary structure developed depending on the membrane system, those with more than one secondary structural motif are classified based on the most abundant and common secondary structure.

Aurein, mellitin, magainin, cecropin, dermaseptins and alamethicin are few examples that belong to α - helical family [9, 42]. The extent of helicity is well correlated to their antimicrobial effect, *i.e.*, increased helicity increases membrane disruption caused by AMPs. Along with increased helicity increase in helix length favors membrane insertion and thus increased penetrability/lysis [44]. β-Sheet forming AMPs are often stabilized by either disulphide bridges or cyclization of the backbone. Protegrin from pigs, tachyplesin from horse shoe crabs and human defensins are some of the commonly known and well-studied peptides that belong to the β-sheet group [18, 40, 45]. Protegrin and tachyplesins adopt a hairpin-like β-sheet structure in a hydrophobic environment [41]. Loop and extended classes of AMPs have received the least attention; of these indolicidin from bovine neutrophils [46] and thanatin from the insect *Podisus maculiventris* [47] are the most well characterized and studied. Indolicidin and thanatin do not act by membrane permeabilization but rather target intracellular targets [46-49]. Several analogs of these peptides have been synthesized by the substitution of one or more amino acids which are more membrane active but all thanatin analogs are found to cause membrane aggregation [47, 49, 50].

Even though AMPs are diverse in their origin, function and structure, there are a number of similarities that apply for most AMPs, namely they are usually relatively short (mainly ranging from 12-50 amino acids), carry a net positive charge of +2 to +9 and are amphipathic in nature. Amphipathicity is often used interchangeably with hydrophobicity in the field of antimicrobial peptides. Thus it is worth noting that amphipathicity represents the relative abundance and orientation of hydrophobic and hydrophilic domains within a protein whereas hydrophobicity is defined simply as the percentage of hydrophobic residues present in a protein. Proteins with the same hydrophobicity can have different amphipathicity. Amphipathicity can be achieved *via* the formation of a variety of protein conformations such as α-helix or β-sheet. The amphipathicity of

α - helical peptides is calculated as the hydrophobic moment which is the vector sum of hydrophobicity indices of individual amino acids, treated as vectors normal to the helical axis [43, 51]. Amphipathicity in α-helices is simple and has a periodicity of three to four residues yielding a segregated hydrophobic and hydrophilic face of the helix. β-sheet peptides are also amphipathic as a result of existence of polar and non-polar faces due to organization of strands. Increased amphipathicity is generally correlated with increased antimicrobial activity of AMPs [51-53]. These studies found that varying gramicidin's amphipathicity by substitution of various residues on different faces of the β - sheet of gramicidin S has a strong effect on the antimicrobial activity of the AMPs. They observed that a small increase in amphipathicity without altering surface charge and hydrophobicity resulted in increased antimicrobial activity along with a decrease in hemolytic activity. However large increases in amphipathicity caused a reversal of the activity [51]. It was suggested that the increase in amphipathicity resulted in directed hydrophobicity which in turn promoted membrane partitioning. Thus identifying the correct windows for amphipathicity and hydrophobicity of an AMP could help in improving antimicrobial activity while decreasing hemolytic activity or host toxicity. In other words identifying the correct amphipathic index for a given AMP could help in improving its therapeutic efficacy.

The cationic nature of antimicrobial peptides is also a common characteristic among AMPs. Thus most synthetic AMPs designed are cationic in nature with charge varying from (+2 to +9). The cationic charge is thought to facilitate the interaction with and increase selectivity for microbial membranes owing to their anionic nature (see section 1.6.1). A higher positive charge on an AMP increases its antimicrobial activity, but a very high positive charge could result in increased host toxicity due to increased interaction with eukaryotic membranes as a result of the membrane potential. Along with increased toxicity, a large increase in the cationic nature of an

AMP could also result in reduced activity, primarily due to the electrostatic penalty as a result of increased electrostatic repulsion between the adsorbed peptides which reduces peptide binding to the membrane interface [54].This suggests that even though an increase in amphipathicity, hydrophobicity and cationic charge could improve their antimicrobial activity, it is important to have the right combination of these properties to identify the most suitable therapeutic AMP candidate with high selectivity towards microbes and low host cell toxicity.

While cationic AMPs are the most commonly reported AMPs, several anionic AMPs such as maximin – H5, enkelytin and dermcidin [55] have also been reported as part of the innate immune system,. These peptides carry a net negative as a virtue of the presence of glutamic and aspartic acid residues. These anionic antimicrobial peptides can adopt amphiphathic structures upon interaction with the microbial membranes and require cations such as Zn^{2+} as cofactors for their activity. The cations act as a linker or bridge between anionic peptides and membranes [39, 55].

1.3.2 Mechanisms of action

Most data regarding the mechanisms of action of AMPs suggest that they act mainly *via* membrane permeabilization. Despite being studied extensively over the past few decades, no common consensus has been reached and it is a topic of huge debate about exactly how these AMPs cause membrane disruption [56]. The molecular mechanism of membrane permeation and disruption of AMPs depends on a number of parameters such as the amino acid sequence, membrane lipid composition and peptide concentration. The majority of studies have focused primarily on the interaction of cationic peptides with model membrane systems. AMPs induced membrane permeabilization can be very fast (causing lysis in a few minutes) or slower (taking hours to complete their action) [39]. Although the precise nature of the membrane permeabilization mechanism has not been suggested, there are few processes such as interaction with membrane,

secondary structure transformation, self-uptake and association or multimerization that are commonly observed to be involved in membrane permeabilization and disruption [43].

1.3.2.1 Initial interaction with membrane

The initial interaction of the peptide with the target membrane surface significantly influences the membrane disrupting effects and process. This initial interaction is affected by the biochemical properties of both the peptide and the target membrane. It has been widely accepted that these initial interactions are due to electrostatic interactions between cationic AMPs and anionic microbial membranes (discussed in detail in section 1.6.1). Numerous studies have confirmed that increasing the cationic charge of AMPs results in an increased membrane disruption activity suggesting why the positive charge of AMPs has been conserved during the process of evolution. For Gram-negative and Gram-positive bacteria, the inner cytoplasmic membrane is surrounded by a tightly packed cell wall comprising anionic lipopolysaccharides stabilized by intercalated cations such as Ca^{2+} and Mg^{2+}.

Even though the exact molecular mechanism of AMPs crossing this barrier is not understood, it is believed that AMPs cross the peptidoglycan barrier by displacement of these cations resulting in the destabilization of the peptidoglycan barrier allowing peptide to pass and interact with the inner membrane. After crossing the peptidoglycan barrier AMPs exert their anitimicrobial action by causing membrane permeabilization. However, D-enantiomers of several AMPs such as melittin, cecropin and magainin exhibited similar activity as L-enantiomers indicating that AMPs do not act primarily by targeting specific receptors on the membrane surface [57]. This is highly advantageous for the therapeutic use of AMPs as the lack of specific receptor mediated mechanisms of bacterial killing makes it difficult for bacteria to develop resistance to these

peptides. Bacteria would have to alter the properties of their membrane as a whole rather than modify specific receptors.

However, there are also some receptor based mechanisms that have been observed for a few AMPs. For instance, nisin exhibits antimicrobial activity by specifically binding to bacterial lipid II, a membrane bound component involved in peptidoglycan synthesis [43]. Similarly, the lantibiotic mersacidin has been demonstrated to interfere with transglycosylation and peptidoglycan synthesis by direct targeting of lipid II [43]. Even though some studies have shown role of receptor mediated mechanisms it has still been widely exhibited that non-specific peptide membrane interactions are the key towards AMPs antimicrobial activity.

1.3.2.2 Membrane insertion

When AMP peptides bind to the cell membrane *via* electrostatic interactions, they can orient themselves in parallel, perpendicular or tilted and/or a combination of these relative to membrane plane[58] (Figure 1-2). Once a peptide reaches a threshold peptide/lipid (P/L) ratio on the membrane surface, it reorients itself to insert deeper into the membranes hydrophobic core which is usually referred to as I – state. The threshold P/L ratio for reorientation is a function of the adsorption binding energy, the elastic constants and hydrophobic thickness of the bilayer, the transmembrane potential and the pH of the medium which in turn effects peptide charge [13, 14, 30]. Thus, the P/L ratio will vary greatly with the lipid composition and the physicochemical conditions of the membrane. The elastic constants of the bilayer will determine the extent to which lipid molecules can deform to accommodate the peptide in the core and this, along with electrostatic and hydrophobic forces, will control the level of insertion of the peptide [59]. Peptide insertion is usually accompanied by a secondary structure transformation. The conformation changes alter the hydrophobic moment and the polar angle of the peptide to allow it to better

accommodate in the membrane hydrophobic environment [43]. At the bilayer interface electrostatic interactions are strongest and the hydrophobic interactions are weakest because the polarity and water content near the charged head group moieties are close to the bulk water values. Hydrophobic interactions become significant only as a peptide partitions deeper into the membrane, away from the bulk water phase.

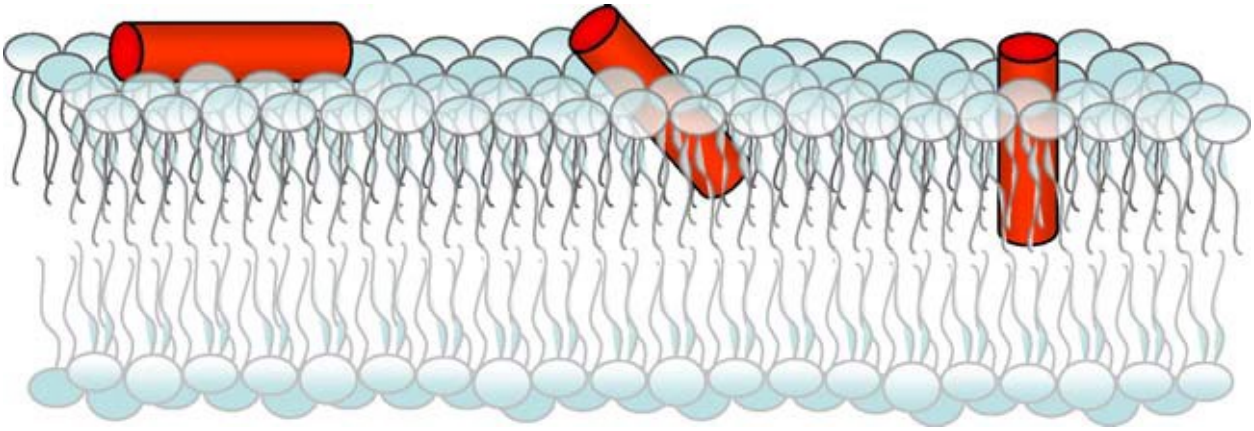

Figure 1-2 Various orientations of AMPs in bilayers.

AMPs can align parallel (left red cylinder), oblique (centre red cylinder) and perpendicular (right red cylinder) to membrane surface. Figure is adapted from Sato *et. al.* [58].

Above these threshold values or in the I-state, AMPs cause membrane disruption resulting in destruction of the transmembrane electrochemical potential defined by the pH and osmotic gradients, loss of important cellular components and eventually complete collapse of the membrane function and cell death. The total membrane electrical potential profile of a lipid bilayer is a complicated sum of multiple components, namely the transmembrane potential, surface potentials, and various internal potentials attributed mainly to the adsorption potentials and the membrane dipole potential (detailed analysis is reviewed by Honig *et. al.* [60]).

The various mechanisms hypothesized so far for AMP's modes of action have been broadly classified into non-pore models such as carpet models and discrete pore models such as barrel–stave pores and toroidal pores[13, 14, 16, 39, 57, 58, 61-64 65].

1.3.2.3 Barrel - stave pores:

In the barrel-stave model the transmembrane pores are formed by bundles of peptides. Initially, AMPs bind as monomers at the surface which then assemble to form multimers on the surface of the membrane (S - state). After reaching a threshold P/L the peptides are inserted (I – state) into the hydrophobic core of the lipid bilayer. In the I – state, the peptides aggregate to minimize the exposure of peptide hydrophilic residues to the hydrophobic membrane interior such that the hydrophilic region of the α-helix or β-sheets forms the interior of the transmembrane pore while the hydrophobic region aligns with the lipid core of the membrane (as shown in Figure 1-3) [43]. Additional peptide monomers are then recruited and attached to the bundle leading to an increase in the size of the membrane pore. A minimum of 22 or 8 amino acids are required for α-helical or β- sheets peptides respectively to transverse the lipid bilayers [62]. Alamethicin is one of the best and most well defined examples of the barrel-stave model of membrane disruption. The alamethicin barrel pore crystal structure was observed almost two decades ago by Fox *et. al.* [66]. They identified that the length of the channel is about 3.2 nm and the channels are of varying diameters ranging from 2-3 Å, corresponding to channels composed of 4-6 membrane spanning peptides [40, 66]. Later, it was observed that stability of the alamethicin pore is a result of strong hydrogen bonding between two glutamine residues of neighbouring peptides which provides stability to the hydrophilic core of the channel [67].

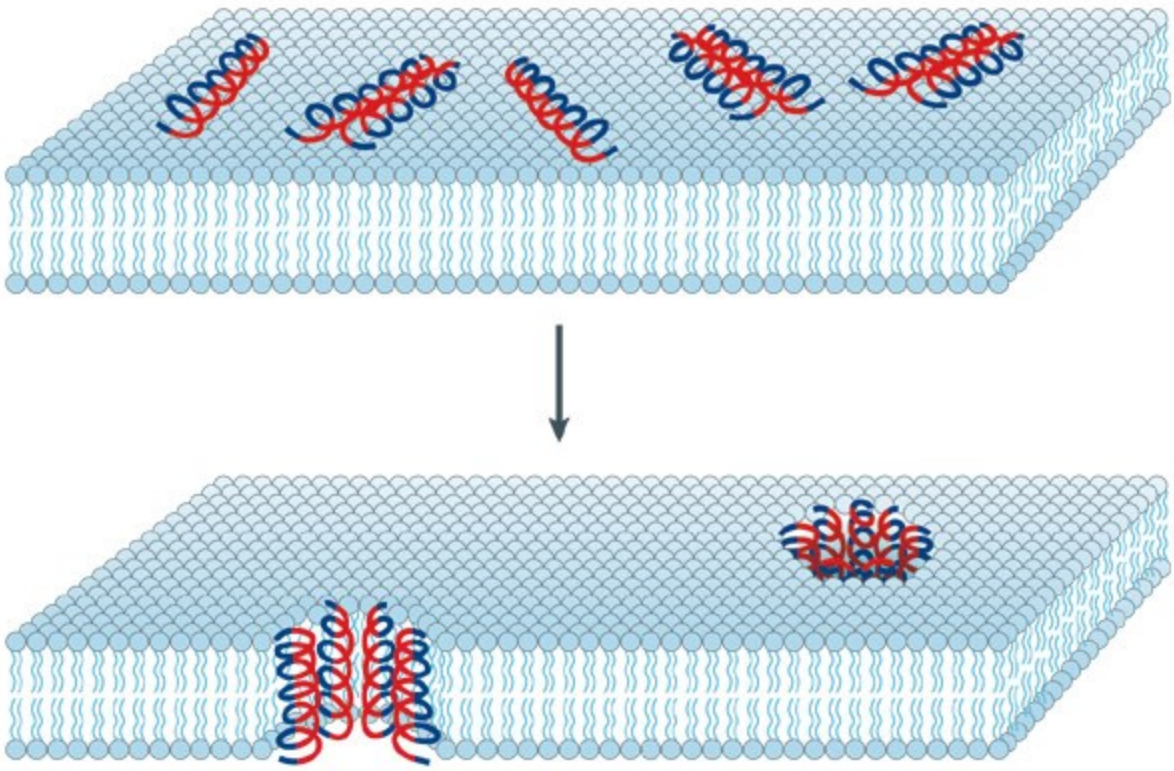

Figure 1-3 Barrel-stave model of antimicrobial peptide induced membrane permeabilization.

Initially peptides bind as monomers and slowly form multimers, after reaching a threshold, peptides insert and aggregate to form channels. Hydrophobic residues (blue) align with the membrane core and hydrophilic residues (red) form the interior of the pore [39].

1.3.2.4 Toroidal pore mechanism:

Although the barrel-stave pore was one of the first identified membrane disruption mechanisms for AMPs, relatively few peptides exhibit this mechanism. More recent studies show that a large group of AMPs exhibit a toroidal pore mechanism. Even though both of these mechanisms form discrete membrane pores, but there are significant differences in the processes by which they are formed. A primary difference between the two mechanism is that in the toroidal pore, the lipids reorient themselves during the peptide insertion and become intercalated between the peptides in the core of the channel (see Figure 1-4). In this mechanism, the peptide initially interacts with the membrane surface due to strong electrostatic interactions and after reaching a threshold concentration on the surface, the peptides generate an excessive lateral pressure, inducing

positive curvature in the membrane. The positive curvature of the membrane surface along with strong interaction between the peptides and the lipid head groups facilitates the bending of the lipid molecules, resulting in a pore lined by both peptides and lipid molecules (Figure 1-4) [39, 40, 43, 45, 57]. The lipids in these openings then connect the two leaflets of the membrane. This is one of the most commonly observed mechanisms of membrane disruption. Magainins, melittins and protegrins are some of the well-studied peptides that exhibit this type of mechanism [45, 58, 68, 69]. This model was proposed based on the observations of magainin-induced lipid flip-flop by Matsuzki *et. al.* [70] and characterized by Ludtke *et. al.* using neutron scattering [71].

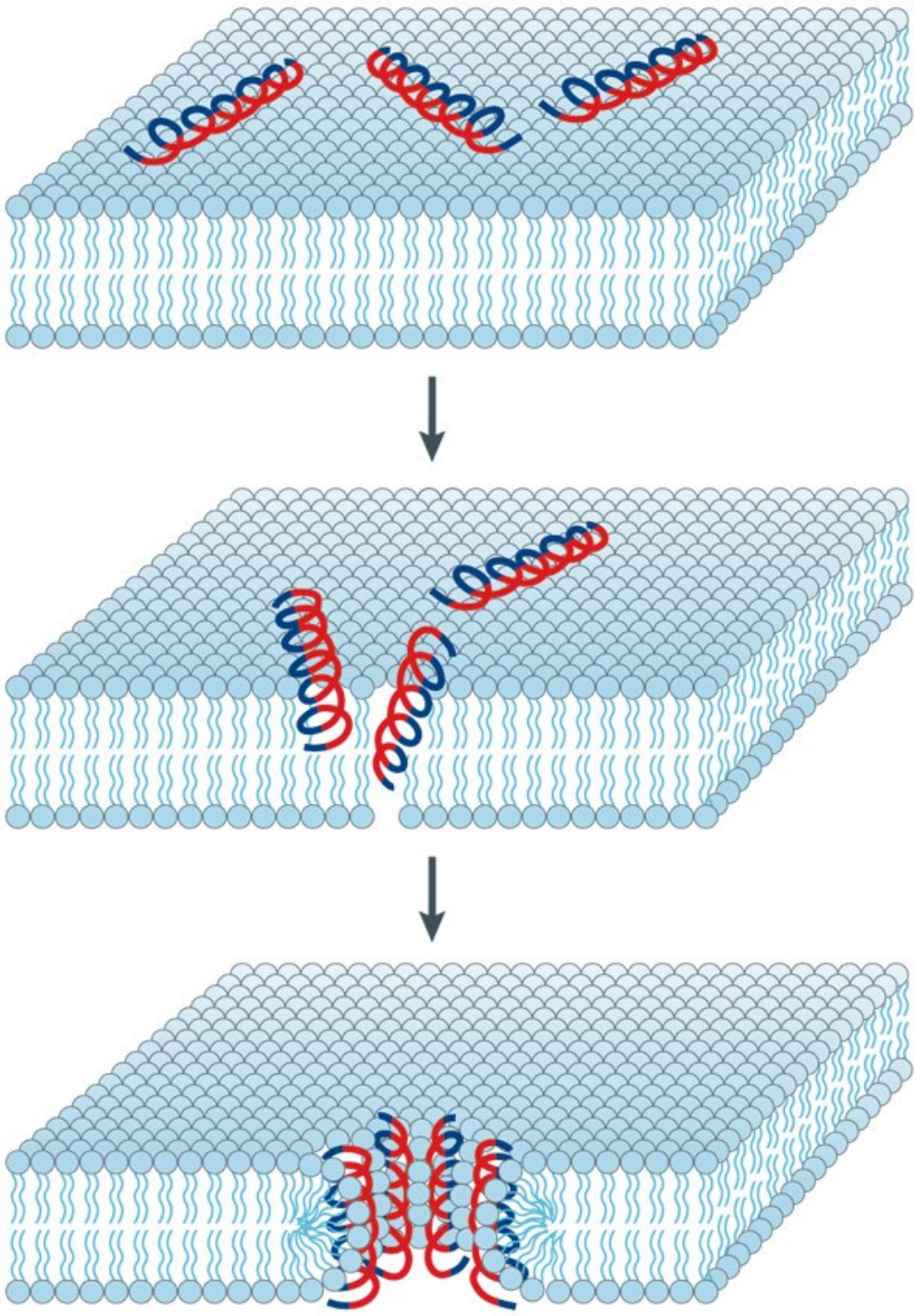

Figure 1-4 The toroidal model of antimicrobial peptide induced membrane permeabilization.

Peptides bind to the surface of the membrane. After reaching threshold, peptides insert and aggregate to form the channels. During channel formation lipid molecules bend with inserted peptides forming a pore lining of both peptides and lipids. Peptides hydrophilic regions are coloured red and hydrophobic regions are coloured blue [39].

1.3.2.5 Carpet model

Some peptides cause membrane permeabilization in a more diffuse manner, *i.e.* without forming any discrete channels which is known as the carpet model. In this mechanism, peptides accumulate at the bilayer surface like a carpet and, above a threshold concentration, the membrane is permeated and disintegrated in a detergent like manner, due to the development of excessive lateral stress or curvature strain on the membrane (as illustrated in Figure 1-5)[40, 58]. The carpet mechanism was first proposed based on the observations of cercopin antimicrobial action. At concentrations high enough to cause membrane permeabilization, it was observed using ATR-FTIR, that the peptide was incorporated parallel to the membrane and did not enter the hydrophobic core [58].

In both carpet and toroidal pore membrane disruption mechanisms, AMPs bind parallel to the membrane and after reaching a threshold P/L ratio cause membrane disruption due to the development of excessive lateral stress on the membrane. However, in the case of toroidal pores peptides insert deeper into the membranes hydrophobic core whereas in the carpet model the peptide remains mainly attached to the membrane interface [58]. It has been suggested that the formation of transient holes or toroidal pores may occur as an early step in membrane disintegration, *i.e.,* toroidal pore formation occurs prior to micellization. It is believed that these toroidal pores might allow the peptide access to the inner core of the membrane, eventually leading to complete disruption or micellization of membranes [39].

AMPs mainly exert their antimicrobial action by causing membrane disruption as explained above and a given AMP can exhibit either one or a combination of these mechanisms. Other than membrane disruption mechanisms, there increasing number of AMPs which interfere with intracellular targets. PR–39, buforin-II and indolicidin are found to block uptake of thymidine,

uridine and leucine in *E. coli*, thus interfering with DNA, RNA and protein synthesis processes[46, 72, 73]. Similarly, pleurocidin and dermaseptin peptides exert bactericidal activity without disrupting or permeabilizing the membranes. Some AMPs interfere with metabolic processes of microbes for example glycine-rich attacins blocked the transcription of the *omp* gene in *E. coli* [74], while some magainins and cecropins induced selective transcription of its stress-related genes *micF* and *osmY* [75, 76]. Some other mechansims that have been reported include enzyme inhibition (HNP-1) [39], non-lytic loss of adenosine triphosphate (ATPs) leading to generation of reactive oxygen species (Bactenicins Bac-5 and -7) [77], inhibition of chaperone assisted protein folding and cytoplasmic membrane septum formation (pyrrhocoricin) [39, 40].

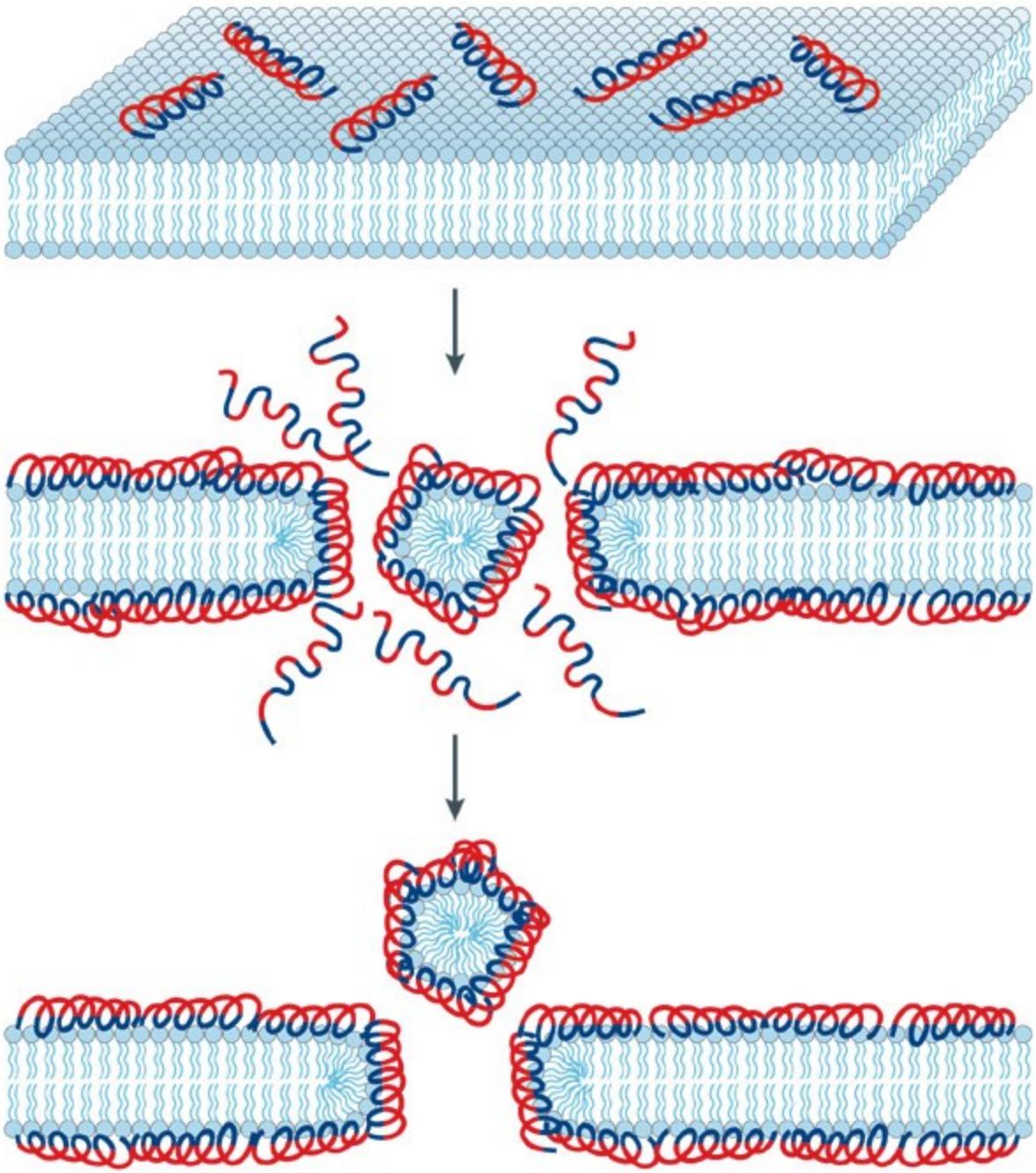

Figure 1-5 The carpet model of antimicrobial peptide induced membrane permeabilization.

Peptides bind to the surface of the membrane without inserting into hydrophobic environment. After reaching a threshold concentration, peptides create excessive lateral stress on the membrane and cause membrane permeabilization. Peptides hydrophilic regions are coloured red and hydrophobic regions are coloured blue [39].

1.4 BACTERIAL RESISTANCE AGAINST AMPS

Bacteria have been inhabiting this planet for millions of years and have evolved strategies to overcome deleterious effect of changing environments and harmful toxins. Conventional antibiotics exerted their mechanism of action by targeting specific receptors or intracellular microbial targets against which bacteria can readily develop mechanisms of resistance either by altering the targets or developing mechanisms to pump the drug out of the cell, thus reducing the concentration below the minimum inhibitory concentrations (MIC). Unlike conventional antibiotics bacteria exhibit a low probability of resistance development against AMPs as they act mainly by altering the membrane structure and function without targeting specific receptors [61]. But we also know that bacteria are masters at adaptation and have evolved strategies to overcome the deleterious effect of almost all antibiotics developed so far. Some bacteria have been identified that can acquire resistance against at least certain AMPs. Some bacteria have been able to alter their surface charge by reducing the anionic nature of the membrane which is controlled by a two component regulator system called PhoPQ which uses PhoQ and PhoP as a sensor and an effector. Some bacterial species secrete proteases and cause proteolytic degradation of AMPs [61].

Daptomycin is a recently developed antibiotic with action against various MDR strains. Daptomycin is a negatively charged lipopeptide which exerts its antimicrobial effect due to heavy calcium complexation which in turn results in charged-based electrostatic interactions with anionic bacterial membranes [78, 79]. Recently, it was observed that *Staphylococcus aureus* exhibits resistance against daptomycin by altering the surface charge of its membrane making it positive and thus resulting in electrostatic repulsion of the peptide [78]. The increase in positive bacterial cell surface charge results from modification of phospholipids in the outer leaflet such

as lysinylation of phosphatidylglycerol leading to lysyl-phosphatidylglycerol (L-PG) and enhanced alanylation of lipoteichoic acids [78, 79]. D-alanylation of teichoic acid in the *S. aureus* cell wall is accomplished by the gene products of a four gene operon, dltABCD [80].

Active energy-dependent efflux also contributes to the resistance of some microbes against cationic AMPs of the innate immune system. For example, *Neisseria gonorrhoeae* expresses an efflux system MTRcde that ejects hydrophobic antibacterial agents and thereby gives increased resistance to antibiotics like penicillin and erythromycin. It has also been demonstrated that gonococcal resistance to the AMPs protegrin-1 and LL-37 is altered by over expression of the same *mtr* genes that control this efflux system. [40].

It is difficult to foresee what will happen if we start to use AMPs extensively as antibacterial drugs. What we do know is that we are in dire need of new antibiotics that can target MDR pathogenic bacteria, and that AMPs may be successful at doing that.

1.5 GL13 PAROTID SECRETORY PROTEINS

The oral cavity is a major port of entry for bacterial infections in humans and harbors over 700 species of bacteria. Most of these bacteria are non-pathologic in healthy individuals but can cause severe diseases in immuno-compromised patients with cancer, AIDS or several other diseases. Oral epithelial cells, neutrophils and salivary glands secrete into the oral cavity a large number of AMPs which kill pathological bacteria and other microorganisms. These AMPs belong to different functional families namely cationic peptides, protease inhibitors, enzymatic activity inhibitors, bacterial agglutinating and metal ion chelators [12, 81].

PSP is a major salivary protein expressed in rat, mouse, bovine and human saliva [82, 83]. Human PSP (hPSP) was identified on chromosome 20q11 expressed on gene C20orf70 [82]. Acinar and

ductal cells of the parotid gland, submandibular gland and in gingival epithelial cells express hPSP [37, 84, 85]. It is a member of the short palate, lung and nasal epithelium clone (sPLUNC) family of proteins that are related to the bactericidal/permeability-increasing protein (BPI), lipopolysaccharides (LPS)–binding protein (LBP), and cholesteryl ester transport protein (CETP). In 2003, Gorr *et. al.* showed that hPSP exhibits antibacterial and anti-inflammatory activity against *Pseudomonas aeruginosa* [37]. hPSP expression is upregulated by inflammatory cytokines such as TNF-α and IL-8 in response to bacterial infection or inflammation similarto β-defensin-2 and-3 suggesting their role in innate immunity [38]. Several peptide sequences (as listed in Table 1-1) have been identified from hPSP based on its structural (see Figure 1-6) and functional similarity with bactericidal/permeability – increasing (BPI) protein and lipopolysaccharide (LPS) binding protein [84, 85]. In BPI proteins the N-terminal domain is needed for bacterial opsonization and the C-terminus is needed for CD-14 binding [37]. While hPSP is only 15% identical and 34% similar to the N-terminal domain sequence of BPI protein it exhibits a high level of structural similarity as suggested by crystal structure fitting of BPI with hPSP [85]. Based on this structural fit between hPSP and the N-terminus of BPI various peptide sequences were identified and synthesized. Some peptides with modifications at carboxyl terminus and point mutations were also synthesized. The antimicrobial activity for selected peptides is summarized in Table 1-2.

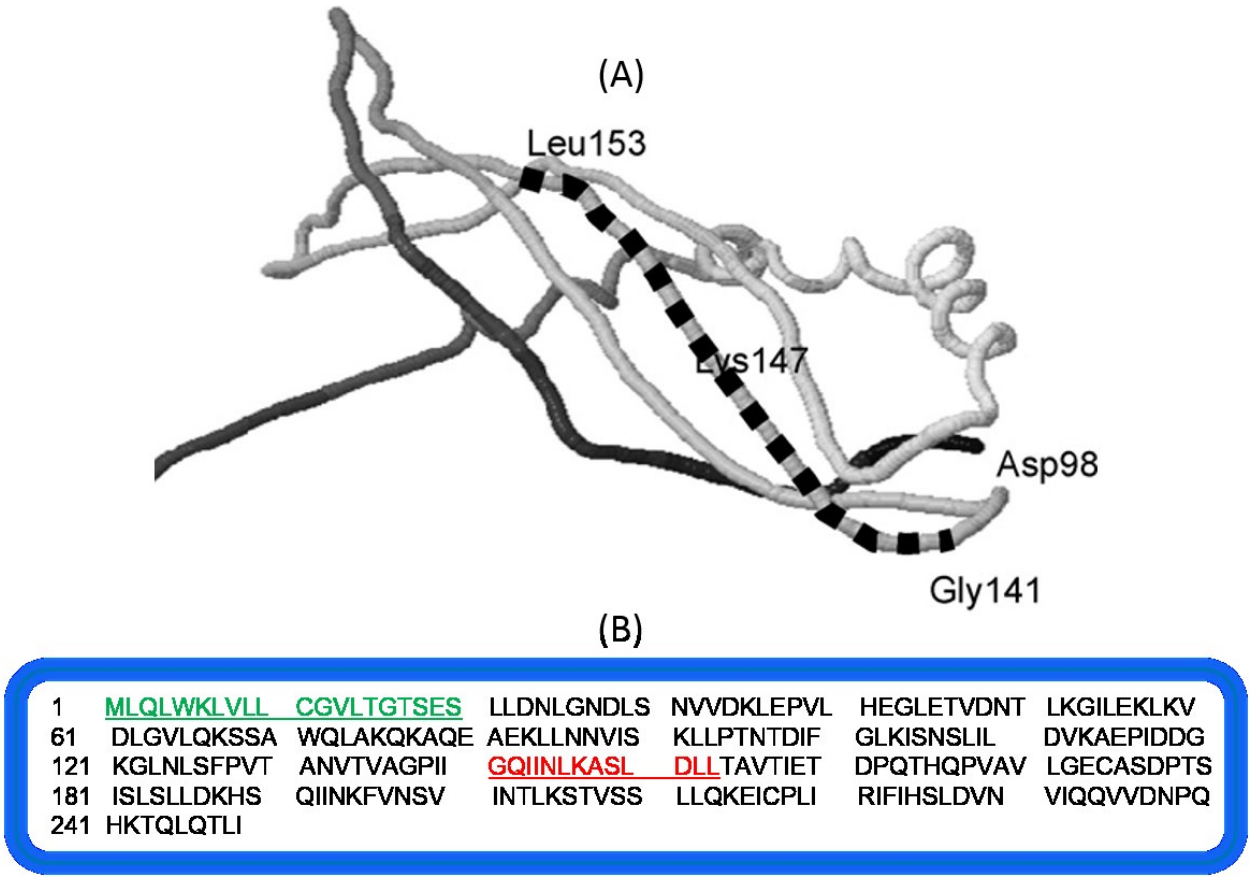

Figure 1-6 Structure and sequence of hPSP.

Structural model of PSP and GL13 peptide is shown as broken line in (A). Sequence of hPSP is presented in (B), where signal peptide is highlighted green and GL13 peptide is highlighted red. This figure is adapted from Gorr et.al. [86]

GL13NH2 which induces bacterial agglutination has an amino acid sequence identical to the native peptide GL13OH (amino acid ranging from position 141 to 153 of hPSP) but with an amide modification of the carboxyl terminus. GL13K was produced by the conversion of glutamine, asparagine and asparatic acid to lyines in the GL13NH2 peptide sequence [87]. GL13K, with 13 amino acids and a +5 charge (at pH 7), has strong anti-inflammatory and antibacterial activity against Gram-negative, Gram-positive and biofilm forming bacteria but low hemolytic and cytotoxic effects [87]. Both GL13K and GL13NH2 inhibit LPS and monophosphoryl lipid A stimulated TNFα secretion from macrophages by binding to lipid A of LPS [84, 87]. GL13K

effectively killed the Gram-negative bacteria *E. coli* and *P. aeruginosa* and Gram-positive bacteria *Streptococcus gordonii* at peptide concentrations of 5-10 μg/ml [87]. Bactericidal effects against *E. coli* were observed to be similar to those of the well characterized antimicrobial peptides LL-37. The presence of saliva had no impact on the activity of GL13K and polymyxin, while LL-37 efficacy was significantly reduced [87]. An alanine scan in which 12 different alanines substituted GL13K variants were analyzed showed that the mutation to lysine at position 2 was responsible for the loss of bacterial agglutination activity and the serine residue in position 9 is responsible for anti-lipopolysaccharide activity of GL13K [87]. The small size, broad spectrum of activity, fast action even at elevated salt concentrations [88], low micromolar MIC values [87] and anti-LPS activity makes GL13K an interesting candidate as an antimicrobial agent.

Table 1-1 Summary of biological activity of some of the hPSP peptides.

Peptide	Sequence	Bacterial agglutination	Bacterial killing	Anti-biofilm	Inhibition of TNF-α secretion	Hemolysis
GK7OH	GQIINLK-OH	No	No	No	Not known	No
GL13OH	GQIINLKASLD LL-OH	Yes	No	No	Yes	No
GL13NH2	GQIINLKASLD LL-NH2	Yes	No	Not Known	Yes	No
GL13K	GKIIKLKASLK LL-NH2	No	Yes	Yes	Yes	No
GL17NH2	GPIIGQIINLKA SLDLL-NH2	No	No	No	No	No

Table 1-2 List of various AMPs synthesized from hPSP.

Peptide properties of hPSP pepides were calculated using Innovagen online peptide property calculator [89] The first and second letter in the peptide name represent the first and last amino acids respectively in the hPSP sequence. The number is indicative of the number of amino acids. OH in the name indicates free carboxyl end and NH2 indicates the amide modification of carboxyl terminus. The peptides highlighted in yellow are the modified peptide sequences with changes shown in blue and red.

Peptide	Sequence	pI	Charge at pH (7.0)
GK7OH	GQIINLK-OH	10.1	+1
GL13OH	GQIINLKASLDLL-OH	6.7	0
GL13NH2	GQIINLKASLDLL-NH2	10.1	+1
GL13DN	GQIINLKASLNLL-NH2	14	+2
GL13K	GKIIKLKASLKLL-NH2	14	+5
GL17NH2	GPIIGQIINLKASLDLL-NH2	10.1	+1

1.6 MEMBRANE COMPOSITION

Biological membranes act as a barrier between the cellular and extracellular environment: however there are differences in the composition of bacterial membranes and mammalian membranes. These differences can be exploited to develop AMPs with selective bacterial toxicity.

1.6.1 Bacterial membranes

Bacteria have survived for millions of years and have evolved in extreme conditions such as heat, cold and toxic chemicals from competing species. The robust bacterial cell walls are one of the several defense mechanisms that bacteria have employed to survive in these harsh conditions. Gram-positive and Gram-negative bacteria are significantly different in their membrane composition. Gram-positive bacteria only have one membrane barrier *i.e.* cytoplasmic membrane, while Gram-negative bacteria have one extra outer membrane barrier after the

cytoplasmic barrier. The cytoplasmic membranes of the two are decorated with peptidoglycans which are the interconnected mesh of cross-linked sugar derivatives and various amino acids. The peptidoglycan layer is several fold thicker in Gram-positive bacteria as compared to Gram-negative bacteria. The outer membranes of Gram-negative and Gram-positive bacteria are decorated with lipoteichoic acids (LTA) and lipopolysaccharides (LPS), respectively (see Figure 1-7). The actual composition of cytoplasmic membranes may vary between various species and strains of bacteria. However, they all carry a net negative charge as a virtue of the negatively charged lipids such as phosphatidylglycerol (PG), phosphatidylinositol (PI), phosphatidylserine (PS) and cardiolipin (CL) [43, 54].

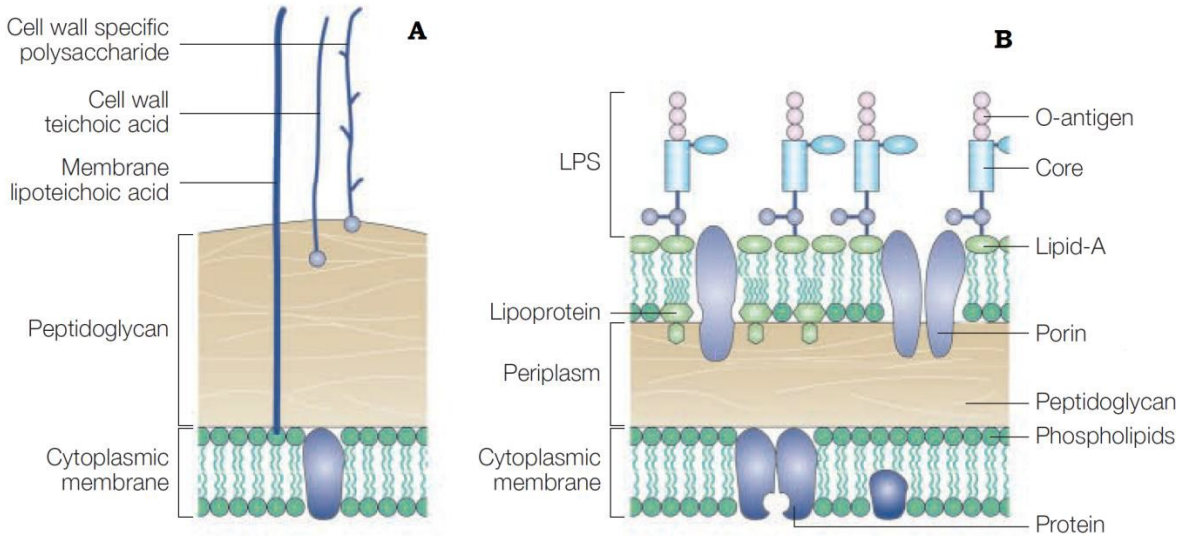

Figure 1-7 Outline of Gram-positive (A) and Gram-negative cell walls (B) adapted from Bucala *et. al.*[90].

1.6.2 Eukaryotic membranes

In contrast to prokaryotic membranes, eukaryotic membranes are largely composed of neutral/zwitterionic phospholipids mainly phosphatidylcholine (PC) and phosphatidylethanolamine (PE) [91]. The two leaflets of eukaryotic membranes are asymmetrical with the outer leaflet carrying a net neutral charge and with the inner leaflet comprised of both

zwitterionic and anionic lipids [43]. They also have a high content of cholesterol (0.2 to 0.5 mol fraction) and sphingomyelin (SM) resulting in increased lipid packing. The presence of cholesterol leads to increased ordering and thickening of the phospholipid hydrocarbon region and this can be detrimental to the insertion of AMPs [92] Differences in eukaryotic and bacterial membrane are represented schematically in Figure 1-8.

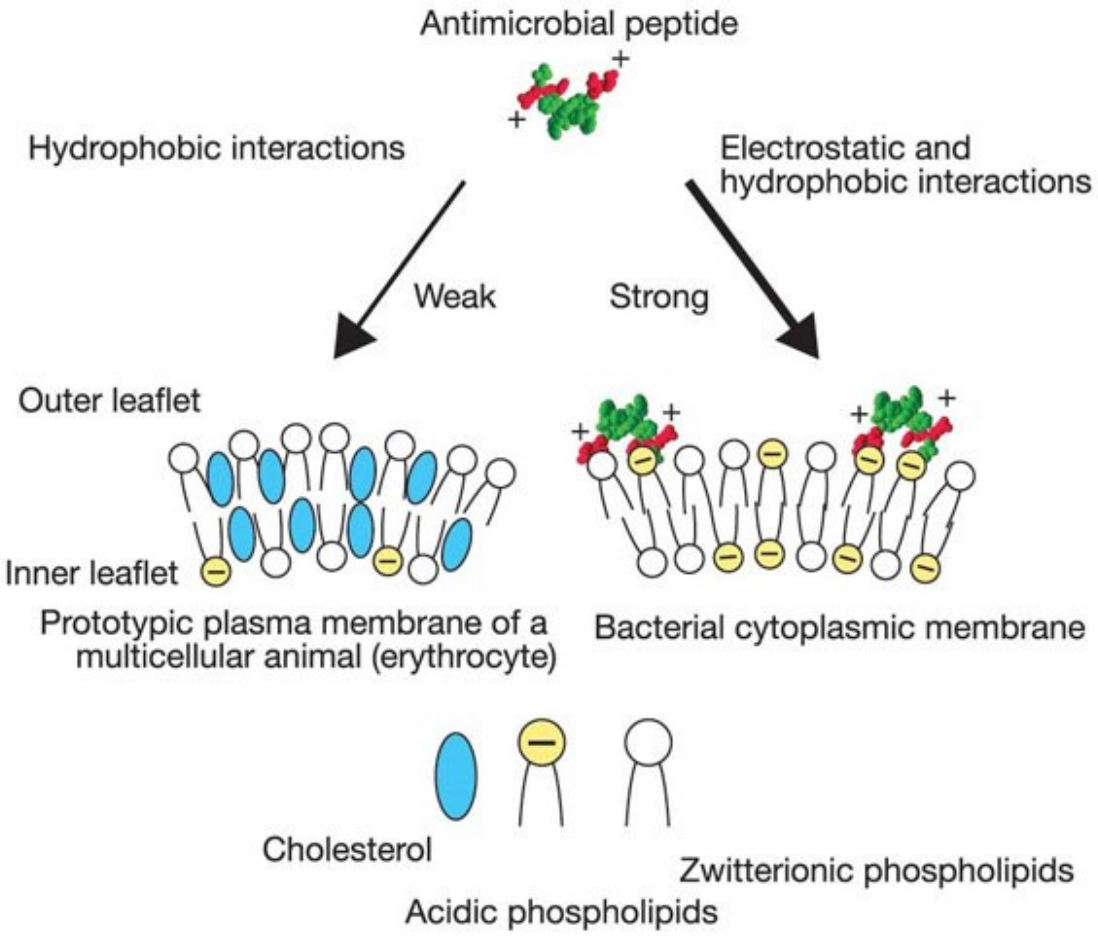

Figure 1-8 Schematic of AMPs interactions with bacterial and eukaryotic membranes.

AMPs target bacterial membranes as virtue of strong electrostatic interactions with anionic lipids. Eukaryotic membranes are mainly zwitterionic in nature with large amount of intercalated cholesterol adapted from Zasloff *et. al.*[13].

1.7 MODEL MEMBRANES

Model membranes have been used extensively to mimic biological membranes. Biological membranes are highly complex so it is very difficult to develop an exact copy of these as model membranes. The use of model membranes enables systematic studies of membrane properties as they offer good control over membrane parameters by varying their composition. The model membranes that we used in this thesis for our peptide lipid interactions studies are supported lipid bilayers (SLBs) and liposomes.

Liposomes were first described in the mid-60s and have been used since then for a wide range of applications ranging from drug delivery, vaccine development, cosmetics, and biophysical studies for peptide/protein membrane interactions and biological fission and fusion processes. Liposomes have an advantage over SLBs in that they allow access to the solution phase on both sides of the membrane. Liposomes can be prepared with a wide mix of lipids to closely resemble the natural membrane, however, the two leaflets of natural membranes are asymmetric and thus difficult to mimic as a whole structurally and functionally using the liposomes which are symmetrical on both sides. Liposomes usually range in size from over 30 nm to several microns. On the basis of the number of the bilayers, liposomes can be classified into unilamellar and multilamellar. In unilamellar liposomes the liposomes have a single phospholipid bilayer enclosing the aqueous solution/core. Whereas multilamellar liposomes have several phospholipid bilayers entrapped in a large membrane barrier.

Since first reported by McConnell *et. al.* in the 1980's [93, 94], SLBs are widely used biophysical models for understanding the functions of biological membranes such as the interactions of biological membranes with membrane proteins or AMPs. Lateral diffusion constant of lipids in in upper leaflet of SLBs is similar to that of biological membranes and liposomes[93, 94]. However,

solid supported SLBs offer a disadvantage in terms of less amount of water being entrapped (1-2 nm water layer) between the substrate and the membranes lower leaflet [95]. This results in reduced accessibility to the other side of the membrane which is particularly disadvantageous for proteins/peptides which have either large transverse membrane domains or cross the membrane to exert there effect. The lower leaflet lipids have a lower diffusion constant compared to the upper leaflet due to substrate coupling.

SLBs are commonly prepared by a liposomal fusion/rupture method. Liposomes in a bulk liquid are allowed to interact with the substrate and this interaction can later induce rupture and fusion of the liposomes to form a planar bilayer after a minimum concentration on the surface is reached. In case, the interactions with the substrate are not enough to cause rupture, then some fusion agents such as divalent calcium ions can be used to diminish repulsive hydration forces and electrical forces between liposomes[96]. Other common methods used for SLB deposition are solvent spreading and Langmuir-Blodgett (LB) deposition. LB deposition offers advantages particularly for the deposition of asymmetric bilayers. This is highly advantageous in mimicking cell membranes which are asymmetric in nature.

1.8 AIMS OF THESIS

The purpose of the present work was to study the molecular mechanisms and forces involved in the activity of various GL13 antimicrobial peptides. This thesis will provide an insight into the role played by various peptide properties such as charge and amino sequence in the activity and selectivity of GL13 peptides. This understanding of important fundamental characteristics of GL13 peptides can then be used to develop a more rational design for more potent hPSP peptides with optimal therapeutic indices.

In this thesis we are particularly interested in understanding the following key properties:

1. The role of peptide structure, in particular, the net charge, amino acid composition and amidation of the carboxy terminus on the activity and specificity of hPSP derived peptides.
2. The role of surface charge and packing density of human and bacterial membranes, which are known to play key roles in bacterial membrane specificity and disruption, on the binding affinity, secondary structure, orientation and insertion of hPSP peptides.

The particular aims and goals of each of the manuscript chapters are discussed in detail herein and in the introduction of the respective chapters.

1.8.1 Scope of manuscript 1 (Chapter 3)

Electrostatic interactions with bacterial membranes are known to play a very important role in the selectivity and activity of AMPs. The peptide, GL13K, having an increased cationic nature was produced by introduction of three lysine residues at equal spacing throughout the peptide length of GL13NH2 (native hPSP peptide with amide modification at carboxy terminus). The modified peptide, GL13K, comprises 13 amino acids (GKIIKLKASLKLL-CONH2) and carries

a net charge of +5 at pH 7. The role of charge on the activity of AMPs has been discussed in detail in section 1.3.1. Lysine substitution of various residues such as glutamine and asparagine at position 2 and 5 resulted in increased peptide water solubility.

We studied the effect of the increased cationic nature of the GL13K peptide on its activity and selectivity. In order to study the effect of electrostatic interactions on the mechanism of action of the GL13K peptide, we used membranes constructed from two synthetic lipids, anionic DOPG and zwitterionic DOPC, as model systems to study the effect of charge without altering the lipid packing. As salt concentrations are significant in biological systems, we studied the effect of increased salt concentrations on the activity and interaction of GL13K with membranes. Finally, we explored the role of electrostatic and hydrophobic forces on the activity of GL13K along with the proposed molecular mechanism of interaction.

1.8.2 Scope of manuscript 2 (Chapter 4)

In chapter 3, single-component (DOPG or DOPC) model membranes were employed to identify the role of electrostatic forces in the activity of GL13 peptides (it was assumed that eukaryotic membranes are zwitterionic in nature). It was important to identify these forces, but natural membranes are much more complex in terms of their composition as explained in detail in section 1.6. Eukaryotic membranes are zwitterionic on the outer leaflet but exhibit a net negative potential due to the presence of some negatively charged lipids on the inner leaflets and the electrochemical gradient which results from the varying extents and rates of proton movement across the membrane [43]. This could result in favourable interactions between GL13K peptides and eukaryotic membranes resulting in cytotoxicity. However, as mentioned in section 1.6.2, eukaryotic membranes also contain a large amount of cholesterol which leads to increased lipid packing and charge dilution. This increased lipid packing might limit any favourable interactions

between GL13K and the eukaryotic membrane. In this chapter we studied the role of cholesterol on the activity and specificity of GL13K. 40 mol% Cholesterol was incorporated into DOPC and DOPG model membranes to study the effect of cholesterol on activity and specificity of GL13K. The percentage of cholesterol was chosen to be towards the higher limit of cholesterol present in eukaryotic membranes which range from 0.2 to 0.5 mol fraction [97] but well below the miscibility limits of 0.67 mol fraction [97, 98].

1.8.3 Scope of manuscript 3 (Chapter 5)

Herein we elaborate on the role of hydrophobicity and reduced charge compared to that of GL13K on the activity and specificity. We studied the native hPSP peptide with an amide modification of its carboxy terminus yielding a net charge of +1 in the resulting peptide GL13NH2. As discussed earlier (section 1.3.1), antimicrobial activity of an AMP is the end result of a combination of its electrostatic and hydrophobic interaction with the membrane. Due to high hydrophobicity and low charge these peptides have low water solubility and are highly ordered. To further identify the role played by the secondary structure of peptide on the activity, we will compare the activity of the GL13NH2 peptide to GL13D/N, which has similar hydrophobicity to GL13NH2 but increased structured components and carries a +2 charge. To study this, model membranes comprising DOPG and DOPC were used as model eukaryotic and prokaryotic membranes to study only the effects of electrostatic and hydrophobic interactions. Zwitterionic DOPC lipids lack electrostatic interactions with cationic peptide thus could serve as model for identifying non-specific interaction. The role of electrostatic and non-specific hydrophobic interactions on the activity of GL13 peptides will be elaborated.

1.8.4 Chapter 6

Chapter 6 will include final discussion and conclusions to correlate the various important observations of the three manuscripts. In this chapter we will discuss some important questions that need to be addressed in future. This section is divided in two sections: short term objectives and long term aspects of the project.

2 MATERIALS AND METHODS

2.1 MATERIALS

Lipids were obtained from Avanti Polar Lipids Inc. (Alabaster, AL, USA). 5-(and-6)-carboxyfluorescein (CF) mixed isomers were supplied by Molecular Probes (Eugene, OR, USA) and used as the sodium salt of CF, obtained by neutralization with two molar sodium hydroxide. Water used for any preparation was of 18 MΩ purity. The peptide GL13K was obtained from the University of Minnesota peptide synthesis facility at better than 95% purity as evidenced by High performance liquid chromatography (HPLC) and mass spectrometry [87]. Peptide stock solutions were prepared by dissolving the desired peptide in water. Sephadex G-50 (fine with a bead size of 20 – 80 μm, ACS grade), sodium phosphate monobasic monohydrate ($NaH_2PO_4 \cdot H_2O$), sodium hydrogenphosphate heptahydrate ($Na_2HPO_4 \cdot 7H_2O$), 4-(2-hydroxyethyl) piperazine-1-ethanesulfonic acid (HEPES), sodium hydroxide (NaOH) and sodium chloride (NaCl) were obtained from Sigma-Aldrich. Unless otherwise stated, all experiments were conducted in 10 mM sodium phosphate buffer at pH 7.4 ("*sodium phosphate*") in this report prepared by mixing appropriate proportion of $Na_2HPO_4 \cdot H_2O$ and $NaH_2PO_4 \cdot 7H_2O$. HEPES buffer was prepared by dissolving the desired amount of HEPES in water and adjusting the pH to 7.4 using NaOH.

2.2 LIPOSOME PREPARATION

2.2.1 Preparation of multilamellar vesicles

Unilamellar liposomes were prepared by downsizing multilamellar vesicles (MLVs). To prepare MLVs, desired lipids were first dissolved in chloroform in a round bottom flask. Chloroform was

then evaporated for 30-40 minutes using a rotary evaporator to yield a thin dry lipid film on the bottom of the flask. These dried lipid films were then hydrated by incubation with the desired buffer solution for ≈2 hours. Hydrated lipid films were then re-suspended to form MLVs by high speed vortexing for 4-5 minutes at room temperature.

2.2.2 Preparation of large unilamellar liposomes by extrusion

Liposomes were prepared by extrusion as described by Mayer *et. al.* [99] using a mini-extruder from Avanti Polar Lipids Inc. (Alabaster, AL, USA). Previously made MLVs (Section 2.2.1) were downsized to get large unilamellar liposomes by forcing them through a polycarbonate filter with a pore size of 0.1 micron. The polycarbonate filter was mounted in the mini-extruder assembly supplied by Avanti Polar Lipids Inc. (Alabaster, AL, USA). The MLV suspension was passed 41 times through the filter with a final pore size (0.1 μm) to ensure liposomes of low polydispersity. This final extrusion through filters with a 0.1 μm pore yielded large unilamellar vesicles (LUV) with a mean diameter of 90-120 nm determined by DLS. Mean particle size depends slightly on lipid composition and was reproducible from batch to batch.

2.3 ISOTHERMAL TITRATION CALORIMETRY

Isothermal titration calorimetry (ITC) is a well established technique to study the interaction of antimicrobial peptides with membranes, yielding thermodynamic parameters such as binding constants, enthalpy, entropy, free energy and binding stoichiometry [48, 68, 100-103]. In an ITC reaction chamber the reference and sample cells are always maintained at the same temperature by supplying the necessary power to the reaction cell. When a chemical reaction or an interaction between a receptor and ligand takes place in calorimeter cell accompanied by a heat release (exothermic) or absorption (endothermic), to compensate for these heat changes and maintain the

constant temperature in the reaction, the power is increased or reduced. Heat signals obtained for each injection during the titration are simply the integrals of this power supplied to the reaction chamber (see Figure 2-1). When the reactant in the cell becomes saturated with added ligand/titrant, the heat signal diminishes until only the background heat of dilution is observed. Lipid–peptide interactions are different from chemical reactions in that no covalent bonds are formed or broken. Instead, the association of a peptide with a pure lipid membrane corresponds to a physical adsorption process [103]. The enthalpy, entropy and free energy changes obtained from the injection of liposomes into peptides or *vice versa* is the net result of a combination of processes such as disruption of peptide aggregates in solution, interaction with the membrane surface, lipid dehydration, aggregation of peptides on the membrane, secondary structure changes, reorientation of the peptides in the hydrophobic core of the membrane, lipid redistribution and/or acyl chain reordering due to membrane disordering or channels formation [102-104]. High sensitivity titration calorimetry can be applied to study lipid–peptide interactions in two different modes. In the first, the calorimeter cell contains lipid vesicles and the peptide is injected into the calorimeter cell. In the second, the two solutions are exchanged i.e. the peptide is contained in the calorimeter cell whereas the lipid is injected [103]. The comparative information obtained from two methods have been discussed in the results section of chapter 3.

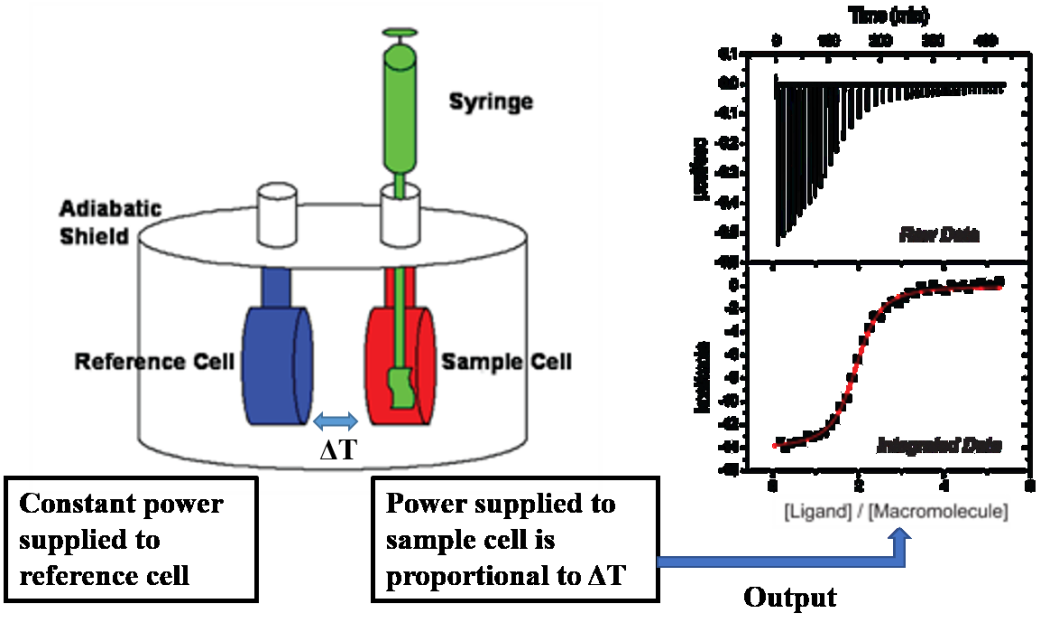

Figure 2-1 Schematic pictorial representation of ITC.

The power supplied to maintain the constant temperature of sample cell is recorded with respect to time as shown in upper half of data view. This can then be used to calculate the molar heat changes occurring upon each injection of titrant (lower half of data view) adapted and modified from [105].

In the thesis all of the ITC experiments were carried out using a VP-ITC Microcalorimeter (MicroCal Inc., Northampton, MA, USA). All solutions were degassed for 30 minute under vacuum with continuous stirring before loading the reaction chamber and syringe. All experiments were performed at 22°C. Data analysis was performed using Microcal Origin® 5.0 software. Diminished heat signals observed after the system reached saturation were used to correct for the heat of dilution. The binding site model was chosen based on the best mathematical fit rather than a mechanistic model as the binding of AMP's with membranes is not due to a specific binding/receptor site. Non linear least square fitting to the binding data using an appropriate fit model was used to calculate various thermodynamic parameters.

For Manuscript 1, in one set of experiments, 4 µl of 1 mM DOPC or DOPG liposomes were injected sequentially into 0.1 mM GL13K contained in the reaction cell. A stirring speed of 300 rpm with injection periods of 8 seconds were chosen with an equilibration time of 4 minutes between each injection to ensure proper mixing and a stable baseline. In another set of

experiments, 3 µl of 1 mM GL13K were injected sequentially into 0.1 mM DOPG liposomes contained in the reaction cell while all other parameters remained the same. These experiments were carried out in sodium phosphate buffer in presence or absence of 107 mM NaCl (as indicated) to study the effect of charge shielding on GL13K binding parameters. All experiments were performed at 22°C.

For Manuscript 2, 7.4 µl of 1 mM DOPC/Ch or DOPG/Ch liposomes were injected sequentially into 0.1 mM GL13K contained in the reaction cell. A stirring speed of 300 rpm with injection periods of 14.8 seconds were chosen with an equilibration time of 4 minutes between each injection to ensure proper mixing and a stable baseline.

For Manuscript 3, all parameters were similar to that of manuscript.

2.4 CIRCULAR DICHROISM

Circular dichroism (CD) relies on the differential absorption of left and right circularly polarized light [106]. The amide chromophore absorbs in the far UV (175 – 250 nm) and the signal varies as a function of the chiral environment produced by different secondary structures. Thus, different secondary structures exhibit characteristic ellipticity changes such as α-helices which exhibit negative double minima at about 222 nm and 208 nm and β-sheets which produce spectra with a negative band at about 210 nm. The CD spectra obtained for a protein represent the contributions from the different secondary structures; these relative contributions are then deduced using secondary structure prediction algorithms such as CONTIN, SELCON 3 [107-109].

CD spectra from 200 nm to 260 nm were recorded using a J-815 spectrometer (Jasco Corporation, Essex, UK) as an average of five scans obtained using a 0.2 cm path length quartz cuvette at 22 °C with data pitch 0.2 nm, scan speed 20 nm/minute and a response time of 1

second. All spectra were corrected by subtraction of the buffer spectra. Wavelength shorter than 200 nm gave high HT (> 600V) values giving a signal-to-noise ratio too low to be used.

Spectra for GL13K, GL13NH2 and GL13D/N in the presence or absence of liposomes were obtained at a fixed peptide concentration of 60 μM for GL13K and GL13NH2 and 150 μM for GL13D/N with varying lipid concentrations to obtain peptide/lipid ratio's (P/L) ranging from 1/15 to 1/2.5. All spectra were corrected for path length and concentration to give the mean residue ellipticity.

2.5 CARBOXYFLUORESCEIN RELEASE ASSAY

It is well established and accepted that AMPs act mainly by causing bacterial membrane permeabilization or lysis. A commonly used method for studying the permeabilization of membranes by peptides or proteins utilizes vesicle-encapsulated fluorescent dyes and quenchers that change fluorescence intensity on release. Self-quenching dyes such as carboxyfluorescein (CF) or calcein and dye/quencher pairs such as ANTS/DPX (8-amino-napthalene-l,3,6 trisulfonic acid/p-xylene-bis-pyri- dinium bromide) and terbium/dipiccolinic acid are the most frequently used marker systems [15, 110-114]. In our investigations, we used CF release assays to study the membrane permeabilization by hPSP peptides. CF is self-quenched when loaded in a high concentration in the core of liposomes [115]. Any disruption of the liposomal membrane will result in efflux of dye and thus reduce the quenching by dilution. Liposomes for CF assays were prepared by hydrating the dried film with 50 mM CF in 10 mM HEPES buffer at pH 7.4 and extruded as explained in section 2.1. Non-encapsulated CF was separated from CF encapsulating liposomes using a Sephadex - G50 column with 10 mM HEPES, 107 mM NaCl at pH 7.4 as an eluent. The lipid concentration was determined using a phosphate analysis based on the method

explained by Bartlett *et. al.* [116]. Complete details about the steps followed in the modified method are listed in Appendix 1. CF leakage experiments were recorded using a Varian Cary Eclipse spectrophotometer (Agilent Technologies, Mississauga, ON, Canada) equipped with a Varian Cary single cell Peltier accessory to control the temperature at 22 °C. The excitation and emission wavelengths were set to 480 nm and 520 nm, respectively. All experiments were performed at a fixed phospholipid concentration (25 μM) obtained by the dilution of the stock solution quantified earlier using modified Bartlett's method. After recording the intensity for two minutes, an aliquot of desired peptide stock was added to achieve the desired P/L ratio and the fluorescence was monitored for 60 minutes. Triton X-100 (3μl of 2% (v/v)) was added to cause complete loss of membrane integrity and resulting fluorescence signal was used as a control for 100 % lysis. The percent release of CF from liposomes was calculated using equation Equation 2-1

Equation 2-1: Percentage CF release.

$$\%\text{CF release} = \frac{F_t - F_0}{F_{max} - F_0} \times 100$$

where F_t is the fluorescence intensity at time t, F_0 is fluorescence intensity before addition of the peptide and F_{max} is the maximum fluorescence intensity after addition of Triton X-100.

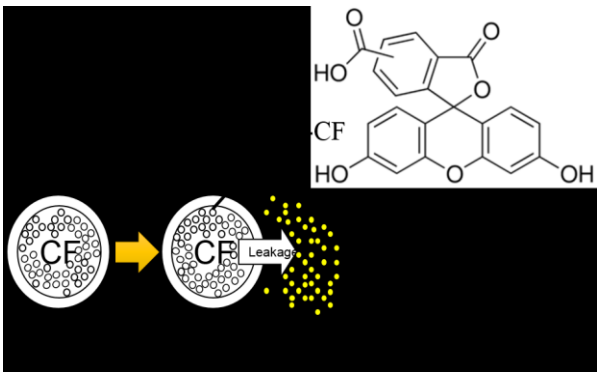

Figure 2-2 Schematic representation of CF release assay.

2.6 FLUORESCENCE RESONANCE ENERGY TRANSFER

Fluorescence resonance energy transfer (FRET) has been used commonly to study membrane fusion processes. This approach relies on the interactions which occur between two fluorophores if the emission band of the energy donor, overlaps with the excitation band of the energy acceptor, and the two probes exist in close physical proximity**.** Under such conditions, the energy from a photon absorbed by the energy donor can be transferred to the acceptor which will then fluoresce as though it had been excited directly [117]. The efficiency of fluorescence energy transfer between two given fluorophores is dependent upon their spatial separation. This can provide a means to study membrane fusion since lipid mixing between two liposomes caused by fusion of membranes will increase the separation distance between labeled lipids. There are two types of FRET assays that are commonly used [118]:

2.6.1 Probe dilution assay

In this method both probes are incorporated into one population of liposomes (labeled vesicles) and they are mixed with another population of non-labeled liposomes containing no probes. Liposomal fusion is followed by dilution and hence a lower surface density of fluorescent probes resulting in decreased energy transfer from the donor to the acceptor.

2.6.2 Probe mixing assay

In this version of the assay, different FRET probes (donor and acceptor) are placed in separate populations of liposomes, and the quenching of donor probe fluorescence and/or increase of acceptor fluorescence upon fusion and mixing is monitored.

The fusion or aggregation caused by GL13K was studied using the probe dilution assay (see section 2.6.1). Head group labeled 1,2-dioleoylphosphatidylethanolamine-N-(7-nitro-2-1,3-

benzoxadiazol-4-yl) DOPE-NBD and 1,2-dioleoylphosphatidylethanolamine-N-(lissamine rhodamine B sulfonyl) DOPE-Rh fluorescent derivatives of phospholipids were used as FRET donors and acceptors respectively. The emission band of DOPE-NBD significantly overlaps the excitation band of DOPE-Rh, so that a very efficient energy transfer (resulting in a decrease of the NBD fluorescence and concurrent increase in the DOPE-Rh fluorescence) occurs between these two probes when they are close to each other [117]. FRET pairs of 2 mol % rhodamine and NBD probes were labeled on one liposome population and another population of liposomes without any labels was prepared. The two liposomal populations then were mixed at an equimolar ratio and incubated with peptide. If the addition of peptide causes liposomal fusion it can be followed as a decrease in the rhodamine fluorescence (at λ_{em} = 592 nm) and an increase in the NBD fluorescence (at λ_{em} = 535 nm).

A Varian Cary Eclipse spectrophotometer (Agilent Technologies, Mississauga, ON, Canada) equipped with a Varian Cary single cell Peltier accessory to control the temperature at 22 °C was used for fluorescence measurements. Emission spectra were recorded by exciting the samples at 460 nm and setting excitation and emission slits to 10 nm each. Emission spectra were recorded from 480 nm to 680 nm and each reported spectrum is an average of 10 continuous scans of the same sample. For the dilution assay, the concentration of lipid concentration for labeled and non-labeled liposomes was 25 μM resulting in a total lipid concentration of 50 μM. Concentrations during the scan for labeled lipid containing liposomes in the absence of peptide were kept at 25 μM so that upon dilution with non-labeled lipids the overall fluorescence intensity of the probes was not altered.

In the case of the control experiments, where the vesicles are labeled with only 2% DOPE-Rh, the excitation wavelength was set to 532 nm and excitation and emission slits were 5 nm and 10 nm respectively.

2.7 DYNAMIC LIGHT SCATTERING

Dynamic Light Scattering (DLS) was used to measure the hydrodynamic diameter of particles in nanometer and micron ranges. DLS works on the principle of Brownian motion of particles in solution. In particular, the DLS instrument uses a laser as the light source to illuminate the sample. The extent of scattering is then calculated by the detector positioned at an angle of 173° to the incident light. The scattering intensity signal from the detector is processed by a correlator and then analyzed by a computer to derive the size information. The amount of scattered light will depend on the size of particles which in turn affects the Brownian motion. Larger particles have slower Brownian motion and *vice versa.* The hydrodynamic diameter values obtained by DLS are actually the diameter of a sphere that will have the same translational diffusion coefficient as the particles [119]. The sizes of the test particles are calculated from the translational diffusion coefficient by using the Stokes-Einstein

Equation 2-2).

The hydrodynamic radius of the liposomes was measured by DLS using a Zetasizer Nano - S (Malvern Instruments Ltd, Worcestershire, UK). All experiments were carried out at a fixed lipid concentration of 25 μM with P/L lipid ratios varying from 1/20 to 1/2.5 with a 10 min equilibration time. For each experiment,five measurements comprising 20 runs each averaged over 20 seconds were recorded. For each P/L ratio, experiments were repeated at least three times with different batches of liposomes.

Equation 2-2 Stokes-Einstein equation for calculation hydrodynamic radius.

$$d(H) = \frac{kT}{3\pi\eta D}$$

Where:

d (H) = hydrodynamic diameter

D = translational diffusion coefficient

k = Boltzmann's constant

T = absolute temperature

η = viscosity

2.8 CRYO-TRANSMISSION ELECTRON MICROSCOPY (CRYO-TEM)

Cryo-TEM is a type of transmission electron microscopy where samples are first frozen and then studied using electron microscopy. Cryo-TEM is becoming increasingly popular for biological samples. Freezing the samples to cryo conditions (temperatures close to that of liquid nitrogen) using liquid ethane minimizes the damage caused by the high intensity electron beam irradiated on the sample. EM microscopy has high resolution as it uses electron beams as a source of radiation (with an equivalent wavelength of 0.02 Å at 300 kV operating voltage) and resolution is inversely related to the wavelength. High power electron beams can destroy biological samples since the high intensity electron radiation can break chemicals bonds to form free radicals, which can have further damaging effect. Thus to image biological samples under these conditions they are either negatively stained with heavy atoms or frozen to liquid nitrogen temperatures and maintained at similar temperatures during imaging. Negative staining is done with heavy atoms which are mainly surface oriented and do not penetrate the biological sample. Negative staining

offers a drawback as it causes the flattening of the samples and loss of the internal cell structure information due to heavy shielding caused by these heavy atoms. Cryo temperatures reduce the radiation damage six fold such that higher intensity electron beam can be used for imaging yielding higher resolution. Further details can be found in Milne *et. al.* [120] and references therein.

Liposomes were imaged in the absence or presence of GL13K as follows: 5 µl of the sample were added to glow discharged Quantifoil (SPI) holey carbon electron microscopy grids. Excess fluid was blotted and the samples were flash frozen hydrated by plunging into a bath of liquid ethane using FEI Vitrobot Grid Plunging System (FEI electron optics). The grids were then stored in liquid nitrogen prior to imaging. Images were acquired using the FEI G2 F20 Cryo-S/TEM microscope (FEI, Inc., Oregon, USA) equipped with a Gatan Ultrascan 4k x 4k Digital (CCD) Camera System at a magnification of 25000× corresponding to a pixel size of 0.45 nm (defocus level ranging from −2.5 to −4.5 µm) under low dose conditions.

2.9 DUAL POLARIZATION INTERFEROMETRY

Dual polarization interferometry (DPI) is an analytical technique that uses dual optical waveguide interferometry for analysing thin films and enables real time measurement of changes in thickness, refractive index, mass and birefringence of an adsorbed layer on the sensor chip. DPI works on the principle of double slit Young's interferometer but is rather more complex than that as it uses two different polarizations namely transverse magnetic (TM) and transverse electric (TE) at the same time. Each polarized light is then passed through two waveguides namely the reference and the senor waveguide of the sensor chip. At the output the polarized light from two waveguides form interference fringes (as they do in a double slit interferometer). If any change happens to the sensing waveguide surface, it will result in the phase shift of fringes

at the output. These changes in the phase shift observed by two different polarizations were then used to calculate the thickness, refractive index, mass and birefringence of an adsorbed layer on the sensor chip. More detailed information about the theory and working principle can be found in these papers and references therein [121-126].

To perform DPI experiments an unmodified *Ana*Chip™ FB 80 from FarField Group Ltd. (Manchester, UK) with dimensions 24 × 6 mm was used to measure changes in the adsorbed bilayer. A 100 µm thick fluorosilicone mask was clamped on the chip to form two microfluidic flow channels of 1 × 17 mm offering a channel volume of 1.7 µl. The sensor chip was then fixed in a dual zone temperature controlled housing maintained at a temperature of 22 °C by a Peltier system. The flow rate through the two channels on the chip surface was controlled using a Harvard Apparatus PHD2000 supplied by FarField.

SLBs on two sensor channels of chip were formed by vesicular rupture by calcium ions according to the method of Mashaghi *et. al.* [125]. The bilayers deposited on sensor surface were further equilibrated with flowing buffer (10mM sodium phosphate) without calcium and allowed to stabilize for at least an hour until stable values for the TM phase and TE phase were obtained (i.e. no or minimal change in mass, thickness and birefringence). Then the peptide was injected consecutively on the same bilayer with increasing concentrations at a 20 µL/minute flow rate for 10 minutes with an equilibration time of 20 minutes between each injection. Data acquisition was done using *Ana*Light® version 2.1.21 software and analysed using *Ana*Light® explorer software.

Phase changes in TM and TE are fitted to calculate the thickness, mass and refractive index of the system. Anisotropic adlayers such as bilayers have different refractive indices perpendicular and parallel to the optical axis known as ordinary (n_o) and extraordinary refractive (n_e) indices

[127]. The difference between n_e and n_o is the birefringence which is related directly to the ordering of the system whereby a decrease in birefringence indicates decreased ordering [124, 128-132]. Birefringence is calculated as a difference in effective refractive index (n_{TM}) and (n_{TE}) measured by TM and TE, respectively. To calculate the bilayer parameters such as thickness, refractive index (R.I.), mass and birefringence either the thickness or R.I. must be known. Herein a fixed isotropic R.I. value of 1.47 was used [129, 131].

Mass values for the adlayer can be calculated using the de Feizter formula:

Equation 2-3 Mass of adlayer.

$$m\ (adlayer) = \frac{d\left(n_{iso}\ - n_{buffer}\right)}{\left(\frac{dn}{dc}\right)}$$

$$n_{iso} = \sqrt{\frac{n_{TM}^2 + n_{TE}^2}{3}}$$

Where m (adlayer) is mass of adlayer, n_{iso} is the average isotropic R.I. of the adlayer, n_{buffer} is the R.I. of the buffer and dn/dc is the specific R.I. increment for the adlayer. In general, the peptide and lipid dn/dc values are taken to be 0.182 mL/g and 0.135 mL/g, respectively [129, 133]. As dn/dc values specific for peptide - lipid complexes are not known, there is a high degree of uncertainty in the calculated mass changes, therefore only changes in birefringence of the bilayers upon interaction with the peptides will be discussed. Changes in birefringence is directly related to bilayer lipid ordering [134].

Bilayers were deposited onto the chip as explained in earlier. Desired amount of pepide was injected consecutively on the same bilayer with increasing concentrations at a 10 µL/minute flow rate for 10 minutes with an equilibration time of 20 minutes between each injection. Data

acquisition was done using *Ana*Light® version 2.1.21 software and analysed using *Ana*Light® explorer software.

2.10 ATOMIC FORCE MICROSCOPY

Lipid monolayers and bilayers supported on solid supports are valuable model systems to mimic biological surfaces (discussed in detail in section 1.7). Atomic force microscopy (AFM) is a surface imaging tool that allows high resolution imaging and scanning of surfaces revealing molecular structures at the nanoscale [135]. AFM imaging is done using a sharp cantilever attached to a tip which is mounted on a tip holder. The AFM tip scans over the surface of the sample and the interaction force between the tip and sample is measured. AFM imaging can be done in either contact mode or tapping mode. In contact mode, the AFM tip is scanned over the sample while the force applied on the cantilever is kept constant. This method of AFM imaging is often used for scanning hard samples. In tapping mode, the cantilever is oscillated at the amplitude close to its resonance frequency while scanning the sample surface. Force amplitude while scanning is kept at minimum to minimize the lateral forces and is particularly important for scanning soft samples. A laser is incident on the cantilever which is then reflected onto a photodiode detector. Any deflection in the cantilever scanning the sample due to height changes are then monitored by photodiode and transformed into a height image [135, 136].

To obtain uniform and defect free bilayers, freshly cleaved mica was immersed in 200 μM of the desired liposomes in 10 mM sodium phosphate, 2 mM $CaCl_2$ at pH 7.4 for 4 hours and then washed twenty times with fresh sodium phosphate buffer without $CaCl_2$ to remove the calcium. To maintain structural and functional integrity the bilayers must be protected from dewetting. These bilayers deposited on mica were then glued to a metal puck which is the fixed on the piezo

scanner. After ensuring the smoothness and uniformity of the bilayers these were then incubated with varying concentration of desired peptide for at least 20 minutes before scanning. AFM measurements were performed using a Nanoscope IIIa MultiMode AFM from Veeco (Santa Barbara, CA, USA). Imaging was done in tapping mode using V-shaped silicon nitride tips with a nominal spring constant of 0.58 N/m. AFM measurements were carried out in environmental mode, *i.e.,* in the presence of buffers. The force applied to the samples was maintained as low as possible by continuously adjusting the amplitude set point during scanning. Image analysis was performed using NanoScope 6.14R1 software and all images are presented after flattening.

3 MANUSCRIPT 1 MEMBRANE SELECTIVITY AND BIOPHYSICAL STUDIES OF THE ANTIMICROBIAL PEPTIDE GL13K

Information provided in this chapter is extracted from material published in **"Balhara, V**.; Schmidt, R.; Gorr, S.-U.; DeWolf, C., Membrane selectivity and biophysical studies of the antimicrobial peptide GL13K. *Biochimica.et Biophysica. Acta,* volume 1828 (2013) pages 2193-2203**"**. The materials and methods section has already been discussed in chapter 2 thus will not be repeated in here.

Author contributions:

I carried out all of the experimental work, data analysis and writing. C. DeWolf helped building the research plan, analyzing the data and contributed to writing the manuscript. R. Schmidt contributed to writing the manuscript. S.-U Gorr supplied the peptide GL13K and contributed to writing the introduction.

3.1 INTRODUCTION

The discovery of penicillin in 1940's led to the beginning of an "antibiotic era" enabling treatment of life threatening infections which was not previously possible. Since then, the development of new and effective antibiotics made it possible to cure many fatal bacterial or microbial diseases. However, in recent decades the extensive and improper use of antibiotics has

resulted in the emergence of new highly resistant bacterial strains and thus leading towards a "post antibiotic era" where we will have only few antibiotics left to combat multidrug resistant bacterial strains [3, 137, 138]. According to a recent report published by the World Health Organization [2], in this post antibiotic era, the development of new effective antibiotic drugs has been diminished which has increased and prolonged illnesses leading to increased mortality rates and socio-economic burden on societies especially in developing nations. Some of the common and life threatening bacterial infections are caused by Gram-negative bacteria and their biofilms, including *Pseudomonas* and *Acinetobacter* [17, 139]. Bacterial biofilms are several folds more resistant to antibiotics compared to their planktonic (floating) states [10, 11, 140].

Antimicrobial peptides (AMPs) seem to be potent antibiotic candidates. AMPs are part of the innate immune system in most organisms (plant/animal kingdoms) [62]. Various bacteria, despite encountering these AMPs for millions of years, have not been able to develop resistance [12, 13]. AMPs do not act *via* a stereospecific protein receptor mediated mechanism but rather target the fundamental difference in membrane composition between the host and the pathogens [13, 14]. Bacteria are less able to develop resistance against AMPs by redesigning their membrane since changing membrane composition and/or lipid organization is not metabolically favourable due to limited membrane lipid synthesis capabilities [137]. This has attracted many researchers to exploit these AMPs and their synthetic analogs as novel antibiotics and an extensive database of almost 2000 known and potential AMPs (antibacterial, antiviral, antifungal and antitumor) has been established [16].

AMPs are reported to act mainly by causing membrane lysis either by barrel-stave, toroidal pore or carpet mechanisms though various other mechanisms are also observed [58, 62, 63]. No single mechanism can be defined for all peptides [141]. Furthermore, membrane disruption mechanisms

for a given peptide can vary depending on lipid composition or other environmental conditions, for example melittin and aurein were found to act by three different mechanisms (barrel-stave, toroidal pore and carpet) depending on the conditions used [42, 142-144]. The interaction of AMPs with membranes can involve a variety of processes including the disruption of peptide aggregates, binding to the membrane surface, secondary structure transformation, reorientation into the membrane, and aggregation within the membrane, disruption of membrane integrity and eventually lysis of the membrane.

It is well accepted that electrostatic interactions can play a major role in the activity and specificity of AMPs not-withstanding the significant roles of hydrophobic forces, membrane curvature and mechanical properties. Despite differences in mechanisms, it can be concluded that AMPs act mainly by binding to membranes and kill bacteria by disrupting membrane packing and organization causing defects in the membrane with the consequent destruction of transmembrane potential and leakage of important cellular contents [13, 56].

GL13K is a small cationic AMP, which was designed by modification of a peptide sequence derived from human parotid secretory protein (hPSP) [145]. PSP is predicted to be structurally similar to BPI protein and lipopolysaccharide-binding protein [82]. This predicted structural similarity of PSP was used to identify potential antimicrobial peptides in the PSP sequence [86]. One of the resulting peptides, GL13NH2, induced bacterial agglutination but was not bactericidal [86]. To produce GL13K, the GL13NH2 peptide was modified by introducing three lysine residues, which switched the activity from agglutinating to bactericidal [87]. Both peptides exhibit anti-lipopolysacharide activity [87, 145]. The modified peptide, GL13K, comprises 13 amino acids (GKIIKLKASLKL-CONH2) and carries a net charge of +5 at pH 7 as calculated using the Innovagen online peptide property calculator [89]. GL13K has strong anti-inflammatory and

antibacterial activity against both Gram-negative and biofilm forming bacteria but exhibits low hemolytic and cytotoxic activity. Also, like polymyxin – B, GL13K binds lipopolysaccharide [87], a component of the outer bacterial membrane. Of particular note, GL13K has been found to be effective against the Gram-negative bacterium *Pseudomonas aeruginosa*. These opportunistic pathogens are associated with infections and biofilm formation in susceptible individuals, including nosocomial infections and cystic fibrosis patients [146].

Herein we present the biophysical studies to understand the membrane disruption mechanism for GL13K. Bacterial membranes are highly anionic in nature whereas outer leaflets of eukaryotic membranes tend to be neutral [18, 45, 147]. Therefore, we chose zwitterionic DOPC and anionic DOPG lipids as models for eukaryotic and bacterial membranes, respectively, to elucidate the effect of electrostatic interactions on the activity and specificity of GL13K.

3.2 RESULTS AND DISCUSSION

3.2.1 Binding affinity with membrane

Strong binding between AMPs and microbial membranes is one of the major driving factors for antimicrobial activity [13, 43]. ITC is a well established technique to study the interaction of antimicrobial peptides with membranes [48, 68, 102, 103, 137] yielding thermodynamic parameters such as binding constants, enthalpy, entropy, free energy and binding stoichiometry. ITC was used to investigate the thermodynamic parameters of the GL13K interaction with DOPC and DOPG model membranes.

Figure 3-1 shows typical titration curves for DOPG into GL13K in 10 mM sodium phosphate buffer in the presence or absence of NaCl. This salt concentration is slightly lower than physiological salt conditions but high enough for reduced electrostatic interactions and

alterations of peptide membrane interactions [69, 148, 149]. Both titration curves show similar behaviour, however in the presence of salt, less peptide binds overall (lower molar ratio at saturation). Also in the absence of salt, when electrostatic interactions are least shielded, enthalpy changes remain high with initial injections whereas in the presence of salt the enthalpy decreases with each subsequent injections. Thermodynamic parameters are summarized in Table 3-1. The interaction of GL13K with DOPG liposomes both in the presence or absence of NaCl yields binding constants in the order of 10^6 to 10^7 suggesting strong binding in both cases. Furthermore, given the high peptide lipid ratios at which interaction occurs, these binding constants can be considered an indication of the partitioning of the peptide to the lipid membrane. Interaction of GL13K with DOPG bilayers is an endothermic process with high positive enthalpy changes. This overall enthalpy is a sum of the enthalpy changes due to a large number of processes such as binding of the peptide to the membrane, aggregation, surface adsorption or insertion, transformation of secondary structure and membrane lipid reorganization or lysis. Free energy changes comprising endothermic enthalpies and large entropic increases have been reported to be associated with processes involving high disordering of lipid membranes [68, 103, 137] although one cannot exclude the solvent entropy changes due to partial dehydration of the peptide hydrophobic face. The large binding constant values and highly negative free energy values suggest a strong binding of GL13K to DOPG vesicles in both absence and presence of NaCl. The higher ionic strength buffer represents the isotonic level required for the CF experiments. The NaCl concentrations are comparable to physiological conditions and thus GL13K seems to be potentially active even at physiological salt conditions, consistent with antibacterial activity data [87]. In the above experiments, liposomes were added to an excess of peptide in solution. In this process, the low lipid/peptide ratio during the first few

injections leads to a significant excess of peptide that must be able to disrupt the membrane barrier function leading to the observed endothermic process. These endothermic heat changes decrease slowly until free peptide and bound peptide reach saturation.

In another set of experiments, GL13K was added to an initial excess of liposomes to probe whether the peptide goes from a surface bound state to a membrane inserted state prior to disrupting the membrane barrier [103]. For some peptides, a heat profile transition from exothermic to endothermic has been observed upon going from a surface bound state to a membrane inserted state [102], if the concentration range for these two states is sufficiently well separated. As seen in Figure 3-2 (A), GL13K initially binds to the excess of liposomes without any significant changes in binding enthalpy upon sequential injections. This suggests that concentration dependence for the different processes is sufficiently similar such that the thermodynamic parameters for individual processes cannot easily be resolved. Minimal heat changes are observed (Figure 3-2 (B)) upon sequential addition of DOPC (zwitterionic) liposomes to GL13K indicating minimal or weak binding to eukaryotic membranes.

Table 3-1 Thermodynamic parameters of GL13K binding to DOPG liposomes.

Values of enthalpy, entropy and free energy change are calculated by the sum of the respective value for two sites of binding.

Titrant	Amount of NaCl (mM)	Total enthalpy change $\Delta H = \Delta H_1 + \Delta H_2$ (kcal/mol)	Total entropy change $\Delta S = \Delta S_1 + \Delta S_2$ (kcal/mol/K)	Total free energy change $\Delta G = \Delta G_1 + \Delta G_2$ (kcal/mol)
Liposomes	0	2.0	0.073	-19
Liposomes	107	1.5	0.070	-19
Peptide	0	2.4	0.037	- 8

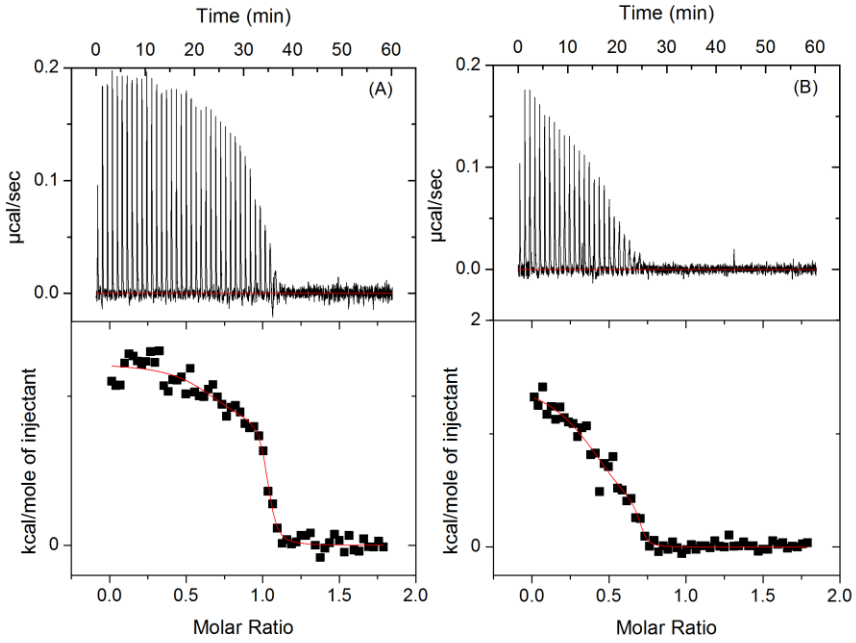

Figure 3-1. ITC binding isotherms for the titration of (1 mM) DOPG into (0.1 mM) GL13K with molar ratio of lipid/peptide.

(A)Titration done in 10 mM, pH 7.4 sodium phosphate buffer, (B) Titration done in 107 mM NaCl, 10mM, pH 7.4 sodium phosphate buffer. Small aliquots DOPG liposomes were injected sequentially into GL13K solution.

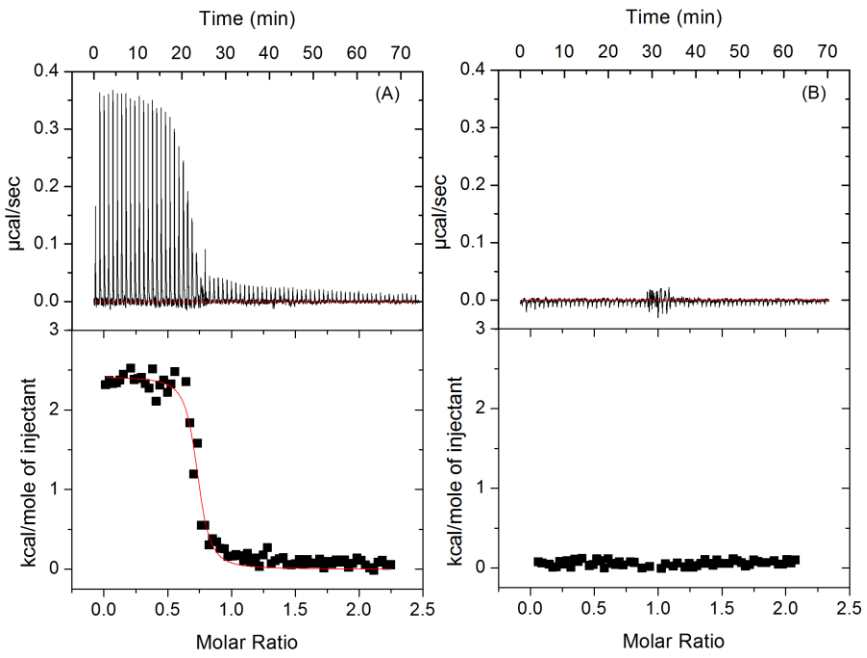

Figure 3-2. ITC binding isotherm for (A) titration of (1 mM) GL13K into (0.1 mM) DOPG contained in the reaction chamber, (B) titration of (1 mM) DOPC into (0.1 mM) GL13K peptides in the reaction chamber.

3.2.2 Secondary structure of GL13K

AMPs can adopt a stable secondary structure upon interaction with a membrane thereby allowing peptides to better accommodate in the hydrophobic environment of membranes. This property of AMPs has been reported to be associated with their antimicrobial activity [150] and often involves formation of an amphipathic structure enabling partitioning to the hydrophobic bilayer core. Furthermore, AMPs can adopt different conformations depending on the membrane environment to which they are exposed [102].

The secondary structure of GL13K in buffer and in the presence of DOPC and DOPG liposomes was investigated using CD (shown in Figure 3-3); secondary structure analysis was performed using SELCON3 [107-109]. GL13K is predominantly unstructured (90%) in phosphate buffer and does not transform its secondary structure upon incubation with DOPC liposomes. However, in the presence of DOPG liposomes, a strong minimum at 217 nm suggests that GL13K adopts a

stable β-sheet structure. Analysis of the spectra indicated that approximately 60% of the peptide transformed from unstructured to β-sheet, while the remaining 40% of the peptide are unchanged. This suggests that electrostatic interactions lead to strong binding with negatively charged membranes which is then followed by the secondary structure changes.

It is known that for some peptides a specific threshold P/L ratio needs to be reached in order to adopt a stable secondary structure upon interaction with membranes [14, 151]. Moreover, a peptide can adopt different conformations in the bulk, surface bound, aggregated and membrane inserted states [103]. The CD spectrum represents the equilibrium between all these states upon interaction with membranes [103]. To better understand this mechanism or possibility for GL13K to adopt different conformations, a fixed concentration of GL13K is incubated with varying concentrations of liposomes of DOPC and DOPG ranging from a P/L ratio of 1/15 to 1/2.5. No significant changes in the CD spectra are observed with incremental increases in lipid concentration for both the DOPC and DOPG membranes as seen in Figure 3-4 (A) and (B). This shows that conformational (secondary structure) changes of GL13K upon interaction with membranes are not concentration dependent (within the given range tested) and that the peptide adopts the same structure in all bound states.

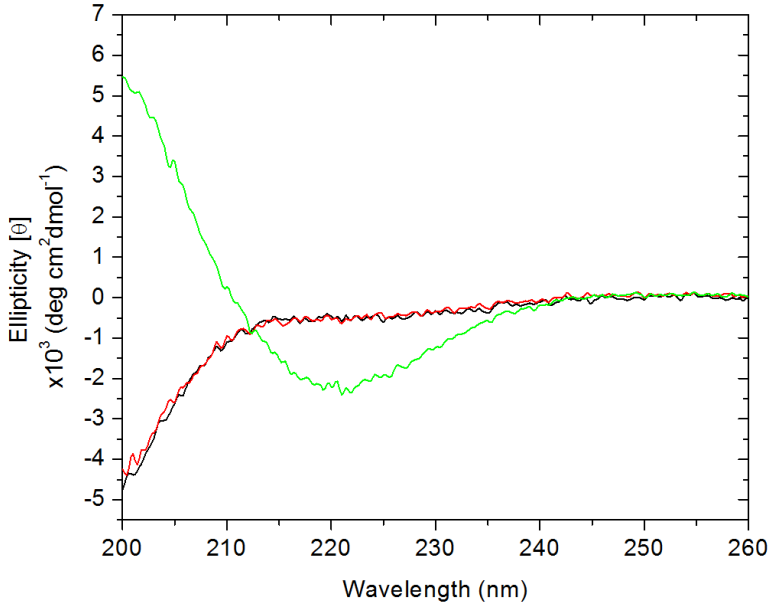

Figure 3-3 CD spectra of GL13K in buffer (black), DOPC (red) and DOPG (green) liposomes at P/L ratio 1/2.5.

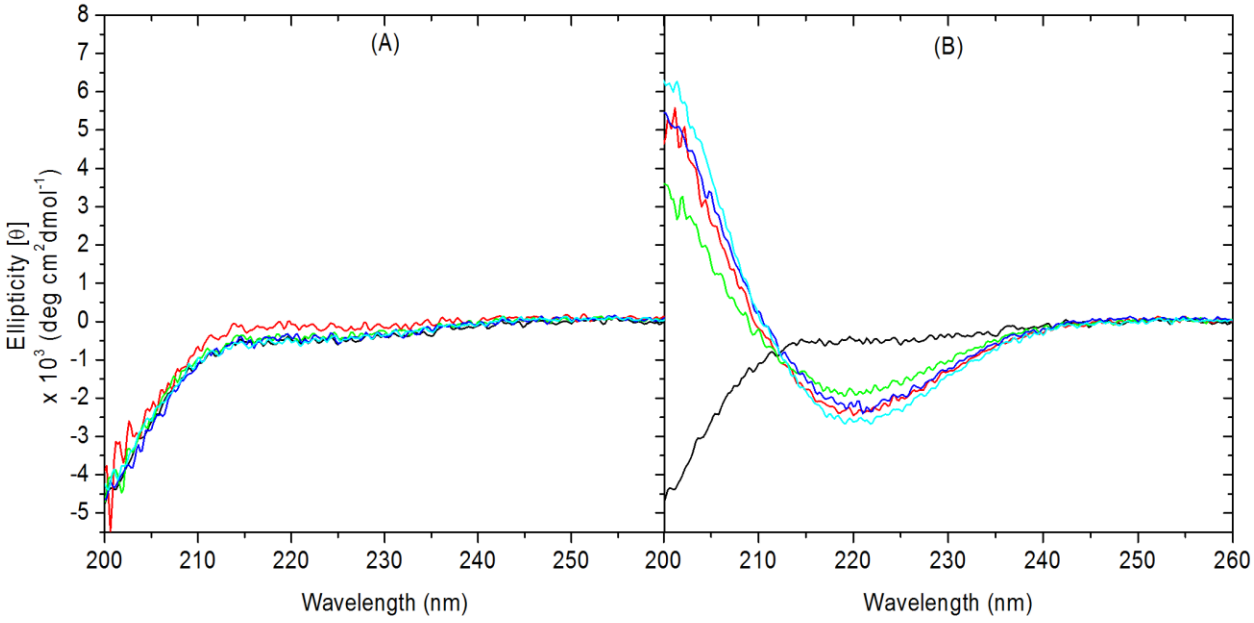

Figure 3-4 CD spectra of GL13K upon incubation with (A) DOPC and (B) DOPG liposomes with varying P/L ratios.

Black (zero), red (1/15), green (1/10), blue (1/10) and cyan (1/2.5).

3.2.3 Membrane integrity

In the bound state AMPs can perturb the membrane barrier leading to disruption of the membrane potential and efflux of cellular contents, eventually leading to cell death. AMPs are thought to act by any of the three major mechanisms as outlined in the introduction. GL13K membrane disruption was studied using a CF leakage kinetics assay. Stable and non-leaky liposomes were formed and yielded no increase in fluorescence intensity (Figure 3-5 (A)) before addition of Triton X 100 which served as a control for 100% lysis.

The addition of peptide to the DOPG liposomes with increasing P/L ratios causes a biphasic release of CF with strong instantaneous release followed by a slow release phase which plateaus within 10-20 minutes depending on the P/L ratio. A similar behaviour has been observed for various other AMPs or other cell penetrating peptides [[152] and references therein]. This concentration dependent gradient release has been attributed to either the formation of transient channels which are stabilized over time [153, 154] or a carpet mechanism of membrane disruption [102, 112]. The extent of release increases with increasing P/L ratios, finally leading to 90-95% release of CF at P/L ratios of 1/2.5 (Figure 3-5 (B)). GL13K does not yield any significant increase in CF release in the case of DOPC liposomes and the percentage CF release is constant with increasing P/L ratios indicating that GL13K does not result in significant lysis of DOPC membranes. The salt concentrations used in these experiments were close to physiological salt concentrations further emphasizing that GL13K seems to have highly selective bacterial membrane lytic activity even in high ionic strength (see section 3.2.1). This appears to be due to strong electrostatic binding and better accommodation in a hydrophobic membrane environment *via* β-sheet formation.

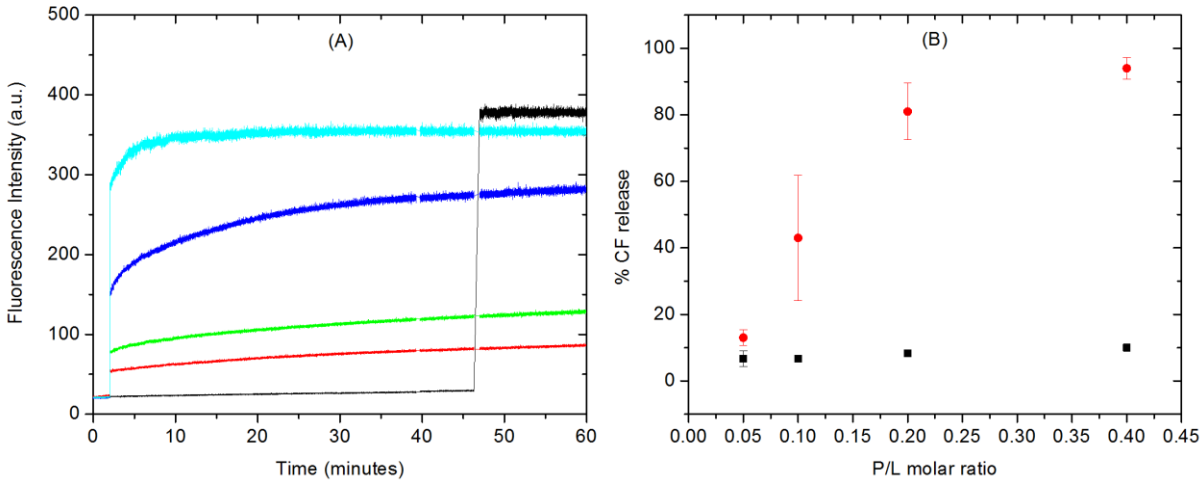

Figure 3-5 CF release profile and percentage release.

(A) Sample set of CF release profiles over 60 minutes upon incubation of CF encapsulating DOPG liposomes with increasing amount of GL13K injected at two minutes. P/L ratios are: 1/20 (red), 1/10 (green), 1/5 (blue) and 1/2.5 (cyan). The black trace shows the absence of peptide followed by 100% leakage and release with addition of Triton X - 100 at 47 minutes.

(B) Averaged percentage of CF released upon incubation of GL13K with DOPG (solid red circles) and DOPC (solid black rectangles). Each data point is an average of three different experiments at same P/L ratio with percentage release calculated at time 60 minutes.

3.2.4 DLS

Instant release of CF from DOPG liposomes which reaches saturation in the first few minutes suggests that GL13K causes membrane lysis either by formation of transient pores or a carpet mechanism [154]. A carpet mechanism of membrane disruption which causes micellization of the membrane should significantly decrease the size of the liposomes as compared to transient pores where only a part of the membrane is destroyed either by sinking raft or translocation of lipo-peptide micelles formed by transient channels. To better understand and distinguish between these two mechanisms, changes in hydrodynamic diameter of DOPG and DOPC liposomes were measured in the absence or presence of GL13K using DLS. Additionally, DLS can be used to monitor aggregation or fusion of membranes (corresponding to an increase in hydrodynamic

diameter), which have been cited as a mechanism by which some AMPs exert their antimicrobial activity [12, 100, 155].

The size of the liposomes in the absence of GL13K peptides varied from about 90 nm to 120 nm in diameter between various batches of extruded liposomes with low polydispersity indices (ranging from 0.07 to 0.12). Incubation of GL13K with DOPC liposomes does not have an effect on the size of the liposomes (as shown in Figure 3-6) or the polydispersity index. GL13K causes a decrease in size for DOPG liposomes with increasing P/L ratios with as high as 50 % of lipids being removed from liposomes at P/L 1/2.5 (Figure 3-7). The liposomal diameter of 60-80 nm at the highest P/L ratio as shown in Figure 3-6 (which resulted in almost 90% CF release) suggests that GL13K is not causing the complete micellization of liposomes and thus does not seem to act *via* a carpet mechanism. A partial or local micellization can be envisioned in which the peptide accumulates and locally removes lipid with a resealing of a then smaller liposome. This would also explain the observed increase in reported error and concurrent increase in polydispersity index (as high as 0.24) as the amount of lipid removal would be a function of the peptide aggregation. Membrane fusion and aggregation can be ruled out as an increase in liposome size is not observed.

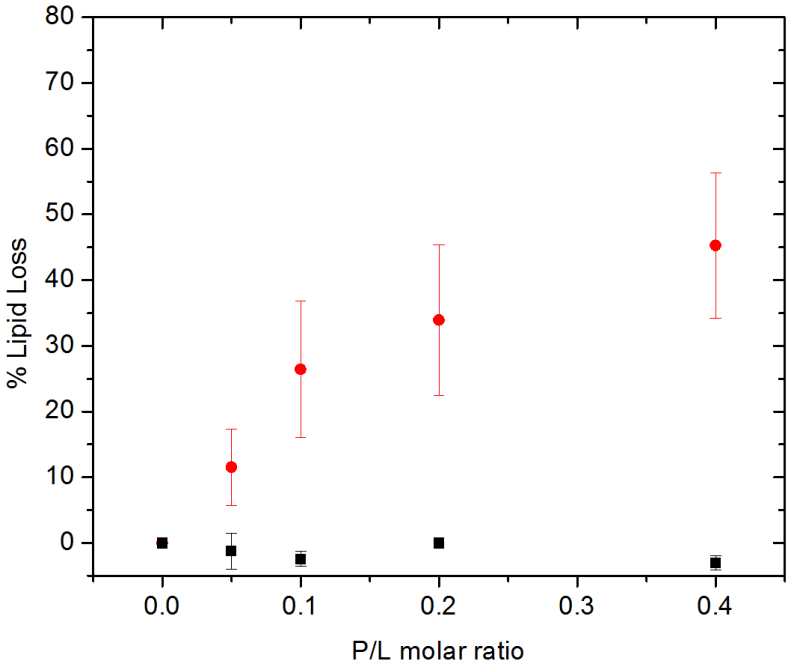

Figure 3-6 Hydrodynamic radius of DOPG (red circles) and DOPC (black rectangles) liposomes with increasing P/L ratio.

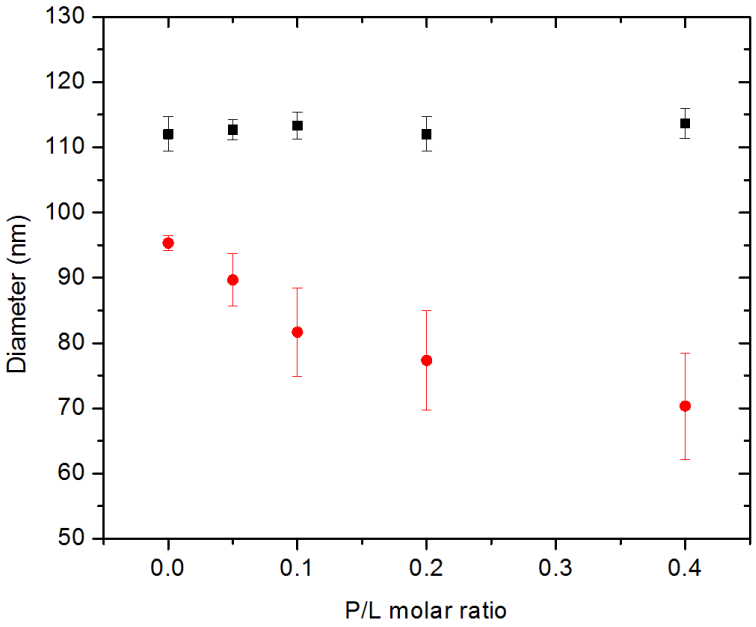

Figure 3-7 Percentage loss of lipid molecules.

Percentage loss of lipid molecules from DOPG (red circles) and DOPC (black rectangles) liposomes initially used upon interaction with increasing P/L ratio. An approximate lipid loss is calculated assuming a fixed area/lipid molecule neglecting any packing differences between the inner and outer leaflets of a liposomal bilayer.

3.2.5 Lipid bilayer ordering

GL13K binding and its effect on SLBs was studied using DPI. First, a stable and uniform bilayer was deposited on the chip surface before injection of GL13K, confirmed by almost stable TM values for at least 30 minutes reaching 10 to 17 radians (see Figure 3-8). The R.I. value was fixed at 1.47 to calculate the thickness, mass, birefringence and density for DOPC and DOPG bilayers as summarized in Table 3-2. Stable and uniform bilayers were treated with an increasing amount of GL13K. The thickness of DOPC bilayers was calculated to be 4.7 ± 0.3 nm which is in good agreement with the reported thickness of 4.5 nm measured by neutron scattering [156]. The thickness calculated for DOPG bilayers was 3.5 ± 0.4 nm which is less than expected (close to DOPC) for a DOPG bilayer. The densities determined for both lipid bilayers are comparable (1.01 ± 0.01 g/cm^3 for DOPG bilayers and 1.01 ± 0.00 g/cm^3 DOPC) suggesting that the decrease in calculated DOPG bilayer thickness might be due to incomplete coverage of the chip surface, as density is calculated as the ratio between mass deposited per unit area and thickness. The thickness measured by DPI is the average thickness of the adsorbed layers over the entire length of the chip calculated from relative phase shifts in TM and TE polarizations, hence partial coverage will lead to lower average thicknesses even if the actual bilayer thickness is the same (Figure 3-9). If void spaces are present, the binding of GL13K to the chip surface adds an extra binding parameter thus complicating data analysis. GL13K binding affinity for the chip was evaluated by injecting GL13K at the same rate as it was injected over bilayers and the peptide was not found to bind even at 16 μM (data not shown). The birefringence which is directly related to the ordering of lipid molecules was calculated to be 0.0149 ± 0.0005 and 0.0124 ± 0.0025 for DOPC and DOPG bilayers respectively, in good agreement with previously reported values [131, 156]. Real time changes in TM and birefringence values after sequential injections of

GL13K on DOPC and DOPG bilayers are shown in Figure 3-8. The birefringence is normalized to the birefringence of complete lipid bilayer coverage to highlight step changes with added peptide.

No significant changes in TM and birefringence for DOPG bilayers are observed for GL13K injections of 6 μM and less. Small changes at 8 μM peptide suggest an initial binding of GL13K. At 10 μM and 12 μM, the mass increases whereas the birefringence decreases significantly. At the higher peptide concentrations, it is evident from Figure 3-8 that upon completion of each injection, changes in TM, mass and birefringence are irreversible, the result of a strong interaction and binding, which leads to a permanent disordering of DOPG bilayers by GL13K [129, 130]. Large changes at 10 μM and 12 μM are then followed by gradual changes suggesting a saturation of the surface [127, 128]. A decrease in adsorbed mass is often correlated to lipid loss from the surface [129, 130]. In this case, a mass increase is observed (Figure 3-10 (A)), however it should be noted that the molecular mass of GL13K is 1423.9 g mol^{-1} almost twice that of DOPG therefore the mass increase at higher GL13K concentration might be due to a combination of both adsorbed peptide and loss of lipid molecules caused by an excess of adsorbed GL13K.

The injection profiles (Figure 3-8) for peptide addition to DOPC bilayers show a weak interaction evidenced from the small net change in TM values (and hence mass and birefringence) occurring for injections at 6 and 8 μM. In addition, for these injections the TM values initially increase upon injection (indicative of binding) and then decrease towards the pre-injection value as the peptide is washed off by the incoming buffer. A small increase in mass with a corresponding small decrease in birefringence (Figure 3-10 (B)) has been suggested previously to be due to surface binding of the peptide [129, 130].

Although the overall trend for both DOPC and DOPG looks similar as shown in Figure 3-10, it should be noted that the relative mass changes for DOPC (≈ 0.1 ng/mm^2) compared to DOPG (≈ 1.08 ng/mm^2) are very small. The normalized birefringence plots in Figure 3-8 also show a significantly lower birefringence change for DOPC bilayers compared to DOPG indicative of permanent and irreversible changes in the membrane ordering of DOPG bilayers and a minimal effect on bilayer ordering for a surface bound state of GL13K with DOPC bilayers [129, 130].

Table 3-2 Properties of DOPC and DOPG bilayers. Values are averaged over at least six different experiments.

Bilayer	Thickness (nm)	Mass (ng mm^{-2})	Birefringence	Density (g cm^{-3})
DOPC	4.67 ± 0.26	4.70 ± 0.23	0.0149 ± 0.0005	1.01 ± 0.00
DOPG	3.47 ± 0.39	3.30 ± 0.54	0.0124 ± 0.0025	1.00 ± 0.01

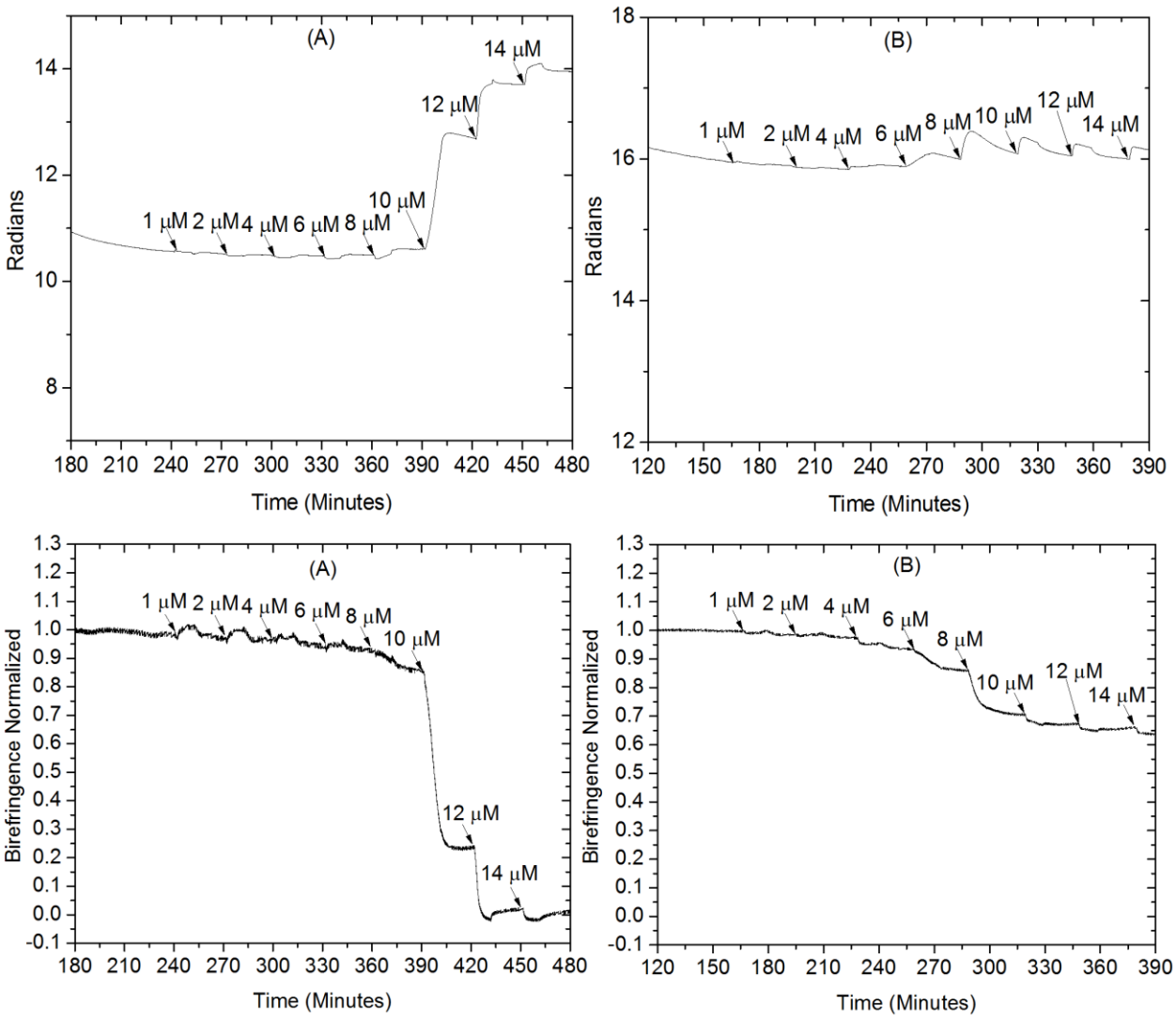

Figure 3-8 Real time changes observed in TM polarization (top) and normalized birefringence changes (bottom) for DOPG (A) and DOPC (B) upon interaction with increasing concentration of GL13K as marked by arrow heads.

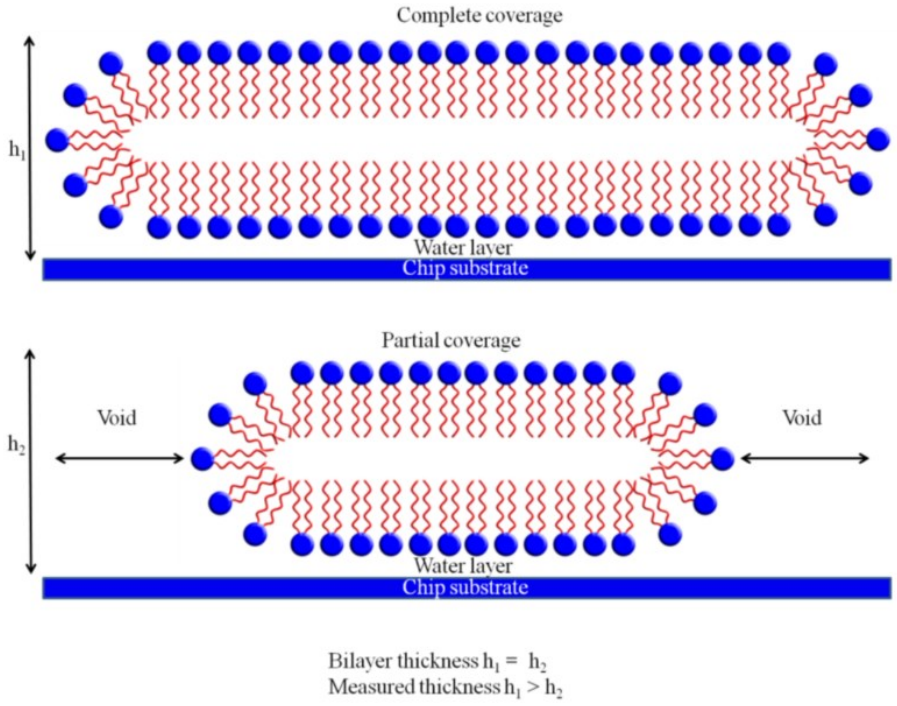

Figure 3-9 Schematic representation of partial and complete coverage of a chip surface by a phospholipid bilayer.

h_1 and h_2 are thicknesses for partial and complete coverage of the chip surface by lipid bilayers of the same composition.

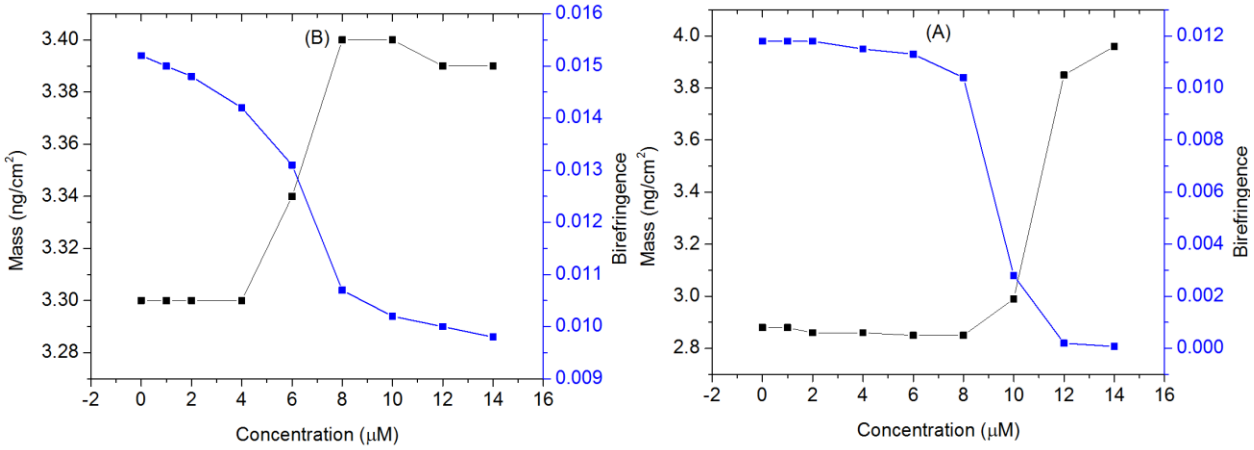

Figure 3-10 Changes in mass and birefringence for (A) DOPG and (B) DOPC SLBs with increasing concentration of GL13K.

3.2.6 Visualization of membrane perturbation by GL13K

Atomic force microscopy provides detailed information about the topography of membranes or other surfaces, and can distinguish height features down to 1 nm [135]. Smooth, uniform bilayers of approximately 4 nm height comprising either DOPG or DOPC (as seen in Figure 3-11 (A)) are deposited by liposomal rupture on freshly cleaved mica. When very low concentrations of GL13K (0.5 μM) are added to DOPG, no changes in membrane topography or adsorption of peptide on the surface are observed (data not shown). Increasing the GL13K concentration to 1 μM as shown in Figure 3-11 (B) disrupted membrane lipid structure and ordering, causing 1 nm to 2 nm deep troughs on the membrane surface. However, a more detailed scan (0.5 μm × 0.5 μm) of the DOPG bilayer incubated with 1 μM GL13K clearly shows membrane thinned regions where a portion of the lipid molecules has been removed (Figure 3-11 (C)). These membrane thinned regions appear since the SLBs have not resealed upon material/lipid loss possibly due to steric constraints arising from substrate coupling [157]. A further increase in the concentration of GL13K to 2 μM leads to an increased number of membrane perturbations and loss of lipids (data not shown). This loss of lipids correlates with the high disordering of DOPG observed using DPI (refer to section 3.2.5)

In case of DOPC bilayers, membrane thinning is not observed but strands (approximately 1 nm high) are observed on the surface as shown in Figure 3-11 (D). Even with higher concentrations (up to 4 μM peptide), only the density of strands increased without membrane thinning (data not shown). This is in agreement with the small changes in birefringence observed in the DPI experiments (refer to section 3.2.5) and can be attributed to surface bound GL13K peptide strands/aggregates. An important question that arises is why there is no or minimal evidence of binding between GL13K and DOPC liposomes, yet AFM and DPI indicate an interaction

between GL13K and DOPC SLBs. There are a number of possible causes. Firstly, this might be an effect of different membrane potentials for liposomes and SLBs. For SLB's these can arise from different dielectric values between the inside (facing the substrate) and outside of the membrane resulting from the organization of entrapped water molecules, as the water layer between the solid support and bilayer is only a few water molecules thick [60, 95, 158]. Additionally, this might be due to non-specific binding of GL13K to small membrane defects present in DOPC bilayers [159] and/or differences in curvature of membrane between liposomes and SLBs [142]. Liposomal membrane interaction studies have been compared often to SLBs due to their similar lateral diffusion rate constants and fluidity [160]. Over the last decade, increasing the spacing and water molecule retention between SLBs and substrates by using hydrophilic polysaccharide and polymeric cushions such as dextran, poly (L-lactide acid), polyethylene glycol and polydopamine have gained significant interest as potential biomimetic models [95, 158, 161, 162]. Resolving the effects of membrane potential, curvature, fluidity and defects on peptide and protein interactions with model membranes is an area which must be addressed in the future.

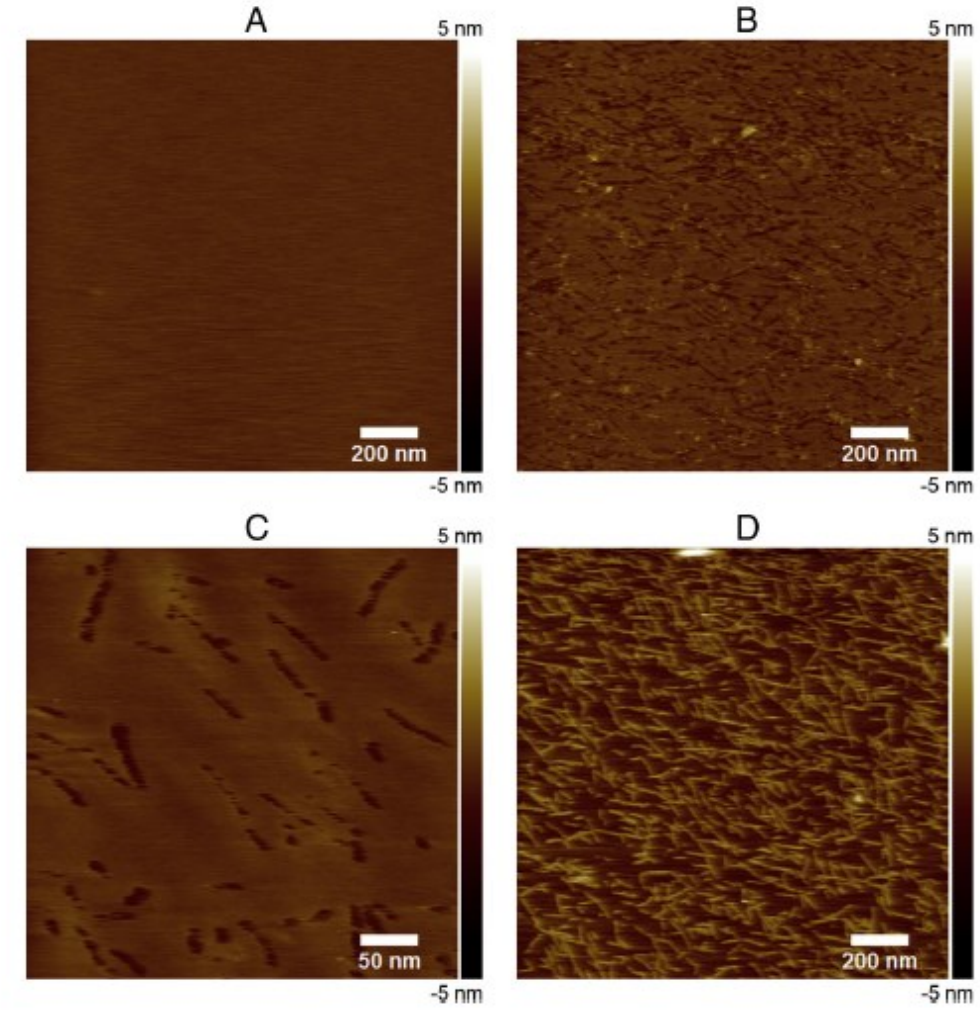

Figure 3-11 Sample AFM images of DOPC and DOPG bilayers under different environments.

(A) DOPG and DOPC SLBs in the presence of buffer, (B) DOPG SLB incubated with 1 μM GL13K, 1 nm – 2 nm deep darker regions were observed, (C) smaller scan of a DOPG SLB incubated with 1 μM GL13K to better visualize and understand the changes in DOPG bilayer, and (D) DOPC SLB incubated with 2 μM GL13K.

3.3 CONCLUSION

Selective toxicity for bacterial cells and fast killing action with a broad antimicrobial spectrum and limited or no resistance are key properties for antimicrobial peptides. Here, we studied for the first time the membrane interaction/disruption mechanism for the antimicrobial peptide GL13K derived from hPSP. The relatively small size and bactericidal effects of GL13K on planktonic and biofilm [87] bacteria makes it an attractive antibiotic candidate. Liposomes and SLBs of DOPC and DOPG lipids were used as model for eukaryotic and bacterial membranes, respectively, to study the role of electrostatic and hydrophobic interactions on activity and specificity of GL13K. Calorimetric and CF leakage studies show that GL13K has a very strong binding affinity and lytic activity against DOPG liposomes even at high salt concentrations without any significant binding to DOPC liposomes even in low salt conditions. The strong membrane lytic activity of GL13K at high salt conditions makes it an interesting candidate for treating diseases such as cystic fibrosis which generates a high local salt concentration [163]. This high salt concentration has been shown to render some host and synthetic AMPs such as β-defensins ineffective [69]. Furthermore, the concentrations required to disrupt the model membranes was of the same order of magnitude (μM) as the MIC values reported for the MIC *E. coli (*4 μM or 5 μg/mL) and *P. aeruginosa (*6 μM or 8 μg/mL) [87].

The activity and selectivity of GL13K is due to a fine balance of its cationic and amphipathic nature. Electrostatic interactions are involved in its strong initial binding to the membrane and the β-sheets formation by GL13K upon interaction with negatively charged DOPG membranes allows it to better accommodate in the hydrophobic environment of the membrane. The concentration dependent and instant release of CF from DOPG liposomes suggests lysis by either a carpet mechanism or by the formation of transient channels or both. For GL13K-DOPG

interactions, the release of liposomal contents appears to be due to a localized removal of lipid from the membrane *via* peptide induced micellization; excessive lateral stress on the bilayer as the peptide adsorbs or inserts causes a localized destabilization of the membrane. To reduce excessive lateral stress and decrease the free energy of the system, a part of the lipids are released along with peptide as small micelles leading to the loss of cellular contents by formation of transient channels which causes bacterial cell death as depicted in Figure 3-12.

In vitro cell studies have shown that GL13K is active against both Gram-negative and Gram-positive bacteria with the capability to kill even biofilm forming bacteria. Here, we showed that electrostatics play a major role in governing GL13K selectivity for bacterial membranes. GL13K disrupts membrane barrier function through a partial micellization and transient pore mechanism.

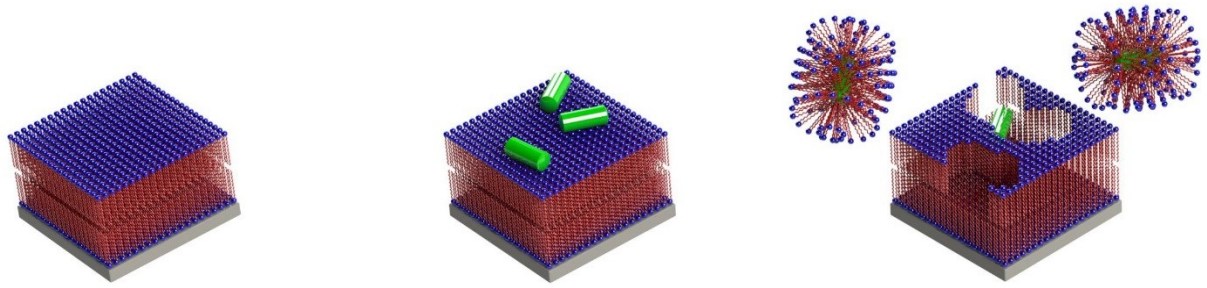

Figure 3-12 Schematic of the GL13K membrane disruption mechanism, (left) planar supported bilayer, (center) GL13K interacts with lipid head groups and (right) after reaching a threshold concentration, GL13K causes membrane destabilization by removing parts of it forming peptide lipid micelles or stable supra molecular structures.

4 MANUSCRIPT 2 ROLE OF CHOLESTEROL INDUCED LIPID PACKING ON THE SELECTIVITY AND ACTIVITY OF GL13K ANTIMICROBIAL PEPTIDE

Information provided in this chapter is extracted from a manuscript under preparation and expected to be submitted to *Biochimica et Biophysica Acta – Biomembranes* with following authors: **Balhara, V**.; Marques, M.A; Schmidt, R.; Gorr, S.-U.; DeWolf, C. The materials and methods section has already been discussed in chapter 2 thus will not be repeated in here.

Author contributions:

I carried out all experimental work, data analysis and wrote the manuscript. C. DeWolf helped building the research plan, analyzing the data and contributed to writing the paper. M.A. Marques performed DLS and CF release control experiments. R. Schmidt contributed to writing the manuscript. S.-U. Gorr supplied peptide GL13K and is a collaborator on the project.

4.1 INTRODUCTION

Bacterial resistance and the development of so-called super bugs is a major concern for health professionals and the scientific community. The infectious disease society of America has recently identified six high priority pathogens namely *Enterococcus faecium, Staphylococcus aureus, Klebsiella pneumonia, Acinetobacter baumannii, Pseudomonas aeruginosa,* and *Enterobacter species* known as "ESKAPE" pathogens [6, 7]. In Europe, some *Klebsiella* isolates have been identified that show resistance against even the last line of antibiotics known as carbapenems [1]. Antimicrobial peptides (AMPs) (specifically membrane active peptides), which

are part of the innate immune system, are potential candidates for design of future antibiotics. However, the exact mechanism of bacterial killing by these peptides is not yet fully understood and is highly debated. The common consensus is that these peptides distinguish between host and pathogens mainly based on the differences in membrane composition. AMPs are generally cationic and amphipathic in nature and their selectivity is due to a balance between membrane charge and packing/fluidity [15]. The fast action and activity *via* non-specific mechanisms do not allow microbes to develop resistance easily against these antimicrobials. However, recently it has been observed that some bacterial strains can actually alter their membrane charge by lipid redistribution to resist against cationic antimicrobial peptides [4, 78, 79].

Human parotid secretory protein (hPSP) is a human salivary protein expressed in acinar and ductal cells of the parotid gland, submandibular gland and in gingival epithelial cells [37, 84, 85]. Several hPSP peptides, each 13 amino acids long, have been identified from hPSP based on its structural and functional similarity with BPI protein and lipopolysaccharide (LPS)-binding protein [84, 85]. GL13K was produced by amide modification of the carboxyl terminus and substitution of three lysine residues in the native peptide sequence [87] and carries a +5 charge (at pH 7). This modified peptide has strong anti-inflammatory and antibacterial activity against Gram-negative, Gram-positive and biofilm forming bacteria and has low hemolytic and cytotoxic effects [87]. GL13K inhibits LPS and monophosphoryl lipid A stimulated TNFα secretion from macrophages by binding to lipid A of LPS [84, 87]. The small size (equating to a lower production cost), broad spectrum of activity, fast action even in presence of high salt concentrations [88], low micromolar MIC values [87] and anti-LPS activity makes GL13K an interesting candidate as an antimicrobial agent.

Previously, we have shown that GL13K adopts primarily a β-sheet structure in the presence of anionic membranes [88]. The specificity of GL13K was found to be mainly due to electrostatic interactions between the cationic peptide and the anionic membranes [88]. However, membrane permeabilization is a net result of electrostatic forces attracting the peptide to the surface and hydrophobic forces promoting accommodation in the membrane core. GL13K causes membrane permeabilization by localized micellization of the membrane resulting in the formation of transient pores [88].

Bacterial and eukaryotic membranes are, however, complex mixtures which differ not only in their surface charges. Cholesterol is present in large abundance in eukaryotic membranes with varying composition from 20-50 mol % [97, 164]. In a phospholipid bilayer, cholesterol orients itself at the interface of the head group and chain region with the hydroxyl group interacting with phospholipid head groups [98]. The presence of cholesterol leads to increased ordering and thickening of the phospholipid hydrocarbon region [92]. Cholesterol also causes increased membrane stiffening due to increased cohesive forces and a decreased bending modulus making bilayers less deformable and less permeable, however, the lateral mobility of the membrane remains unaffected [142]. More recently, it has been shown that cholesterol not only causes stiffening but also causes dewetting of lipid head groups altering the membrane dipole potential [165]. An altered membrane potential and increased packing caused by cholesterol has been shown to affect membrane insertion and folding for various cationic and amphipathic AMPs [166, 167]. Their activity is also attenuated by the presence of cholesterol [142 15 167] with a greater effect on peptides exhibiting a carpet mechanism *via* prevention of the bending of membranes [50 100]. On the other hand, it has also been reported that when cholesterol is present in very low concentrations (≤ 6 mol %) it can cause increased permeabilization due to enhanced membrane

defects [92]. Parker *et. al.*[97] observed that the cholesterol miscibility limit with DOPC is ≈ 67 mol % cholesterol [97] and recently it was observed that PC and PG lipids of similar chain lengths exhibits similar cholesterol miscibility [168]. In the present study, we introduced cholesterol into both DOPG and DOPC membranes at 40% molar ratio (much below their cholesterol miscibility limits and within the physiologically relevant concentrations range [168]) in order to determine the impact on the activity and mechanism of GL13K peptides. Most of biophysical experiments are done in this range (0.3 to 0.5 mol fraction) [54, 137, 169-173] to study the effect of presence of cholesterol as it is below miscibility limits and towards the upper limit of biological membrane cholesterol composition. Unsaturated DOPC and DOPG were chosen over other saturated lipids to ensure that the lipid ordering caused by cholesterol, does not effect the Transition temperature (T_m) in the temperature studied in these experiments (22 °C). DOPC and DOPG lipids T_m values are approximately -20 °C and packing caused by presence of cholesterol will result in T_m values which should still be much below the temperature used in these experiments.

4.2 RESULTS

4.2.1 Membrane binding affinity

ITC was used to determine the thermodynamic parameters for GL13K interacting with DOPG/Cholesterol (Ch) and DOPC/Ch liposomes with 40 mol % cholesterol since strong and selective binding of AMPs with microbial membranes is very important for their use as potential therapeutics. Measured enthalpy, entropy and free energy changes obtained from injection of liposomes into peptides or *vice versa* are the net result of a combination of processes such as disruption of peptide aggregates in solution, interaction with the membrane surface, lipid dehydration, aggregation of peptides on the membrane, secondary structure changes, reorientation of the peptides in the hydrophobic core of the membrane, lipid redistribution and/or acyl chain reordering due to membrane disordering or channels formation [102-104].

Sequential injections of DOPG/Ch liposomes into excess of GL13K contained in the reaction cell show a strong endothermic binding (Figure 4-1 (A)). The heat signals decrease gradually with sequential injections as the amount of free or unbound GL13K decreases with each injection; saturation is only reached after the 40^{th} injection and at lipid/peptide ratios above 2. Fitting the data yielded an overall endothermic enthalpy change of ≈ 1.7 kcal/mol with large entropic change values of ≈ 0.064 kcal/mol/K. Binding constants in the range of 10^6 indicate reasonably strong binding. In contrast, neutral DOPC/Ch liposomes (which lack electrostatic attraction) do not show any significant interaction with GL13K as observed by the negligible enthalpy changes for various injections (Figure 4-1 (B)). The strong endothermic change for one injection is an artifact and may be due to a residual air bubble in the reaction cell from the cell loading process. Previously, we reported enthalpy, entropy and binding affinity in a similar

range, but with somewhat higher values (ΔH=2.0 kcal/mol and ΔS = 0.073 kcal/mol/K), for GL13K interactions with DOPG liposomes in the absence of cholesterol [88]. Thus, the presence of the cholesterol has only a small effect on the net binding affinity of GL13K to negatively charged DOPG vesicles, despite the differences in membrane packing and charge density. It may be that the thermodynamic parameters are dominated by the strong electrostatic interactions with the membrane surface, regardless of the degree of penetration or extent of membrane permeabilization. However, in the absence of cholesterol, equilibrium is reached at the lower P/L ratio of 1.0 [88] compared to over 2.0 in the presence of cholesterol, indicating that the overall amount of peptide bound to membrane is reduced by the presence of cholesterol and consequently much higher amounts of peptide are required to achieve the same effect. One possibility is that increased packing caused by cholesterol attenuate the reorientation of the peptide in the membrane core and thus overall less peptide is bound as it can only bind to the surface.

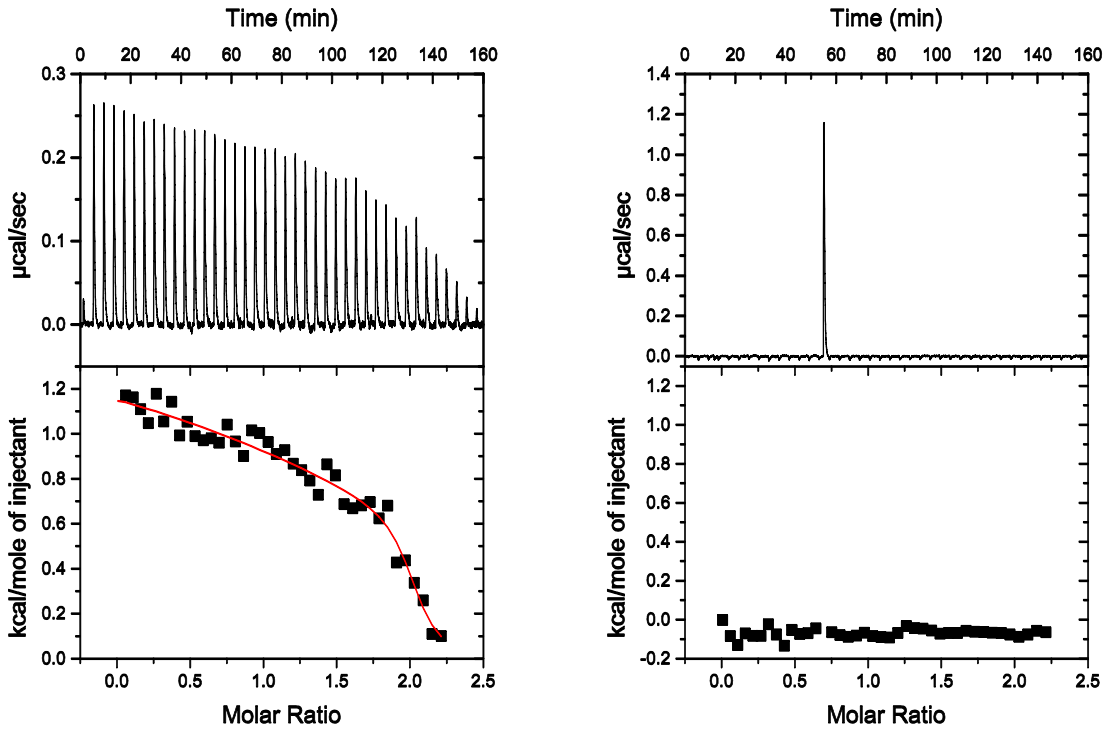

Figure 4-1 ITC binding isotherms for the titration of (1 mM) DOPG/Ch (left) and DOPC/Ch (right) liposomes into (0.1 mM) GL13K peptide. Molar ratios reported in (A) and (B) are P/L ratio.

4.2.2 Secondary structure transformation

Changes in secondary structure for a peptide upon interaction with membrane are known to be an important part of antimicrobial peptide activity [150] usually by facilitating partitioning into the membrane hydrophobic core upon adoption of an amphipathic structure. Our previous studies have shown that the DOPG membrane environment induces a secondary structure change in GL13K from unstructured to predominantly β-sheets [88]. Cholesterol may inhibit the partitioning by preventing insertion of the peptide into the membrane and may therefore prevent the associated secondary structure change. The conformational changes in GL13K upon interaction with cholesterol-rich DOPG and DOPC liposomes were followed using CD spectroscopy. AMPs can adopt different structures in the buffer, at the membrane surface and at deeper inserted states, thus the spectra recorded with CD spectroscopy are a representative of all possible secondary structures [102, 103, 174, 175].

CD spectra for GL13K in presence of buffer and different membrane environments are shown in Figure 4-2. GL13K is mainly unstructured (≈ 90%) in buffer and in the presence of DOPC/Ch liposomes, whereas the presence of the negatively charged DOPG/Ch membranes causes ordering and a transformation of peptide to mainly β-sheets (≈ 53%) and remaining being unstructured (≈ 35%) and α-helix (≈ 12%). With DOPG liposomes (*i.e.,* without cholesterol), approximately ≈ 60% of the GL13K peptide transformed to a β-sheet conformation, slightly more than in the presence of cholesterol. The lower extent of secondary structure transformation in the presence of cholesterol is attributed to less membrane bound peptide which correlates well with the higher P/L ratios required for saturation found by ITC.

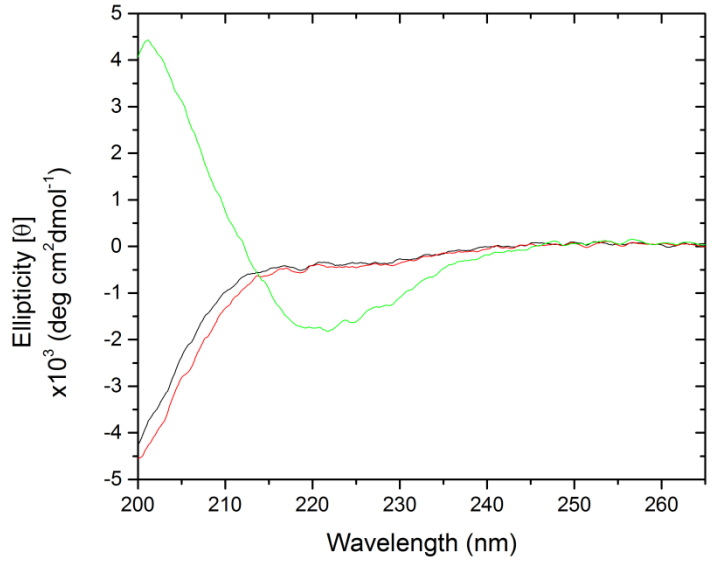

Figure 4-2 CD spectra of GL13K in buffer (black), DOPC/Ch (red) and DOPG/Ch (green) at P/L (1/2.5).

4.2.3 Membrane disruption or lysis

Disruption of membrane barrier functions, leading to the loss of vital cellular metabolites of microbes, is the most common mechanism for the antimicrobial activity of AMPs. In the bound state GL13K is known to disrupt negatively charged membranes by causing the localized micellization and forming transient channel formation [88]. Cholesterol can act as a barrier to membrane disruption by increasing the packing density of the membranes, limiting the depth of membrane penetration of the peptide. The effect of cholesterol on membrane disruption by GL13K was followed by CF release from liposomes in the presence of increasing amounts of GL13K. Stable and non-leaky liposomes were formed as no significant increase in fluorescence signal is observed over time in the absence of peptide (Figure 4-3 (A)). Triton X, which causes complete micellization of liposomes, served as a control for 100 % lysis.

Figure 4-3 (A) shows the changes in CF fluorescence intensity before and after addition of GL13K to DOPG/Ch liposomes. Minimal or no release below P/L ratios of 1/20 suggests that a

minimum threshold of membrane bound peptide is needed to cause liposome lysis. The maximum release at P/L ratio of 1/2.5 was 95% for DOPG liposomes which is reduced to 70% release in the presence of cholesterol. At lower peptide concentrations, the reduction in CF release is even greater. As the DOPG liposomes have already reached 90% lysis at a P/L ratio of 1/2.5, this is the highest ratio used for comparison of the absence and presence of cholesterol. However, the linearity in the plot of percentage release versus concentration and the lack of a plateau (see Figure 4-3 (B)) indicate that saturation has not been reached and a further increase in the P/L ratio may yield an even higher percentage release. An instantaneous release of CF followed by a slow release is observed at higher P/L ratios similar to that seen in the absence of cholesterol [88]. The attenuation of CF release in the presence of cholesterol suggests that cholesterol induced membrane packing might help to stabilize the membrane against peptide induced defects and thus reduced overall leakage. However, the similarity in release profile to DOPG liposomes indicates that the overall membrane disruption mechanism and associated kinetics remain unaltered when sufficiently high P/L ratios are used. For zwitterionic membranes of DOPC/Ch where minimal interaction and no secondary structure transformation is observed, GL13K is not able to cause any liposomal rupture. The salt conditions (107 mM NaCl) used in the CF leakage assays are high enough (close to physiological conditions) to cause diminished electrostatic interactions. This suggests that membrane lytic activity of GL13K results from a fine balance of its cationic charge and amphipathicity.

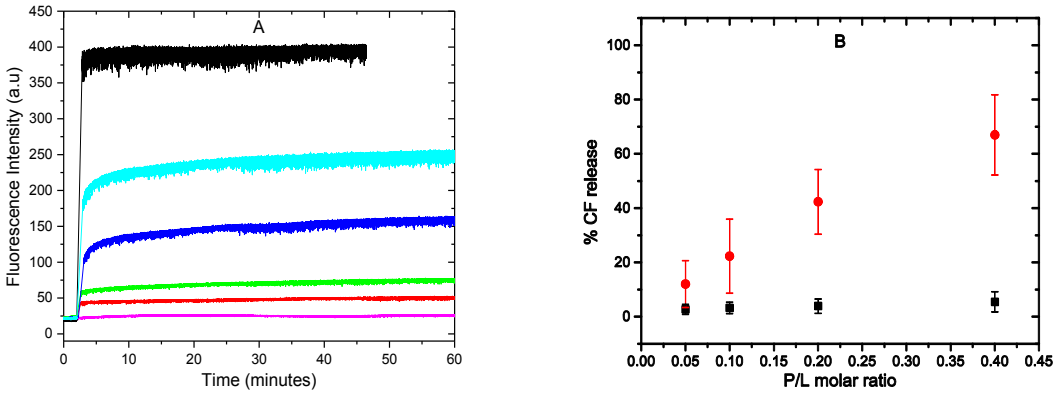

Figure 4-3 CF release profiles and percentage release in presence of cholesterol.

(A) Sample set of CF release profiles over 60 minutes upon the incubation of CF encapsulating DOPG/ Ch liposomes with increasing amount of GL13K added at time t=2 minutes to obtain varying P/L ratios such as 1/20 (red), 1/10 (green), 1/5 (blue) and 1/2.5 (cyan). In absence of peptide there is no CF release as shown by the magenta trace, while the addition of Triton X - 100 (black trace) causes 100 % leakage and release.

(B) Averaged percentage of CF released upon incubation of GL13K with DOPG/Ch (solid red circles) and DOPC/Ch (solid black rectangles). Each data point is an average of three different experiments at same P/L ratio with percentage release calculated at time 60 minutes.

4.2.4 Vesicular size

Light scattering was used to follow the changes in liposomal size upon incubation with peptide at similar P/L ratios as used for the CF leakage assay. It was observed that the size of the vesicles initially (up to P/L = 1/5) decreases to ≈80% of the initial size (see Table 4-1), which is a similar decrease as was observed for DOPG in absence of cholesterol. Therefore, GL13K can still induce the loss of lipid molecules from liposomes which then reseal to form smaller liposomes. Above P/L ratios of 1/5, the interaction of GL13K with DOPG/Ch liposomes yields an additional population of liposomes with sizes ranging in the micron range. This larger population could either be a fusion product of liposomes, aggregates of smaller liposomes or aggregates of fused liposomes.

Liposome fusion, which results in the mixing of lipids from different liposomes, can be distinguished from aggregation with no lipid redistribution between liposomes by a FRET dilution assay as explained in sections 2.6.1 As shown in Figure 4-4 (A), the mixing of labeled with non-labeled liposomes in equimolar ratios in the absence of peptide does not cause any significant change in fluorescence intensity, indicating that there is no fusion-generated lipid transfer between liposomes. However, upon addition of GL13K, a small and progressive decrease in the fluorescence intensity of rhodamine is observed with increasing P/L ratios up to P/L 1/5. No shift in the intensity maximum for rhodamine was observed; a similar effect has been observed in DNA strand interaction studies [176]. At the higher P/L ratio of 1/2.5 (for which a size increase was observed in DLS) a strong decrease in rhodamine fluorescence is observed, although the fluorescence intensity of NBD does not exhibit the corresponding increase expected for an energy transfer process. However, rhodamine is a highly environment sensitive probe whose fluorescence signal is strongly affected by the polarity of the medium. It may be that the fluorescence changes observed are the result of a local environment change caused by the binding and aggregation of GL13K to the liposome surface rather than a fusion of liposomes.

Liposomes containing 2 mol % of DOPE-Rh without any DOPE-NBD were prepared to examine the role of the local environment on rhodamine fluorescence. If GL13K causes any fusion of these liposomes, a significant change in rhodamine fluorescence should not be observed but a change in a local environment (either due to peptide binding and/or liposome aggregation) would yield a decrease in rhodamine fluorescence. Figure 4-4 (C) shows that the rhodamine fluorescence signal decreases with increasing peptide concentration. In the case when the peptide does not interact with membranes, no quenching of rhodamine fluorescence should occur. Therefore, FRET experiments are done by mixing DOPC/Ch liposomes containing DOPE-NBD

and DOPE-Rh 2 mol % each with equimolar non-labeled DOPC/Ch liposomes. These are then incubated with increasing concentrations of GL13K; no change in fluorescence signal is observed for either NBD or rhodamine (Figure 4-4 (B)). These results support the conclusion that changes in rhodamine fluorescence with DOPG/Ch liposomes are the result of peptide aggregation onto the liposomes surface or liposomal aggregation altering the local environment of the rhodamine label. The fluorescence is reduced by peptide binding and aggregation on the membrane, an effect which is amplified at very high P/L ratios, likely due to aggregation of liposomes.

Table 4-1 Size of DOPG/Ch liposomes before and after incubation with increasing amounts of GL13K to obtain various P/L ratios.

Peptide/Lipid ratio	**Average diameter (nm)**
0	123 ± 7
1/20	105 ± 8
1/10	98 ± 4
1/5	108 ± 4
1/2.5	1163 ± 290

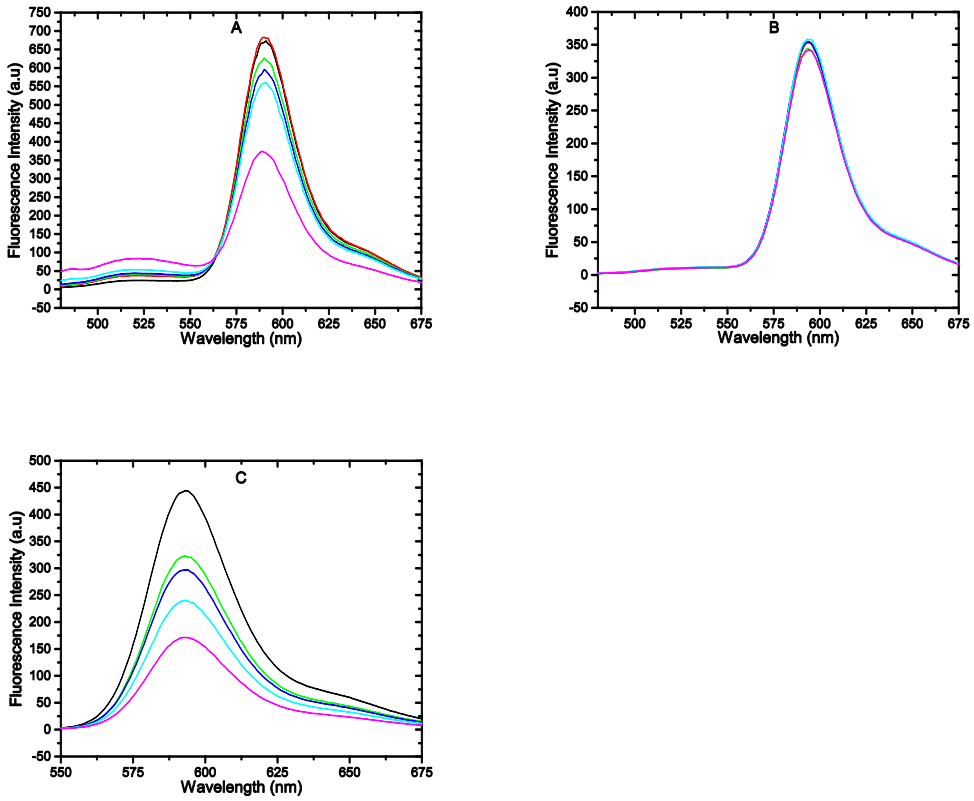

Figure 4-4 FRET changes for different membrane systems in presence of GL13K.

(A) DOPG/Ch liposomes and (B) DOPC/Ch liposomes fluorescence spectra for 25 μM labeled lipids containing 2 mol % of both DOPE-NBD and DOPE-Rh (black), 50 μM labeled/non-labeled (1/1)in the absence of peptide (red), P/L ratio; 50 μM labeled/non-labeled (1/1) in the presence of peptide at the following P/L ratios:1/20 (green), 1/10 (blue), 1/5 (cyan), 1/2.5 (magenta). (C) Fluorescence spectra of DOPG/Ch containing 2 mol % DOPE-Rh; 25uM Rh labeled liposomes (black) and P/L ratios; 1/20 (green), 1/10 (blue), 1/5 (cyan), 1/2.5 (magenta).

4.2.5 Liposome aggregation

Cryo-TEM was used to observe the morphology changes and aggregation of liposomes caused by GL13K. Figure 4-5 (A) shows representative images of DOPG/Ch liposomes. Liposomes with well-defined boundaries along with some small liposomes trapped in the larger ones are observed. GL13K peptides do not seem to cause any significant change in the morphology of the liposomes at a P/L ratio of 1/20 (see Figure 4-5 (B)). At a P/L ratio of 1/2.5 large aggregated structures are observed (Figure 4-5 (C)). Aggregates observed in the cryo-TEM images are much larger than those observed in the DLS due to increased localization of aggregates during the freezing of samples. Liposomes in this image do not show clear boundaries; the contrast has been lost due to complete coverage of the surface of liposomes by the GL13K. In some images for this P/L ratio, mixed populations of liposomes are seen in which partially covered liposomes with distinct boundaries co-exist with aggregates. Note that the size of the structures observed within these aggregates is much smaller than the size of liposomes observed in Figure 4-5 (A) and (B). This suggests that the structures observed in Figure 4-5 (C) are the aggregates of smaller liposomes formed by loss of lipid molecules due to partial micellization. It clearly can be seen in Figure 4-5 (C) that the morphology of the liposomes has been distorted and the surface coverage of DOPG/Ch liposomes causes aggregation after a threshold surface coverage is reached. Representative images were selected where a sufficient concentration of liposomes was observed in the field of view; imaging in presence of peptide was only done for P/L ratios of 1/20 and 1/2.5. The number density of liposomes bound to the substrate was reduced compared in the absence of peptide induced aggregation and thus a lower density of liposomes was observed. This could be either due to changes in surface charge before and after the peptide addition and/or a better interaction of large aggregates with the substrate.

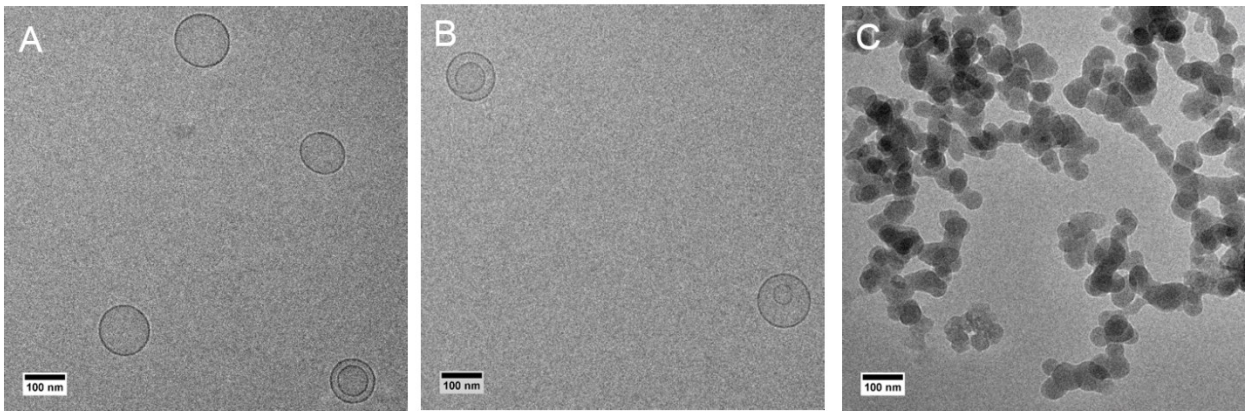

Figure 4-5 Cryo-TEM images of DOPG/Ch liposomes.

(A), DOPG/Ch liposomes with P/L (1/20) and P/L (1/2.5) (B) and (C) respectively

4.2.6 Bilayer ordering

DPI was used to study the effect of GL13K interaction on bilayer ordering. The birefringence is directly related to bilayer ordering *i.e.* a decrease in birefringence indicates decreased bilayer ordering[124, 129, 130, 133]. Stable and uniform bilayers are deposited on the sensing waveguide of the chip prior to the injection of GL13K. Structural parameters for the bilayers are calculated using the isotropic R.I. of 1.47 for lipid bilayers [128-130]. The bilayer thicknesses calculated for DOPG/Ch and DOPC/Ch bilayers are 3.9 nm and 5.6 nm respectively. The decrease in expected thickness of DOPG/Ch bilayers could be due to incomplete coverage which yields overall reduced thickness (explained in detail in section 3.2.5)

The GL13K interaction with bilayers of DOPG/Ch and DOPC/Ch is followed by real time changes in TM, mass and birefringence upon sequential injections of increasing peptide concentrations over pre-deposited bilayers as shown in Figure 4-6 and Figure 4-7. Small, partially reversible changes in TM values are observed for DOPG/Ch bilayers up to peptide concentrations of 12 μM. These small changes suggest an initial binding of GL13K. Irreversible and large increases in TM values are observed at high concentrations of peptide, namely 16 μM

and 20 μM. At these concentrations, the increase in mass is followed by a decrease in birefringence where the changes observed are irreversible. This suggests that the peptide binds very strongly to the DOPG/Ch bilayer which in turn causes increased disordering of the bilayer in a concentration dependent manner [124, 129, 130]. At concentrations of 24 μM and above, net changes in TM, mass and birefringence decrease gradually suggesting a saturation of the surface [127, 128, 133]. At these concentrations binding is reversible, particularly at 28 μM and 32 μM, that is bilayer disordering is reversible during washing by incoming buffer where with dissociation of peptide and associated mass decreases and birefringence values that recover close to that of pre-injection values. We have previously shown that GL13K causes irreversible disordering of DOPG bilayers at the lower threshold concentration of 10 μM and that the bilayer is saturated at 12 μM [88]. The presence of 40 % cholesterol increases these threshold values to 16 μM and 24 μM for irreversible disordering and saturation, respectively. Furthermore, cholesterol decreases the extent of bilayer disordering as suggested by smaller changes in birefringence in presence of cholesterol.

The injection of GL13K over DOPC/Ch bilayers does not have any significant effect on TM, mass and birefringence. However, at higher concentrations a small change is observed during the injection which then recovers to original values similar to pre-injection values. This suggests that GL13K has minimal affinity for zwitterionic DOPC/Ch bilayers. The gradual decrease in mass and birefringence observed during the experiment suggests that the bilayer was not completely stabilized prior to the GL13K injections and the small continuous change is a result of bilayer stabilization process. In the absence of cholesterol, GL13K was found to interact with DOPC bilayers [88] but the presence of cholesterol seems to minimize these interactions. Increased packing caused by cholesterol might have minimized the non-specific hydrophobic interactions.

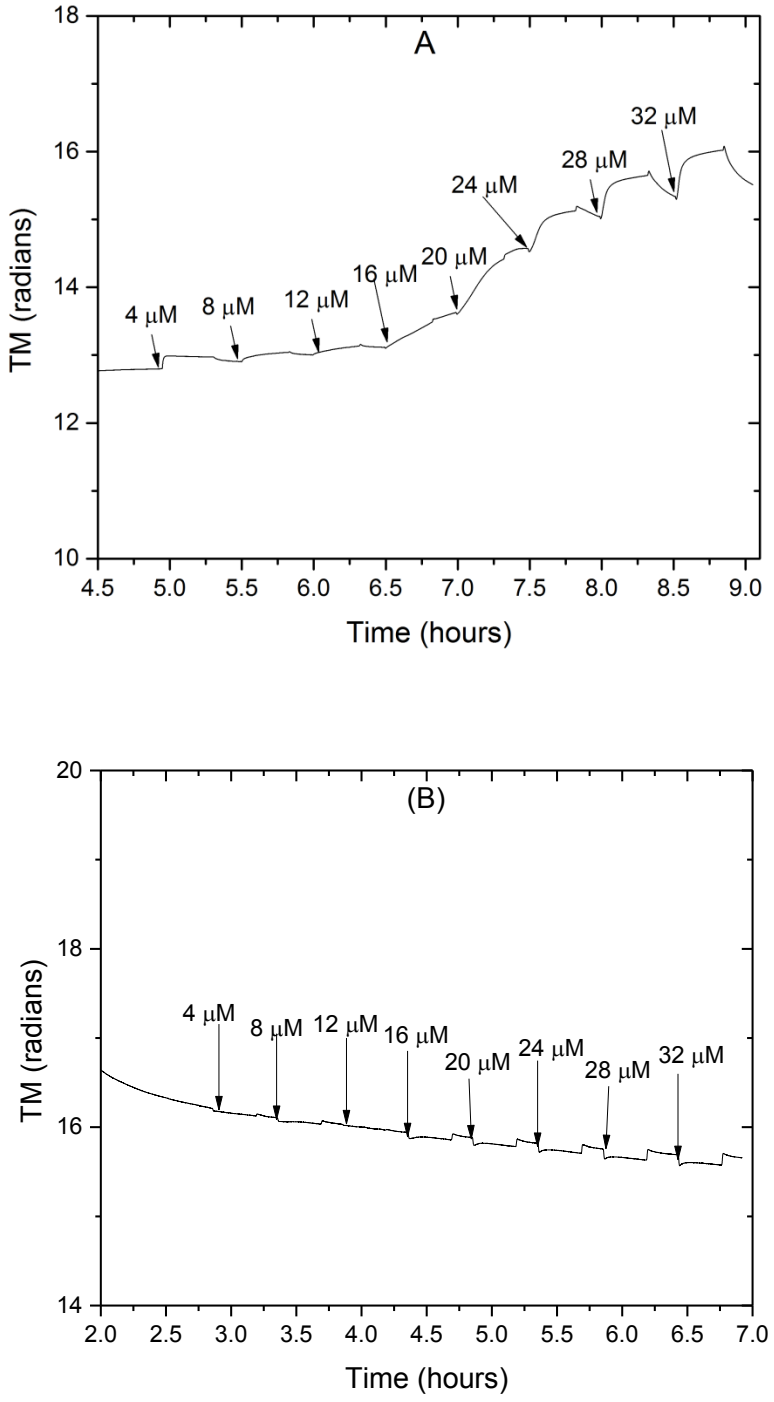

Figure 4-6 Realtime changes in TM polarization.

Changes for DOPG/Ch (A) and DOPC/Ch (B) bilayer upon incubation with increasing concentration of GL13K as shown by arrow heads in the respective plots.

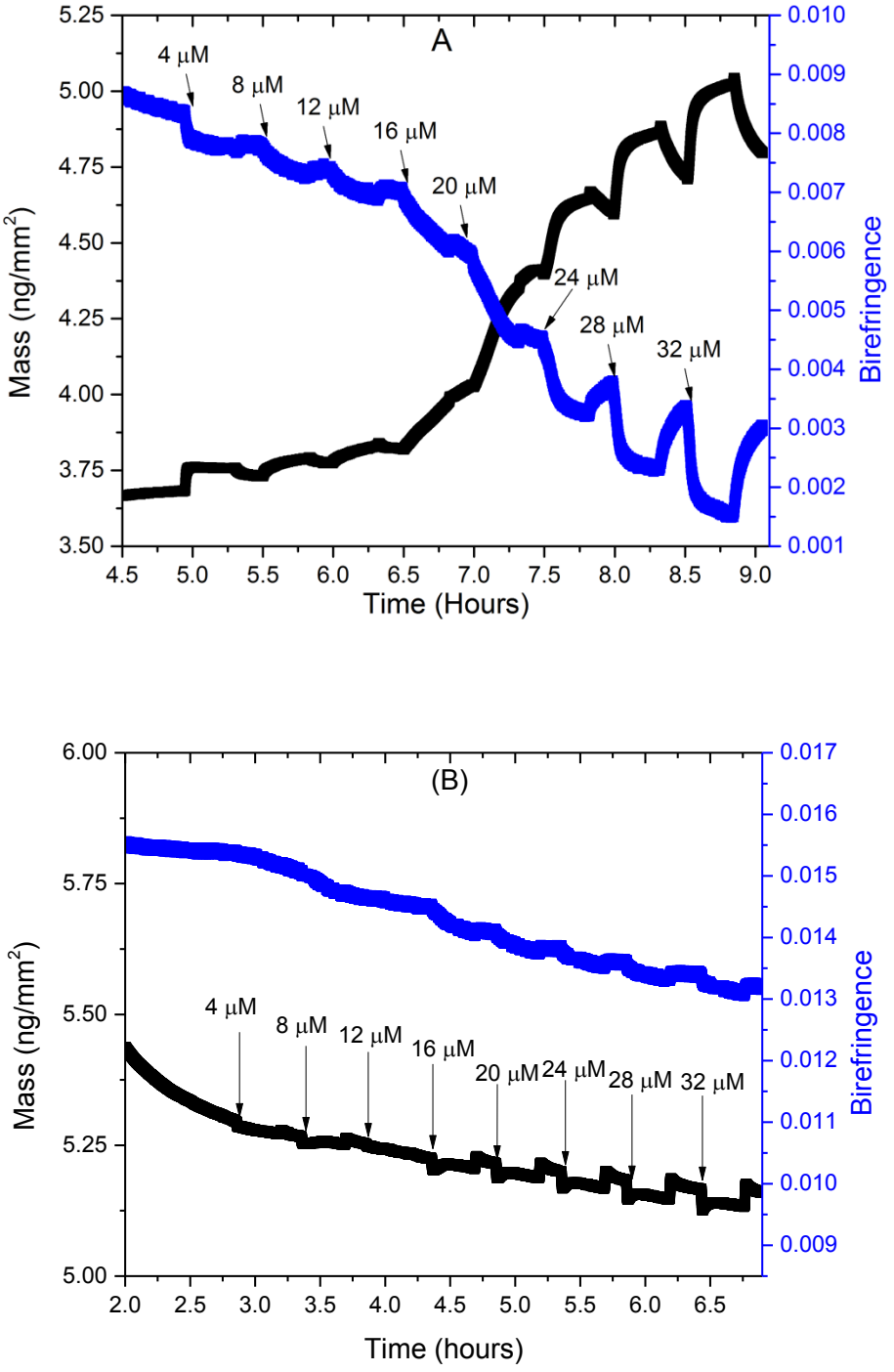

Figure 4-7 Realtime changes in mass and birefringence.

Changes for DOPG/Ch (A) and DOPC/Ch (B) bilayer upon incubation with increasing concentration of GL13K as shown by arrow heads in the respective plots.

4.2.7 Bilayer imaging

Atomic force microscopy was used to image the bilayers before and after incubation with peptide. Smooth and uniform bilayers of DOPG/Ch and DOPC/Ch were deposited on the freshly cleaved mica surfaces as shown in Figure 4-8 and Figure 4-9. Only bilayers which meet these criteria were used to further investigate the peptide interactions. For DOPG/Ch bilayers no significant changes were observed for incubation with 4 μM or less GL13K. When the GL13K concentration is increased to 6 μM, GL13K covered the bilayer surface like a carpet with the majority of these raised features measuring between 0.2 nm to 0.5 nm in height and 10 nm to 20 nm in length (see Figure 4-8). A further increase in GL13K concentration to 8 μM leads to the formation of some 1-2 nm deep and 40-50 nm wide holes as observed in Figure 4-8 (bottom left). However, in some areas, mixed regions exhibiting membrane holes and raised peptide aggregates on the membrane are also observed (see supplementary figure). In some regions, smaller membrane defects about 0.5 nm deep and 30-40 nm wide are also observed as shown in Figure 4-8 (bottom right). This suggests that the extent of membrane disruption caused by GL13K is not uniform over the entire sample. In the absence of cholesterol, GL13K forms much larger holes at concentrations as low as 1 μM [88]. Thus, the presence of cholesterol increases the stability of the bilayer against GL13K disruptive action. However, in the case of DOPC/Ch bilayers GL13K does not have any effect on the topography of bilayer even at concentrations as high as 16 μM (see Figure 4-9). In the absence of cholesterol, we reported that the GL13K can nonspecifically interact with the surface of DOPC SLBs [88]. However, the presence of cholesterol increases the lipid packing and decreases the defects in planar bilayers. This minimizes non-specific hydrophobic interactions between the peptides and the cholesterol containing DOPC SLBs.

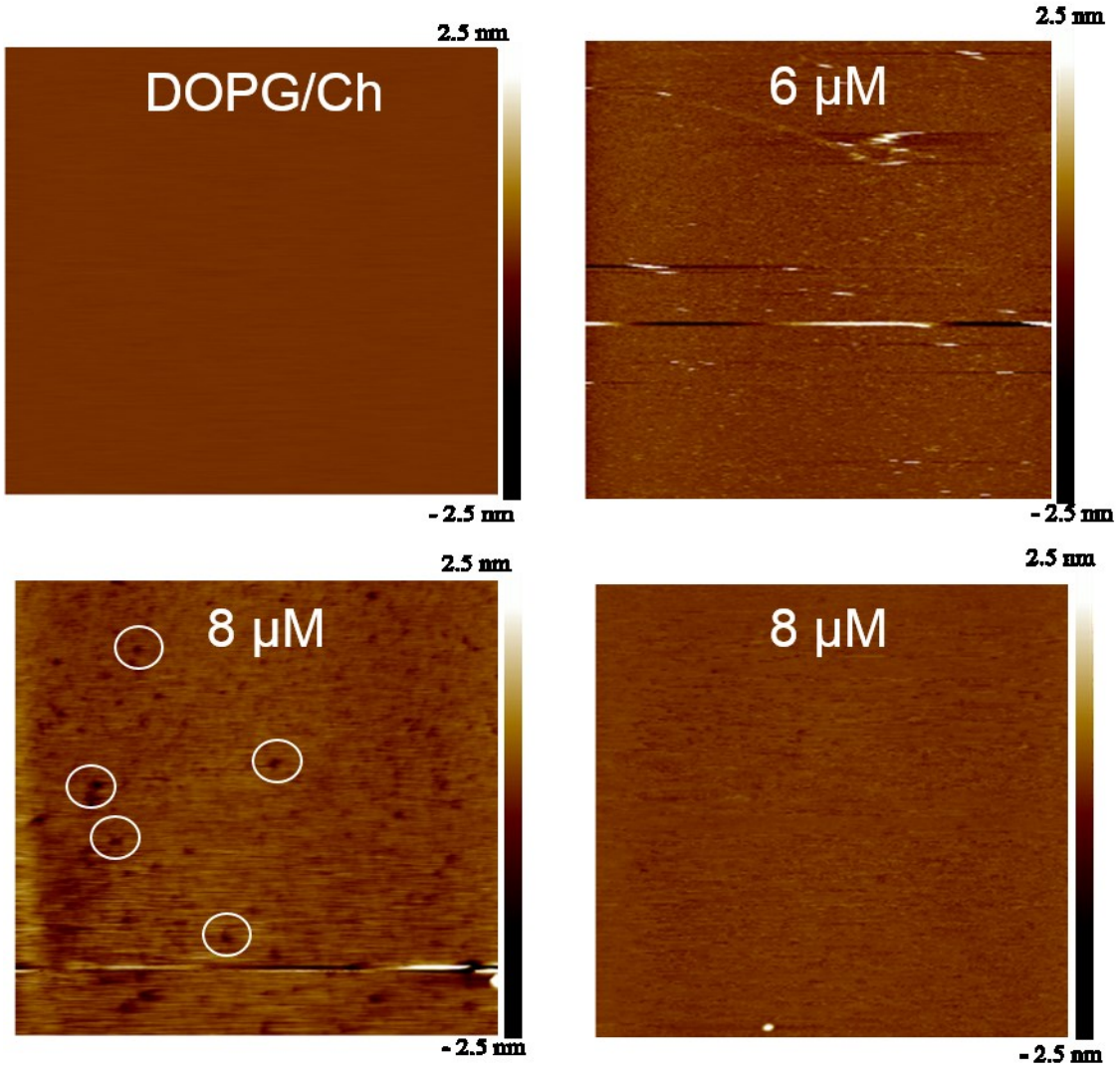

Figure 4-8 Sample AFM images of DOPG/Ch bilayers with varying concentration of GL13K.

DOPG/Ch bilayers (top left), DOPG/Ch bilayer with 6 µM GL13K (top right), 8 µM (bottom left and right). All AFM images were taken with scan size of 2 µm * 2 µm. Circles in the image shows the dark holes in the membrane.

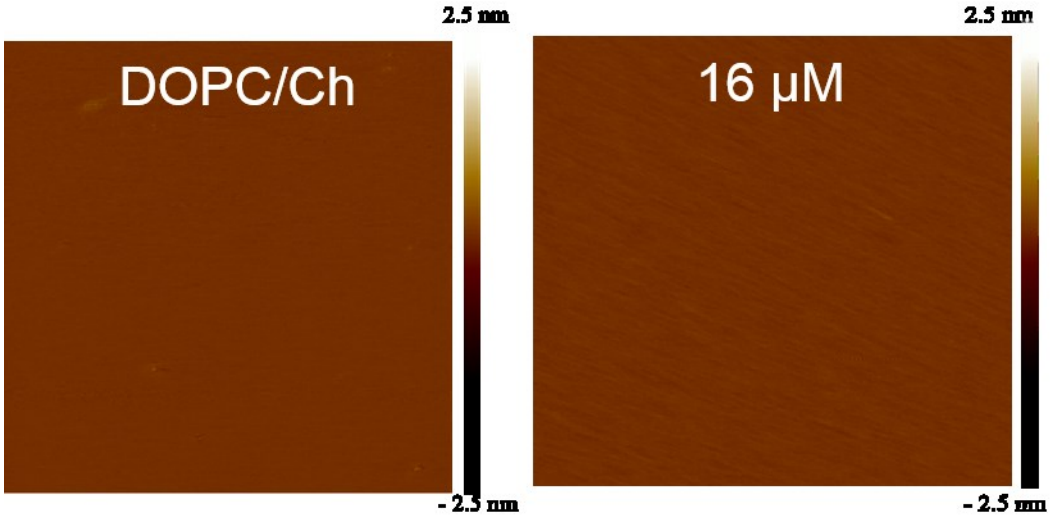

Figure 4-9 Sample AFM images for DOPC/Ch bilayers with varying concentration of GL13K.

DOPC/Ch bilayer (left) and DOPC/Ch bilayer with 16 µM GL13K (right). All AFM images were taken with scan size of 2 µm * 2 µm.

4.3 DISCUSSION AND CONCLUSIONS

Specificity towards bacteria without any adverse effects on eukaryotic or erythrocyte cells is an important property for any AMP to become a successful therapeutic. Most of the unsuccessful AMPs were denied approval either due to their cytotoxic effects or insufficient evidence of their efficacy compared to current antibiotics [13, 40]. It is important to rationally develop new AMPs with higher specificity and activity. Previously we reported [88] that GL13K acts in a charge dependent manner by causing localized micellization of bilayers. We also observed that GL13K had some affinity for zwitterionic SLBs with non-lytic action against zwitterionic liposomes.

Although the outer leaflet of eukaryotic membranes is zwitterionic, the inner leaflet is negatively charged. This difference in the charge between the two leaflets and the charge gradient across the eukaryotic membrane results in a negative membrane potential that can favour GL13K interactions and possible toxicity against eukaryotic cells. However, bacterial and eukaryotic membranes not only differ in terms of charge: eukaryotic membranes also contain a large amount of cholesterol. Cholesterol is known to attenuate AMPs activity and even alter the mechanism of action for AMPs possibly by acting as a barrier to peptide intercalation in the membrane [167, 173].

Cholesterol incorporation results in increased bilayer ordering [92] which limits GL13K peptide insertion into the membrane core, reduces membrane disruption and potentially limits the amount of peptide bound to the membrane. In the presence of 40% cholesterol, the amount of peptide transformed to β-sheets was reduced by 15% and the extent of membrane permeabilization was reduced by ≈40% at P/L ratio of 1/2.5 compared to that in its absence. Furthermore, DPI showed a reduced extent of overall membrane disordering. Despite this, the liposomal contents release kinetics remains unaltered. An instantaneous release of CF followed by slow release observed for DOPG liposomes in the presence of cholesterol is similar to that

observed in its absence [88] although the extent of release is reduced. The large, initial fast release may occur due to the formation of transient channels while small membrane defects result in the second slower release as the membrane stabilizes against these defects over time. Similar release profiles have been observed previously and are reported to be a result of either the carpet mechanism or by formation of transient channels by AMPs [15, 100, 143, 177]. Although, the carpet mechanism and transient channels exhibit similar release profiles, it has been suggested that the formation of transient holes or toroidal pores may occur as an early step in membrane disintegration prior to micellization caused by the carpet mechanism [39]. Such membrane defects formed by transient channels are large enough to cause the leakage of even large molecules from the core of liposomes [143, 177].The carpet mechanism is often associated with detergent-like, membrane disruption resulting in complete loss of membrane integrity while transient channels due to a surface orientation of peptide causes membrane defects and thinning of bilayers at certain areas and forms transient defects or pores without compromising the gross structure of liposomes [57, 64, 65, 143]. Toroidal pores however should not cause the loss of lipid material from the membranes as they are formed by the incorporation of peptides into the membrane core.

Even in the presence of cholesterol, GL13K appears to act *via* a carpet mechanism. Unlike the conventional understanding of a carpet mechanism, here the interpretation is amended to include peptide oriented on the surface that causes localized micellization resulting in transient or toroidal pores and local defects. We have shown that the extent of membrane permeabilization is reduced and the size of membrane pores are much smaller in the presence of cholesterol incorporation than were observed in its absence. Toroidal pores are less likely to occur if insertion is limited, however, a detailed analysis of peptide orientation relative to the membrane would be necessary to exclude the possibility that some peptide may adopt this orientation.

Moreover, even in the presence of 40% cholesterol there is evidence of lipid loss and membrane resealing to form smaller liposomes (as shown in Figure 4-10). However, the extent of loss is limited with eventual aggregation of these smaller liposomes. It may be that at 40% cholesterol, the peptide can still insert sufficiently to cause some lipid loss, with a preference for the DOPG anionic lipid in the micellized lipid-peptide aggregate. The resealed liposome would become enriched in cholesterol which would further hinder peptide insertion. If the peptide then remains surface oriented, with the charged hydrophilic face of the β-sheet oriented to interact with the anionic lipid head groups, the hydrophobic face would be left exposed. The associated reduction of the hydration repulsion forces between the liposomal membranes and exposed hydrophobic face of surface bound peptide would eventually lead to the aggregation of liposomes (as observed by DLS and TEM) after surface bound peptide reaches threshold concentration on the membrane surface *via* the hydrophobic effect (refer to schematic in Figure 4-10). Similar liposomal aggregation effects have been observed previously for other amphipathic β-sheet AMPs such as S-thanatin and gomesin which are not able to insert deep into the membrane [50, 100].

Cholesterol is major constituent of eukaryotic membranes, thus the reduced activity of GL13K against these membranes will protect against human cell toxicity and in particular hemolysis. Some bacterial strains are observed to render some AMPs ineffective by increasing their membrane packing [80]. In such cases, GL13K could potentially act by causing the aggregation of bacterial cells similar to the effect observed in the presence of cholesterol for negatively charged membranes. Aggregated bacterial cells could then be cleared by the macrophage cells of our immune system and thus the chances of bacteria being able to develop resistance against GL13K are minimized due to its different modes of action.

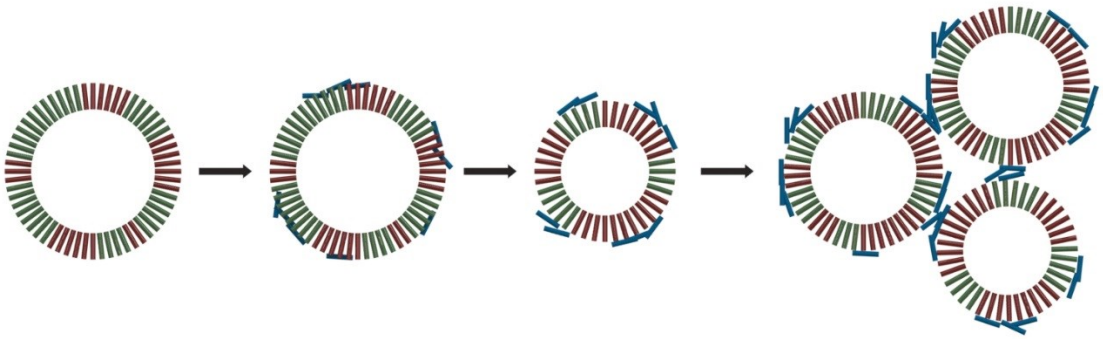

Figure 4-10 Schematic representation of a mechanism of action of GL13K in presence of cholesterol.

Left if a DOPG/Ch liposome where DOPG and cholesterol lipids represented by green and red cylinders respectively. Initially the peptide interacts with liposomes (second left) and after reaching a threshold concentration causes transient destabilization of the membrane forming transient pores resulting in the loss of lipid molecules (mainly DOPG lost as lipid-peptide micelles; micelles not depicted) to form smaller liposomes rich in cholesterol (second right). Finally these small liposomes aggregate (right).

5 MANUSCRIPT 3 ALTERED CATIONIC CHARGE AND AMPHIPATHICITY OF NATIVE HUMAN PAROTID SECRETORY PROTEIN ANTIMICROBIAL PEPTIDE: EFFECT ON ACTIVITY AND SELECTIVITY

Information provided in this chapter forms part of a manuscript in preparation and expected to be submitted to *Biochimica et Biophysica Acta – Biomembranes* with following authors: **Balhara, V**.; Escalante-Cornejo, I.-E.; Schmidt, R.; Gorr, S.-U.; DeWolf, C., Some of the information in methods section has already been discussed in chapter 2 thus will not be repeated in here.

Author contributions:

I carried out all experimental work, data analysis and wrote the manuscript. C. DeWolf helped building the research plan, analyzing the data and contributed to writing the paper. I.-E. Escalante-Cornejo performed CD, DLS and CF release experiments for GL13D/N peptide; I carried out the interpretation of the data. R. Schmidt contributed to writing the manuscript. S.-U. Gorr supplied the peptide GL13K and is a collaborator on the project.

5.1 INTRODUCTION

Resistance of multi drug resistant (MDR) bacteria to several classes of antibiotics results in a serious lapse in treatment of bacterial infections caused by these MDR strains leading to serious social and economic problems [1-5]. Bacterial resistance is increasing at an alarming rate which has resulted in increased mortality and morbidity. This period of increased bacterial resistance and lack of antibiotics is referred to as either the "Pre-antibiotic era" or the "Post-antibiotics era. Antimicrobial peptides (AMPs) which are part of our humoral immune system have been suggested as potential replacements to conventional antibiotic therapies. These AMPs act by targeting the fundamental differences in membrane composition between bacterial and eukaryotic membranes (see section 1.6 for details). hPSP is an AMP secreted into our oral cavity by parotid glands, submandibular glands and gingival epithelial cells [37, 84, 85]. It belongs to the short palate, lung and nasal epithelium clone (sPLUNC) family of proteins that are related to the BPI, lipopolysaccharides (LPS)–binding protein (LBP), and CETP [37]. Based on the structural fit between hPSP and the known N-terminal antimicrobial domain of BPI responsible for bacterial opsonizatio) various potential AMP peptide sequences have been identified and synthesized by Gorr et .al [84, 85]. Sequences and details of their *in-vivo* studies are explained in detail in section 1.5.

GL13NH2, the native peptide (residues 141 to 153 of hPSP) but with an amide modification of the carboxy terminus, induces bacterial agglutination [87]. GL13NH2 also inhibits LPS and monophosphoryl lipid A stimulated TNFα secretion from macrophages by binding to lipid A of LPS [84, 87], thus exhibiting an anti-inflammatory response. GL13NH2 carries a net charge of +1 due to the amide modification of the carboxy terminus. The single substitution of an aspartic acid by an asparagine at position 11 yielding GL13D/N increases the net charge and hemolytic

activity of the peptide (see Table 1-1 for details about the peptide sequence and their properties). Both GL13NH2 and GL13D/N have poor water solubility due to the presence of a large number of hydrophobic residues (as suggested by the sequence and calculations of peptide property calculator [89]). This reduced water solubility might affect the secondary structure of the peptide in buffer which in turn might alter the activity and selectivity of these peptides. Activity and selectivity of the majority of AMPs are known to vary with membrane composition as well as the charge, hydrophobicity and amphipathicity of the peptide[43, 51, 53, 62]. In order to rationally develop more efficacious and selective GL13 AMPs, it is important to identify and understand the role of various peptide properties towards the activity and specificity ofthe peptides. Herein hPSP peptides with lowered charge and reduced water solubility compared to the previously characterized GL13K.

Table 5-1Peptide sequences for various hPSP peptides synthesized.

Coloured residues indicate where the changes in amino acid residues were made compared to native peptide

Peptide	Sequence	pI	Charge at pH (7.0)
GL13NH2	**GQIINLKASLDLL-NH2**	**10.1**	**+1**
GL13DN	**GQIINLKASLNLL-NH2**	**14**	**+2**
GL13K	**GKIIKLKASLKLL-NH2**	**14**	**+5**

5.2 RESULTS AND DISCUSSION

5.2.1 Effect of secondary structure transformation on activity

The extent of secondary structure transformation and the type of secondary structure are well known to have an effect on the activity and even mechanism of action of AMPs. Helical wheel and β-sheet representations of GL13NH2 (Figure 5-1) and GL13D/N (Figure 5-2) show that these peptides can adopt both amphipathic α-helical and β-sheet structures. GL13NH2 and GL13D/N have very low water solubility possibly due to the large number of hydrophobic residues present in these peptide (see sequences in Table 5-1). These hydrophobic residues induce aggregation and increased intermolecular hydrogen bonding between peptide molecules, thus promoting formation of amphipathic secondary structures in buffer (refer to Table 5-2 for the contributions of the different secondary structures as a function of environment obtained from CD data deconvolution) as observed previously in the cases of penetratin, PGLa and magainin [41, 178].

DOPC liposomes do not induce a significant change in the secondary structure of GL13NH2 (see Table 5-3 and Figure 5-4), whereas the presence of DOPG liposomes, which are negatively charged, increases the proportion of the peptide which is structured and significantly favours the formation of α-helices. Deconvolution of recorded spectra of GL13NH2 and GL13D/N reveals that they are 60% and 73% structured in buffer, respectively. While this amount of structured peptide is different for GL13NH2 and GL13D/N, the proportional contribution of α-helices (42%) and β-sheets (58%) to the total structured peptide is same in buffer. α-Helices could promote deeper insertion of the peptide in the membrane hydrophobic core. Thus it is clear that the initial GL13NH2 interaction is still primarily governed by attractive electrostatic interactions

with the anionic membrane despite the low (+1) net charge. However, once the peptide has reached the membrane surface, there is a secondary structure transformation to α-helices which likely promotes accommodation of the peptide deeper into the membrane hydrophobic core. Incorporation of 40% cholesterol into DOPG liposomes which results in increased lipid packing and reduced membrane insertion lowers the overall proportion of the peptide which is structured.

As noted above, GL13D/N is more structured in buffer than is GL13NH2 albeit with the same relative proportions of α-helices and β-strands. Upon incubation with either DOPG or DOPC liposomes, a slight increase in structured peptide is observed but much more evident is the increase in the proportion of α-helices (from 42% in buffer to 67-71% in the presence of liposomes), the helical form clearly being more suited to membrane accommodation. The increased structuring of GL13D/N was enough to promote interaction with zwitterionic DOPC membranes as suggested by the increase in helical content from 42% in buffer to 67% in DOPC environment.

By comparison, the GL13K peptide studied in previous chapters was only 10% structured in the presence of buffer and formed predominantly β-sheets when structured. The absolute number of hydrophobic residues has not been altered between these peptides. However, GL13K carries 4 lysine residues distributed over the entire length of the peptide which results in electrostatic repulsion and in turn increased water solubility and reduced aggregation-promoted secondary structure in buffer. Once this peptide is exposed to DOPG membranes with which it can interact electrostatically it adopts mainly a β-sheet structure. Helices might not be favourable for the GL13K as four lysines are uniformly distributed over two faces of the helix which might prevent peptide aggregation in the membrane due to charge repulsion between the helices. However, one quality that is universal among the peptides is that on favourable interaction with membranes

they can transform their secondary structures to accommodate in membrane hydrophobic environment. This finding is consistent with other AMPs findings in the literature where secondary structure transformation is an important condition for the AMP activity.

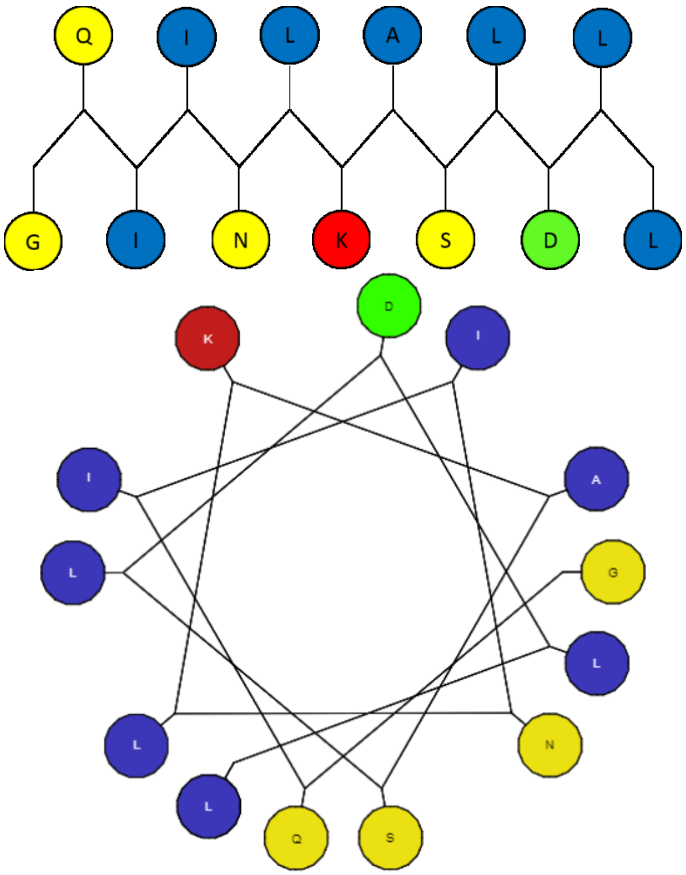

Figure 5-1 Helical wheel and beta sheet representation for GL13NH2.

Non polar residues (blue), polar residues (yellow), negatively charged (green) and positively charged (red)

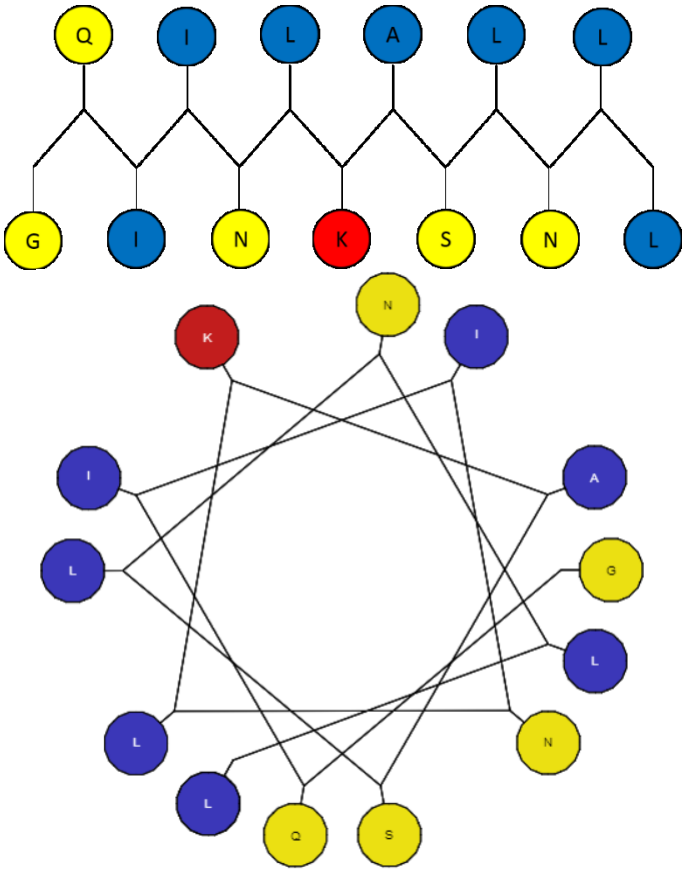

Figure 5-2 Helical wheel and beta sheet representation for GL13D/N.

Non polar residues (blue), polar residues (yellow), negatively charged (green) and positively charged (red)

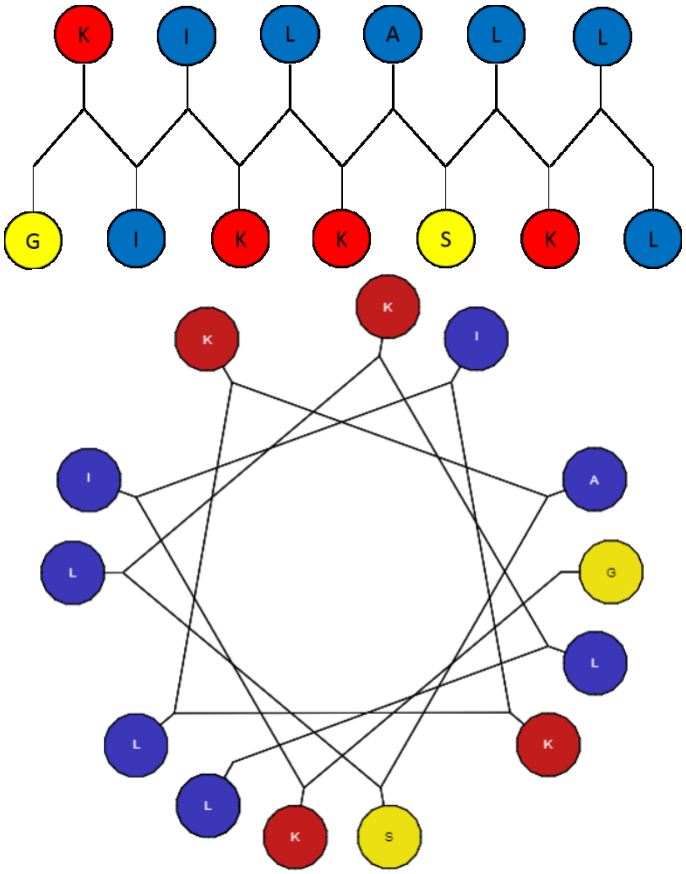

Figure 5-3 Helical wheel and beta sheet representation for GL13K.

Non polar residues (blue), polar residues (yellow), negatively charged (green) and positively charged (red)

Table 5-2 Percentage contributions of structured and unstructured GL13NH2, GL13D/N and GL13K in buffer. Secondary structure deconvolution is done using SELCON3 [107-109].

Peptide	Structured (%)	Unstructured (%)
GL13NH2	60	40
GL13D/N	73	27
GL13K	10	90

Table 5-3 Percentage contributions of various secondary structures of GL13NH2 and GL13D/N in different environments.

Secondary structure deconvolution is done using SELCON3 [107-109]. Values in parentheses indicate the proportion of structured peptide associated with that secondary structure. The secondary structure deconvolution in lipid environment was done at P/L of 1/2.5.

Peptide	*Environment*	*α-helices (%)*	*β-sheets (%)*	*Unstructured (%)*
	Buffer	25 (42%)	35 (58%)	40
	DOPG	75 (88%)	10 (12%)	15
GL13NH2	DOPC	27 (47%)	30 (53%)	43
	DOPG/Ch	48 (69%)	22 (31%)	30
	DOPC/Ch	20 (33%)	40 (67%)	40
	Buffer	31 (42%)	42 (58%)	27
GL13D/N	DOPG	55 (71%)	22 (29%)	23
	DOPC	53 (67%)	26 (33%)	21

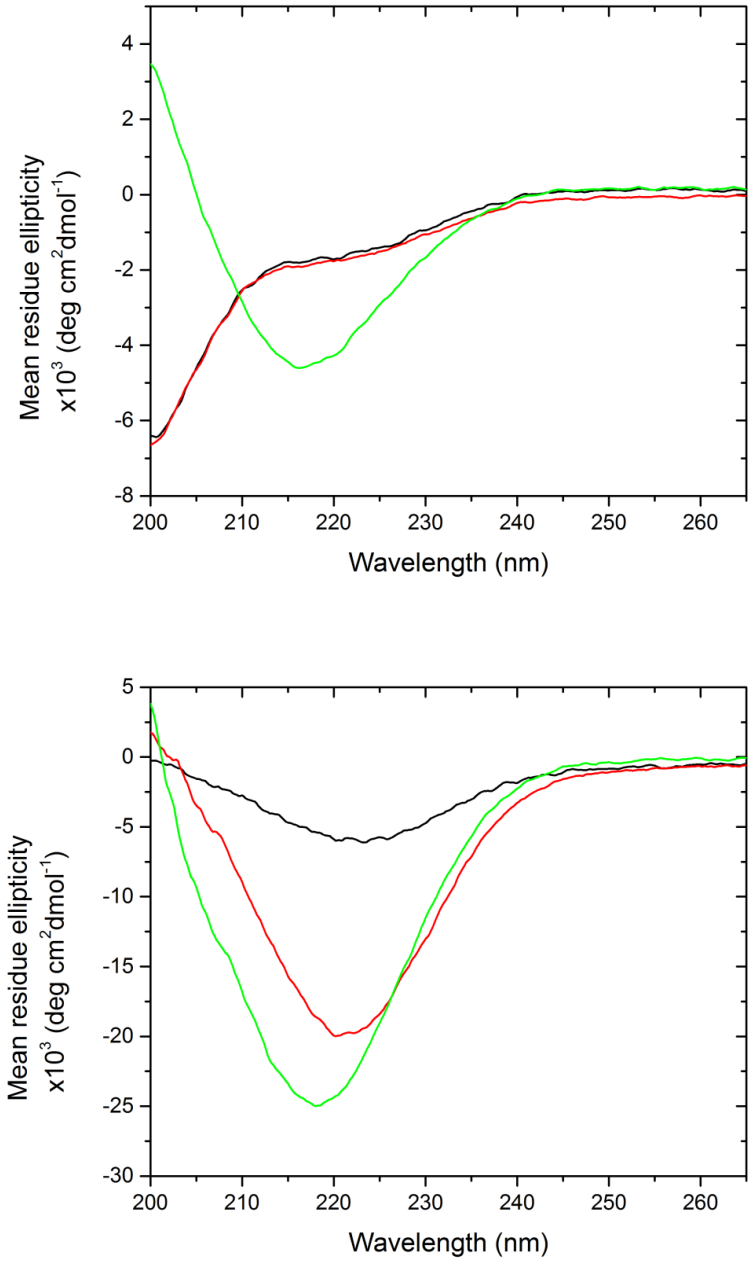

Figure 5-4 CD spectra of GL13NH2 and GL13D/N in various environments.

CD spectra of GL13NH2 (upper) and GL13D/N (lower) in buffer (black), DOPC (red) and DOPG (green). In presence of liposomes spectra were recorded at P/L ratio of 1/2.5. The concentration of lipid used was 60 μM and 150 μM for GL13NH2 and GL13D/N respectively.

5.2.2 Membrane disruption activity

Membrane disruption was followed by CF release from liposomes in presence of increasing amounts of the peptides. Stable and non-leaky liposomes were formed as no significant increase in fluorescence signal was observed over time in the absence of peptide (Figure 5-5). Triton X, which causes complete micellization of liposomes, served as a control for 100 % lysis.

As discussed in the previous section, both GL13NH2 and GL12D/N show significant secondary structure formation in buffer with a greater proportion of helices formed relative to GL13K (which was shown to only fold into ordered structures in the presence of anionic membranes and with a complete preference for β-sheets). This difference was attributed to the increased hydrophobicity of GL13NH2 and GL13D/N which leads to an increased tendency to fold and aggregate. This leads to a much reduced specificity for causing membrane leakage by GL13NH2 and GL13D/N as seen in Figure 5-6. If one considers the release at P/L = 1/2.5 which corresponds to the P/L ratio used for CD experiments, a significant release for both peptides with both DOPC and DOPG liposomes is observed. Had this been solely due to the charge reduction (and not the increased hydrophobicity or amphiphilicity) one would expect greater specificity for GL13D/N which has a higher charge of +2 compared to +1 for GL13NH2. In fact, at this P/L ratio, GL13D/N shows very little specificity towards an anionic (bacterial model) membrane. The generic membrane disruption appears to be correlated to the secondary structure transition to a α-helix. For example, GL13NH2 is 60% structured in buffer with an almost equal mixture of α-helices and β-sheets. In the presence of an anionic membrane it transforms to 85% structured with the majority α-helices and causes high release. Moreover, while the amounts of helices (and total structured GL13NH2) in the presence of DOPC zwitterionic liposomes remains unchanged (compared to buffer), the release is still significant implying that the pre-formed helices can

interact with the membrane and cause disruption. The evidence for helices preferentially interacting with the membrane is stronger with GL13D/N. Here, the peptide is significantly structured in buffer, again with an almost equal distribution of helices and sheets, and this total structured amount remains unchanged in the presence of a membrane. However, upon interaction with either DOPC or DOPG membranes there is a strong shift to α-helices and approximately 85% CF release. The presence of cholesterol moderates the effect for both DOPG and DOPC membranes. Here, one can observe the contribution of electrostatic attraction. Despite the cholesterol, a +1 charge on the GL13NH2 peptide is sufficient to discriminate between an anionic and zwitterionic membrane with a corresponding increase in α-helical content.

If one considers both the release as a function of P/L ratio (Figure 5-6) and the real-time CF release profiles (Figure 5-7 and Figure 5-8), it becomes clear that there is a different mechanism of action for GL13NH2 with DOPG/Cholesterol and GL13D/N with either DOPG or DOPC. They exhibit a slower initial release compared to that of GL13NH2 with DOPG (particularly at low P/L ratios). Furthermore, the presence of cholesterol resulted in relatively little release at low P/L ratios compared to one in the absence of cholesterol. Only upon reaching a high threshold amount of bound peptide a large release and significant membrane disruption is observed. It is assumed that the cholesterol can attenuate the non-specific interactions of the amphipathic helices with the hydrophobic core of the membrane by increasing lipid packing and preventing peptide insertion. This results in surface orientation of peptide causing permeabilization by local destabilization of membrane lipids due to excessive lateral stress generated by peptide binding. The similarity in profile would suggest that the GL13D/N is also surface bound in the presence of DOPC membranes. This is further supported by the real-time profiles (Figure 5-7 and Figure 5-8) for both these systems as well as GL13D/N with DOPG liposomes (Figure 5-5). In these

three cases, the instantaneous release is replaced with a much slower process yielding slower overall kinetics of CF release with long times to stabilization (plateau in the CF release). For GL13D/N interacting with DOPC liposomes this effect is amplified with an initial slower release followed by an increased rate of release as peptide surface accumulation increases which presumably leads to greater disruptions. The details of the mechanism are still under investigation.

DLS experiments were done to address the effects of the membrane permeability on the size of liposomes and to see if the peptide-induced lysis is accompanied by the loss of lipid molecules or by aggregation. No significant effect on the size of DOPC and DOPG liposomes is observed upon incubation with GL13NH2 (see

Table 5-4). Therefore, GL13NH2 does not cause either aggregation or significant loss of lipids from the liposomes.The pre-formed helices likely associate to form pores in the DOPC membranes which cause the continual increase in lysis as more peptide is added to the system. With GL13D/N and DOPG on the other hand, the appearance of multiple large-sized, highly polydispersed populations appears (data not shown) to be correlated with CF release and membrane disruption. These appear as early as P/L = 1/5 for DOPG liposomes but not until P/L = 1/2.5 for DOPC. These findings suggests that GL13D/N might exhibit its activity by a combination of different mechanisms which are yet to be studied. GL13D/N was excluded from the remaining studies (subsequent sections) because of its high lytic activity towards DOPC liposomes and lack of discrimination between bacterial and eukaryotic model membranes.

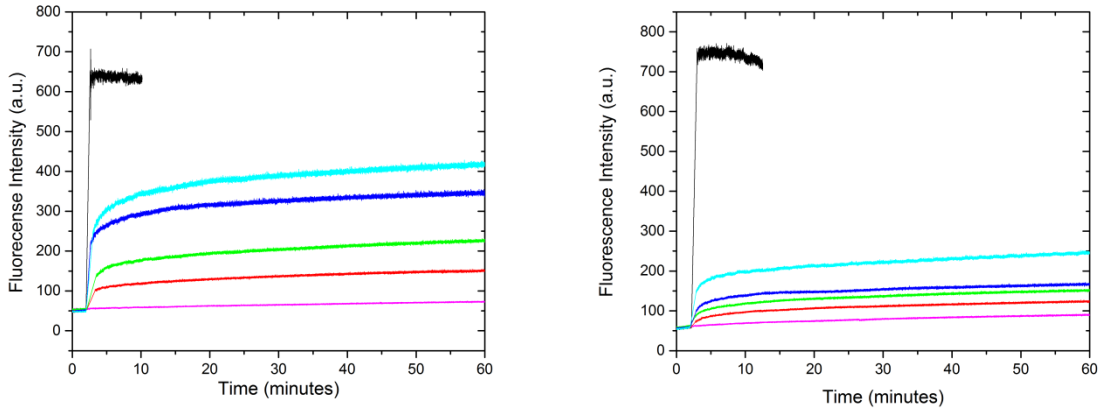

Figure 5-5 CF release profile for DOPG and DOPC membranes with varying amount of GL13NH2.

Sample set of CF release profiles over 60 minutes upon incubation of CF encapsulating DOPG liposomes (left) and DOPC liposomes (right) with increasing amount of GL13NH2 at time two minutes to obtain varying P/L ratios. In absence of peptide there is no CF release as shown by the magenta trace, while addition of Triton X - 100 (black trace) causes 100 % leakage and release. With increasing P/L ratios such as 1/20 (red), 1/10 (green), 1/5 (blue) and 1/2.5 (cyan) an instantaneous release followed by a slow release was observed.

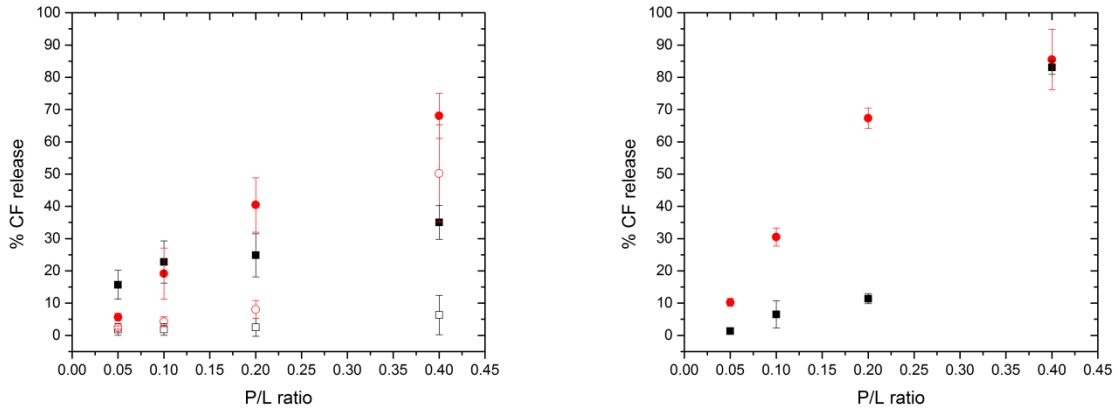

Figure 5-6 Percentage CF release of various membranes caused by GL13NH2 and GL13D/N.

Averaged percentage of carboxy fluorescein released from various liposome compositions upon incubation with GL13NH2 (left) and GL13D/N (right). Lipid composition represented as DOPG (solid red circles) and DOPC (solid black rectangles), DOPG/Ch (hollow red circles) and DOPC/Ch (hollow black rectangles). Each data point is an average of three (GL13NH2) and two (GL13D/N) different experiments with different liposome preparations at same P/L ratio with percentage release calculated at time 60 minutes. Cholesterol experiments for GL13D/N were not performed thus not presented here.

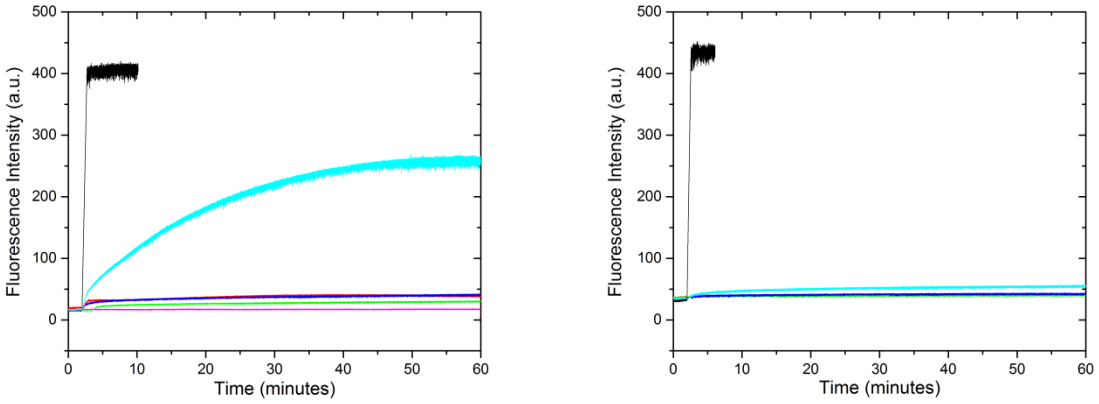

Figure 5-7 CF release profile for DOPG/Ch and DOPC/Ch membranes with varying amount of GL13NH2.

Sample set of CF release profiles over 60 minutes upon incubation of CF encapsulating DOPG/Ch (60/40) liposomes (left) and DOPC/Ch (60/40) liposomes (right) with increasing amount of GL13NH2 at time two minutes to obtain varying P/L ratios. In absence of peptide there is no CF release as shown by the magenta trace, while addition of Triton X - 100 (black race) causes 100 % leakage and release. Various P/L ratios are represented as 1/20 (red), 1/10 (green), 1/5 (blue) and 1/2.5 (cyan)

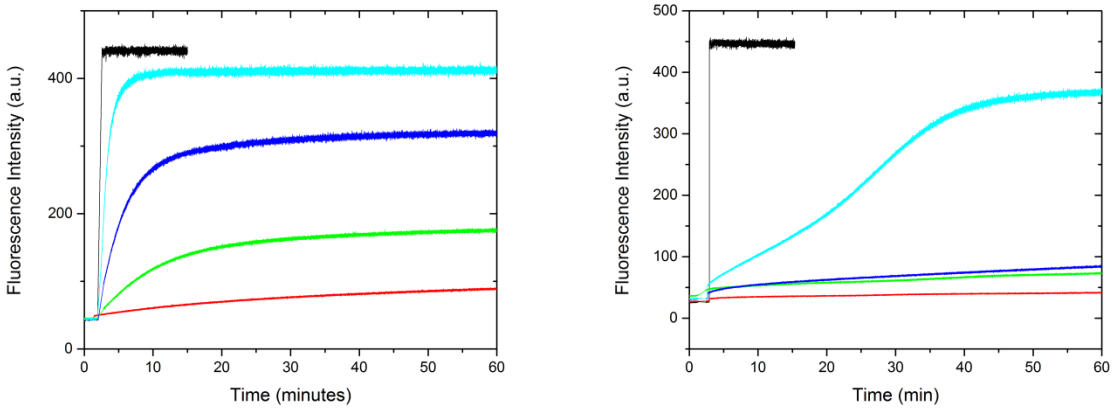

Figure 5-8CF release profile for DOPG and DOPC membranes with varying amount of GL13D/N.

Sample set of CF release profiles over 60 minutes upon incubation of CF encapsulating DOPG liposomes (left) and DOPC liposomes (right) with increasing amount of GL13D/N injected at time two minutes to obtain varying P/L ratios. Release caused by addition of Triton X - 100 (black trace) and varying P/L ratios such as 1/20 (red), 1/10 (green), 1/5 (blue) and 1/2.5 (cyan) are presented.

Table 5-4 Size of DOPG and DOPC liposomes before and after incubation with increasing amount of GL13NH2 to obtain various P/L ratios.

Peptide/Lipid ratio	Average diameter of DOPG liposomes (nm)	Average diameter of DOPC liposomes (nm)
0	104.1 ± 5.9	120.6 ± 11.3
1/20	105.9 ± 3.9	121.0 ± 11.5
1/10	107.6 ± 5.5	120.3 ± 10.8
1/5	107.2 ± 3.7	124.0 ± 9.7
1/2.5	108.7 ± 4.3	121.7 ± 10.8

5.2.3 Membrane affinity

Thermodynamic parameters for the interaction of GL13NH2 with DOPG or DOPC liposomes were studied using ITC. Strong and selective binding of AMPs with microbial membranes is very important if they are to be used as a potential therapeutic. Liposomes composed of either DOPG or DOPC lipids were titrated into GL13NH2 contained in the reaction chamber. Figure 5-9 illustrate the enthalpy changes and binding isotherm obtained upon sequential injections of DOPG and DOPC into GL13NH2. Each injection of DOPG liposomes resulted in an exothermic heat of reaction which decreases in magnitude with consecutive injections as the amount of free or unbound GL13NH2 decreases; saturation is reached after the 15^{th} injection. Fitting the data yielded an overall exothermic enthalpy change of ≈ - 1.8 kcal/mol with entropy values of ≈ 0.019 kcal/mol/K. Binding constants in the range of 10^5 suggests reasonably strong binding even though it is an order of magnitude lower than the GL13K peptide (as observed with similar ITC

experiments in Section 3.2.1 and 4.2.1), the latter likely attributable to the reduced charge. In contrast, neutral DOPC liposomes (which lack electrostatic attraction) do not show any significant interaction with GL13NH2 as suggested by the negligible enthalpy changes for all injections (Figure 5-9 (B))**.** An important question that arises here is why we do not see GL13NH2 binding with DOPC liposomes using ITC whereas in previous section 5.2.2 we reported the lysis of DOPC liposomes caused by GL13NH2 at all P/L ratios studied. While the weak interactions between GL13NH2 and DOPC due to hydrophobic interactions might be enough to cause some disruption they do not yield strong heat changes measurable in ITC. In this case heat changes due to disruption of peptide solution aggregates, peptide interactions with lipids, secondary structure changes and energy costs associated with lipid disordering might have been balanced and resulted in a net low heat changes.

GL13NH2 exhibited exothermic heat changes compared to GL13K which exhibited endothermic heat changes [88]. Entropy changes were relatively much larger for GL13K (0.073 kcal/mol/K) [88] compared to GL13NH2 (0.019 kcal/mol/K). Endothermic heat changes with large entropy values might be due to a high level of restructuring of liposomal lipids caused by partial membrane micellization. DOPG vesicles do not exhibit loss of lipid molecules in the presence of GL13NH2 although liposomal lysis is seen. This suggests that the two peptides act by somewhat different mechanisms.

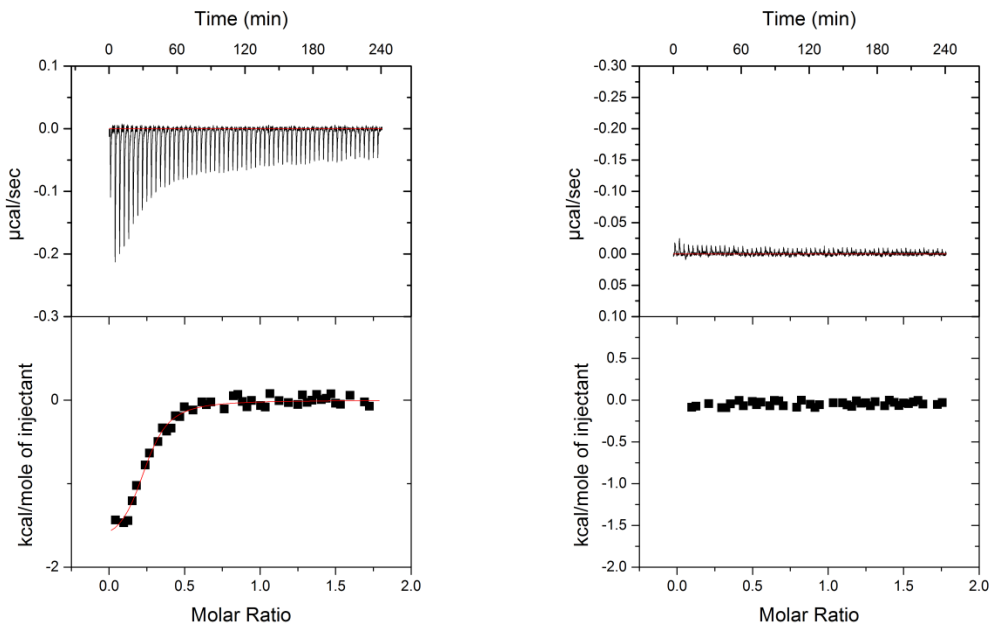

Figure 5-9 ITC binding isotherms for DOPG and DOPC with GL13NH2.

Binding isotherms for titration of (1 mM) liposomes (left) DOPG and (right) DOPC into (0.1 mM) GL13NH2 peptide. Molar ratios reported in here are P/L ratio

5.2.4 Interactions with SLBs

5.2.4.1 Bilayer ordering

DPI was used to study the effect of GL13D/N interaction on DOPG and DOPC bilayer ordering. The bilayer thicknesses calculated for DOPG and DOPC bilayers were 4.0 nm and 3.8 nm respectively. The thickness measured by DPI is the average thickness of the adsorbed layers over the entire length of the chip calculated from relative phase shifts in TM and TE polarizations, hence partial coverage leads to lower average thicknesses even if the actual bilayer thickness is the same (explained in section 3.2.5).

GL13NH2 interaction with bilayers of DOPG and DOPC was followed by the real time changes in TM and TE upon sequential injections of increasing peptide concentrations over pre-deposited bilayers which were used to calculate thickness, mass and birefringence using Maxwell's equations. Small partly reversible changes in mass values are observed for the DOPG bilayer up to peptide concentrations of 16 μM. These small reversible changes suggest an initial weak binding of GL13NH2 to the membrane which is then washed off by the incoming buffer after the injection is complete. At higher concentrations (20 μM peptide), injection results in an initial increase in mass and birefringence followed by decreases in both to below the original values at the end of the dissociation period. This suggests a weak interaction between the peptide and the membrane which leads to a loss of lipid molecules from the membrane surface and a net loss of lipid ordering. The effect is further enhanced at 24 μM peptide concentration, although further additions (28 μM and 32 μM) suggest saturation. The onset of significant changes in birefringence occurred at 10 μM for GL13K [88] compared to 20 μM for GL13NH2. This suggests that more of the GL13NH2 peptide is needed to bring a similar effect as the GL13K peptide. A

similar trend was observed for CF leakage results where the percentage release caused by GL13NH2 was lower than that of GL13K at a given P/L ratio.

The injection of GL13NH2 over DOPC bilayers do not have any significant effect on mass and birefringence up to concentrations of 28 μM (see Figure 5-10). At these high concentrations, a small increase in mass is observed during the injection with no recovery to pre-injection values, indicating a weak binding of GL13NH2 peptides to the DOPC membranes. At even higher concentrations (32 μM), GL13NH2 injections result in an initial large increase in mass. The majority of this weakly absorbed peptide is washed off but there is a net increase in mass at the completion of the injection period. It is not known whether the mass values can reach pre-injection values if sample is allowed to equilibrate for long enough time periods. The interaction of GL13NH2 to the DOPC membranes does not induce a significant change in birefringence, indicating that it may be surface bound but does not cause significant bilayer disordering.

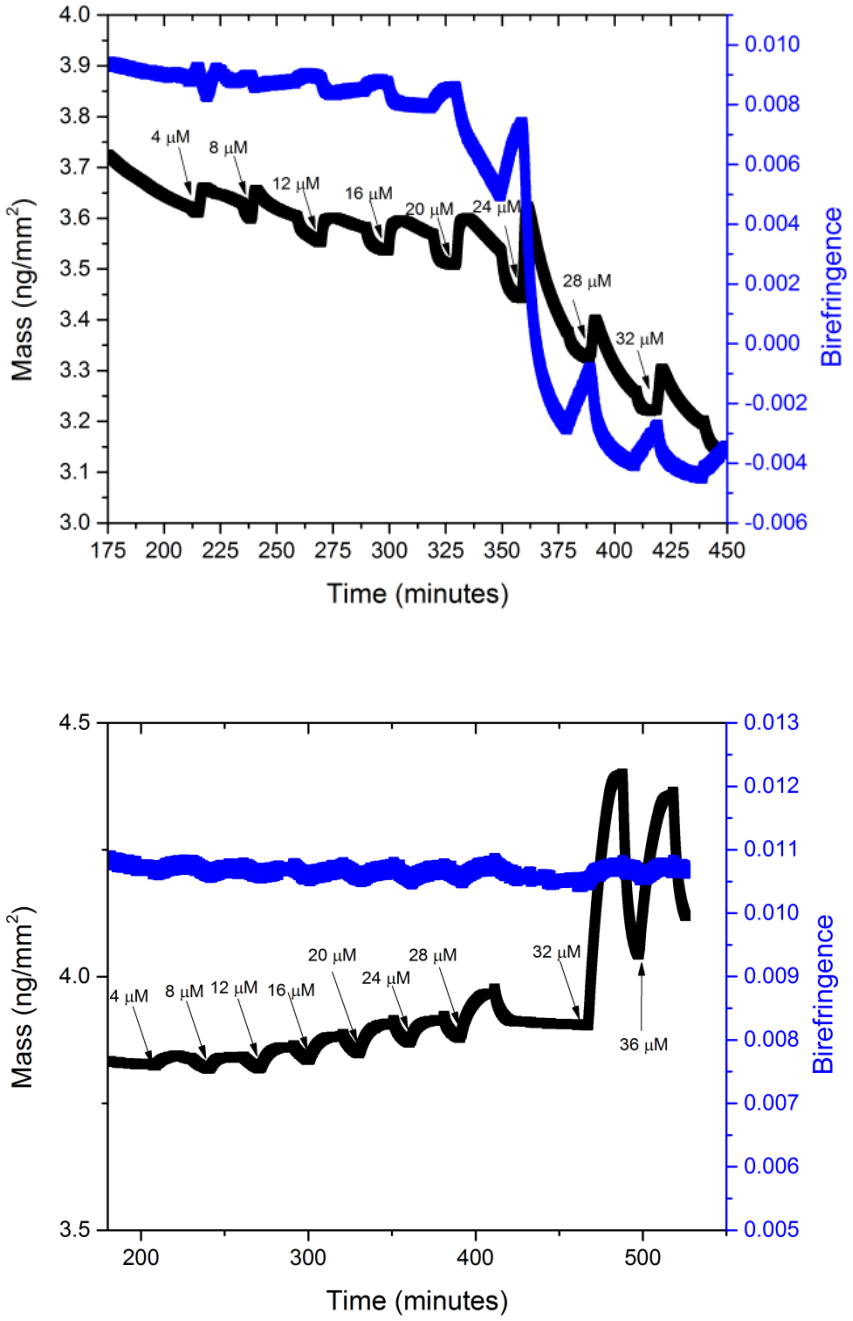

Figure 5-10 Realtime changes in mass and birefringence of DOPG and DOPC bilayers.

Mass and birefringence changes for DOPG (top) and DOPC (bottom) bilayer upon incubation with increasing concentration of GL13NH2 as shown by arrow heads in the respective plots

5.2.4.2 Bilayers imaging

Smooth and uniform DOPC and DOPG bilayers are deposited on the freshly cleaved mica substrates (data not shown). When these bilayers are incubated with 2 μM GL13NH2, small aggregates (1.5 nm to 2 nm high and 20 nm to 40 nm wide) are observed on the surface, with a higher density of aggregates in the case of DOPG bilayers (Figure 5-11). When the concentration of GL13NH2 is increased to 10 μM it lead to the formation of 3-4 nm high strands on the surface of the bilayer (refer to Figure 5-11). Stranded and small aggregates are also observed in some areas at intermediate concentrations (Supplementary Figure 5-1). The density of strands formed on the surface of DOPG bilayers is higher than that seen on DOPC bilayers. The increased electrostatic interactions between the peptides and the negatively charged DOPG membranes as compared to the DOPC membranes favor higher accumulation of peptide on the DOPG membrane surfaces. However, the hydrophobic forces due to the highly hydrophobic nature of GL13NH2 are enough to cause the interactions with zwitterionic DOPC membranes. Strands and aggregates observed in some scan areas (as shown in Figure 5-11) are highly aligned in one direction. To confirm that these highly regular strands were not an artifact of the scanning or tip movement, the same area was scanned in the opposite direction and the same image was obtained (see Supplementary Figure 5-1). These images obtained for low density of strands (Supplementary Figure 5-1) clearly indicate that these aggregates are aligned on the membrane surface without the formation of holes. In contrast to the AFM experiments which show surface bound structures, DPI showed a decrease in the mass at higher peptide concentrations. This may be due to differences in experimental procedures. In the case of DPI, the surface is continuously flushed which might result in the washing away of weakly bound peptide whereas in AFM the

SLB is incubated with and imaged in a solution of peptide.

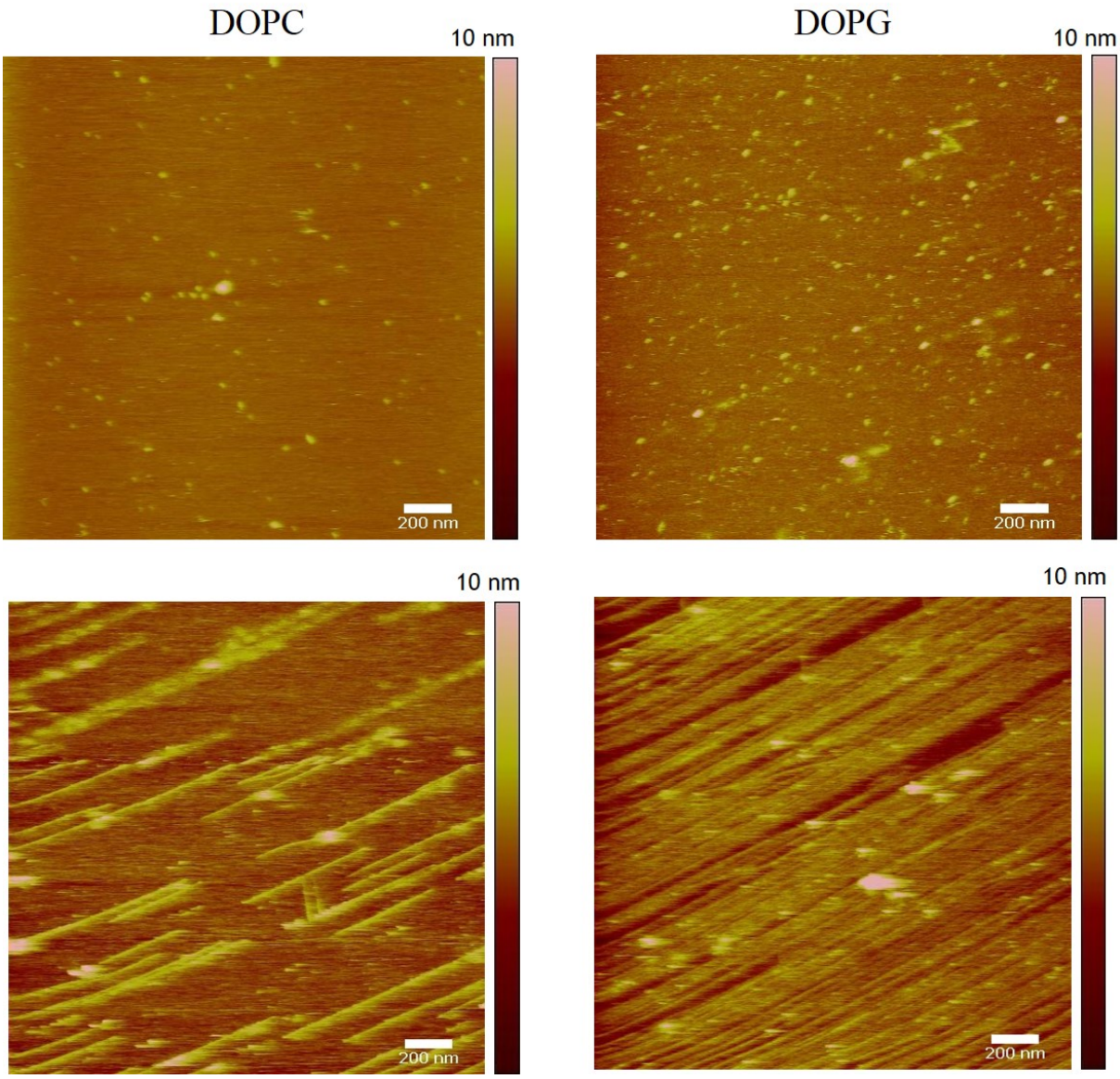

Figure 5-11 AFM images of DOPC and DOPG bilayers with varying amount of GL13NH2.

AFM images for DOPC (left) and DOPG bilayers (right) with 2 μM GL13NH2 (top) and 10 μM (bottom). All AFM images were taken with scan size of 2 μm * 2 μm.

5.3 CONCLUSIONS

GL13NH2 and GL13D/N have low solubility in water and carry seven hydrophobic residues of a total of thirteen amino acids. This results in the aggregation of these peptides which in turn promotes the secondary structure transformation of these peptides to t α-helices or β-sheets. The high degree of structured peptide in solution and a further secondary structure transformation to predominantly helices, appears to be responsible for promoting non-specific hydrophobic interactions with the membrane core. This increased activity against zwitterionic DOPC membranes is not favourable in terms of biological applications as this might promote hemolytic activity.

GL13D/N which carries a +2 charge compared to the +1 charge of GL13NH2 exhibited much stronger lytic activity against DOPG liposomes but it also showed a much higher level of non-specific interactions with DOPC liposomes. This suggests that electrostatic interactions promote the activity of GL13 AMPs but the net effect is a sum of both electrostatic and hydrophobic interactions. This correlates with *in vitro* studies in which GL13D/N exhibited increased hemolytic activity even in presence of serum while hemolytic activity was not observed for GL13NH2 [81, 84]. Thus, a fine balance of electrostatic and hydrophobic interactions is necessary to have an optimal window of antimicrobial activity without hemolytic activity.

These peptides seems to act by multiple mechanisms similar to the toroidal and carpet mechanisms. It is hard to differentiate which one is occurring at which step or whether they occur concurrently. Further investigations need to be carried out to differentiate between the two mechanisms. Regardless of the mechanism, these peptides seem to exert their lytic activity by transient membrane destabilization without significant loss of lipid molecules. Finally, even though an increase in hydrophobicity and amphipathicity is important for increased antimicrobial

activity (in particular for low cationic charged peptides) an excessive increase in these properties might result in increased cytotoxicity.

5.4 SUPPLEMENTARY DATA

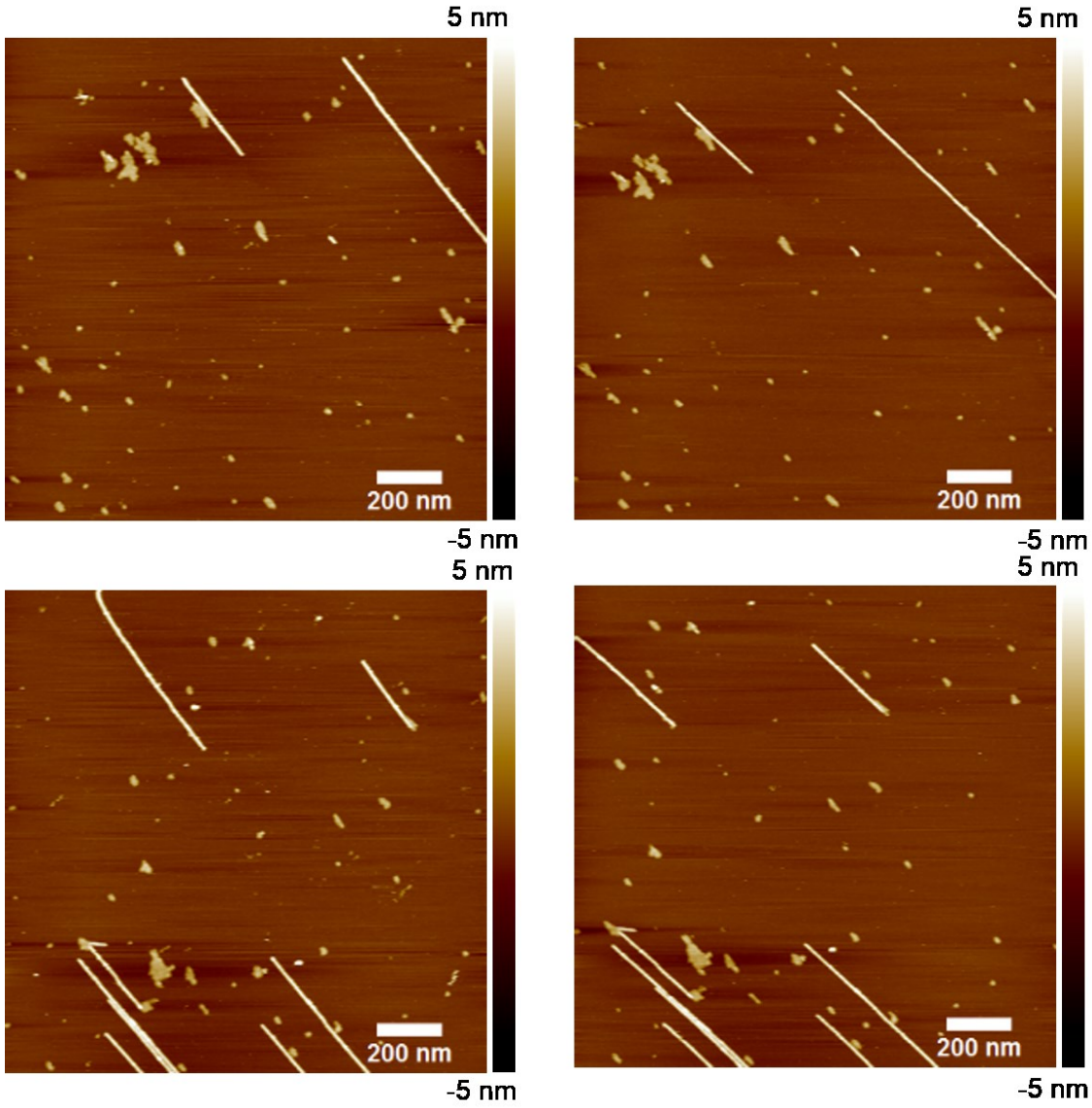

Supplementary Figure 5-1 Sample AFM images for DOPC and DOPG bilayers with 7 µM GL13NH2.

Top and bottom panels represent two different areas scanned bottom to top (left) and top to bottom (right). All AFM images were taken with scan size of 2 µm * 2 µm. A small drift is observed in the samples but the two features observed in left panel scan are unaltered in right panel scan.

6 FINAL CONCLUSIONS

From these studies various conclusions that can be drawn are summarized here. The conclusions are divided into four sections: (i) role of membrane properties, (ii) role of peptide charge and structure, (iii) mechanism of action and, (iv) selection of potential candidates for therapeutic use.

6.1 ROLE OF MEMBRANE PROPERTIES

The membrane composition can have a strong impact on the activity and mechanism of action of AMPs. In the case of GL13 peptides, the membrane charge is the major driving force for their selectivity and activity toward bacterial cell model membranes as opposed to eukaryotic membranes. GL13 peptide lytic activity and the extent of interactions with bacterial model membranes composed of DOPG lipids followed the order of their cationic charge (GL13NH2 < GL13D/N < GL13K) particularly up to P/L ratios of 1/5. Increased cationic charge favored stronger interactions with the anionic membrane. GL13NH2 and GL13D/N peptides also exhibited activity against zwitterionic membranes (eukaryotic model). The electrostatic interactions between these peptides and DOPC should not contribute to their activity. Instead hydrophobic forces seems to be the major driving forces in this case and, in particular, an increased level of helix formation, driven by low solubility and increased hydrophobicity. The interaction between the peptide and the phosphate of the phosphocholine can also be a contributor for their interactions with DOPC membranes. Incorporation of 40% cholesterol resulting in increased lipid packing thus reducing non-specific interactions, attenuated the membrane lytic activity of GL13 peptides (particularly for GL13K and GL13NH2, as GL13D/N was not tested).. Cholesterol is a major constituent of eukaryotic membranes. Thus, the presence

of cholesterol will hinder the lytic activity of GL13 peptides towards membranes of healthy eukaryotic cells and, hence, yield a reduced hemolytic effect. .

6.2 ROLE OF PEPTIDE PROPERTIES

Various peptide properties that were shown to be important for AMPs activity are cationic charge, hydrophobicity and high amphipathicity (for details refer to section 1.3.1). All GL13 peptides studied have seven hydrophobic residues thus their hydrophobicity is not a variable in the present studies. GL13NH2 and GL13D/N were not soluble in water while substitution of lysine residues at various positions in GL13K results in increased solubility by limiting the solution aggregation *via* electrostatic repulsion. Thus these peptides exhibited different degrees of structuring in buffer with GL13K being mainly unstructured while GL13NH2 and GL13D/N were highly structured with almost equal contributions from both α-helices and β-sheets. Upon interaction with charged membranes, GL13K transforms to form a majority of β-sheets while GL13NH2 and GL13D/N form a majority of α-helices, thus it appears that these peptides belong to two different classes even though they have similar origin.

As discussed in section 6.1 increased cationic charge of the peptide has resulted in increased membrane lytic activity. However the overall effect of the GL13 peptides is the net result of both electrostatic and hydrophobic forces. Hydrophobic forces and secondary structure changes play an important role in helping peptide to be accommodated in the membrane hydrophobic environment. As observed with other AMPs in the literature [51-53] even though increased amphipathicity helps to improve the antimicrobial activity of the AMP an excessive increase in it is usually associated with increased toxicity. We observed a similar phenomenon, whereby GL13NH2 and GL13D/N which had an increased structured component even in buffer alone

resulted in a lack of specificity as suggested by their activity against the eukaryotic DOPC models. In general, the greater the degree of structuring in the solution, the higher the lytic activity against eukaryotic models and the increased toxicity towards healthy cells. Knowledge of the proper window of charge, hydrophobicity and amphipathicity is necessary to design a peptide with high selectivity and activity for bacteria without any toxicity to the host. GL13K peptides are highly efficient in bacterial killing with high specificity (without any effect on eukaryotic membranes) as a virtue of the loss of ordered structures in buffer and the presence of high cationic charge

6.3 MECHANISM OF ACTION

GL13K and GL13NH2 interact with t negatively charged membranes and form aggregates on the surface of the membrane. The size of the aggregates was much smaller for GL13K as compared to GL13NH2. However the release profile of these peptides showed an instantaneous release followed by a slower release. The instantaneous release might be associated with the transient destabilization of the membrane followed by a larger disruption when an excess of peptide is bound at the surface. AFM imaging of GL13K suggests that it results in the loss of lipid molecules after reaching a threshold concentration on the membrane surface. GL13K thus acts by a carpet mechanism and disrupts membrane barrier function through a partial micellization and transient pore mechanism see Figure 6-1.

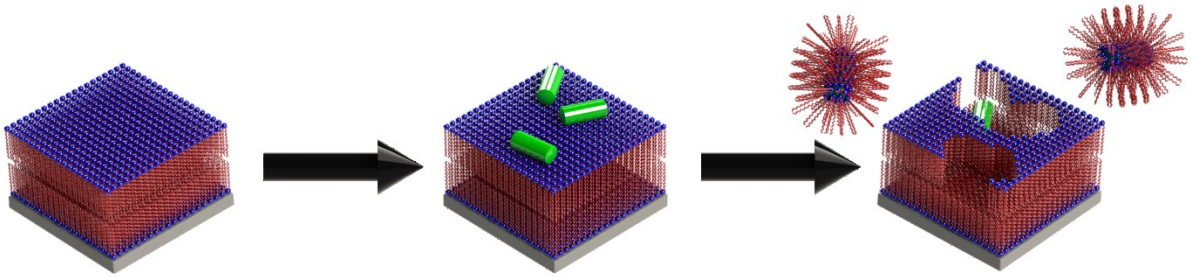

Figure 6-1 Schematic of the GL13K membrane disruption mechanism.

Effect of increasing peptide on the bilayers is highlighted, planar supported bilayer (left), initially GL13K interacts with lipid head groups (center) and after reaching a threshold concentration (right), GL13K causes membrane destabilization by removing parts of it forming peptide lipid micelles or stable supra molecular structures.

However, in the case of GL13NH2 the peptide seems to be covering the membrane like a carpet without any observed discrete holes in the bilayers. Our studies suggest that GL13NH2 causes membrane permeabilization by a carpet mechanism resulting in local membrane defects and transient holes without causing the loss of lipid molecules or micellization of the membrane.

GL13D/N is a highly structured peptide, even in buffer and has a +2 charge. The release profiles observed for GL13D/N show initial sharp increase followed by a slow release for anionic membranes while for zwitterionic membranes they show a slow initially which then increases and finally stabilizes following a sigmoidal curve. Certainly, it is acting by different mechanisms in two membrane systems. More detailed studies need to be done before concluding on the mechanism of action of this peptide. This type of variance in mechanism upon changing membrane properties has been observed previously for various other AMPs including melittin and aurein. They were found to act by three different mechanisms (barrel-stave, toroidal pore and carpet) depending on the conditions used such as the hydrophobic length of bilayer, the lipid packing and the charge distribution[42, 142-144]

6.4 GL13 PEPTIDES FOR THERAPEUTIC APPLICATIONS

The various GL13 peptides studied exhibit different levels of activity and specificity toward bacterial and eukaryotic model membranes. GL13NH2 exhibited activity toward bacterial model membranes (DOPG) but its lytic activity was much lower as compared to GL13K. The activity of GL13NH2 against negatively charged membranes was further reduced (almost to zero) by incorporation of cholesterol into the membrane unless a very high P/L ratio (1/2.5) was reached. Bacterial membranes lack cholesterol but they contain saturated phospholipids which might result in increased phospholipid packing. Thus the reduced charge in the cells and lipid packing might lead to decreased lytic activity of GL13NH2. This would result in higher doses of it being needed in case it has to be used as an antibiotic. This is not a preferred condition as very high doses are associated with other side effects and narrow down the drug safety window and therapeutic applications. Further modifications need to be done to this peptide (e.g. further increasing its charge) to improve antibacterial activity and decreasing its hydrophobicity and to reduce possible cytotoxic effects.

GL13D/N showed strong activity towards bacterial model membranes but a lack of specificity causing strong lysis of eukaryotic model membranes (particularly at high P/L ratio). Thus, this peptide will not meet the specificity requirements as a potential antimicrobial without further modifications in its sequence to increase its charge with a concurrent decrease in its hydrophobicity which might help in improving its selectivity and activity.

GL13K exhibited high selectivity and activity towards bacterial membrane models. GL13K has low micromolar range MIC values for the *E. coli (*4 μM or 5 μg/mL) and *P. aeruginosa* (6 μM or 8 μg/mL) and is active against both Gram-positive and Gram-negative bacteria [87]. Non-hemolytic activity of GL13K suggested that it can be used for systemic circulation. GL13K

exerts its activity even in the presence of serum and at high salt concentrations. This makes it a very important candidate for treatment of cystic fibrosis. In cystic fibrosis, the local salt concentrations are elevated which render some of the β-defensin peptides and other drugs ineffective[69, 163, 179]. GL13K has strong antibacterial activity against *P. aeruginosa* biofilms [180] which is one of the major causes of cystic fibrosis [146]. All these properties make GL13K a very potent candidate for antibiotic therapeutics where its efficacy can be further improved by a proper formulation development process. GL13K has recently been tested for its application in dental and orthopedic implants where it was incorporated into the titanium coating and observed to reduce morbidities and improve long term clinical efficacies of these implants [181]. Thus of all three peptides studied, GL13K is the most suitable antimicrobial candidate for future applications.

6.5 SHORT TERM SUGGESTED FUTURE WORK

In this thesis we studied the mechanisms of action of various GL13 peptides. Our attempts provided an insight into how these peptides act. However, there are questions that were left unexplained:

- **What can we extract from the biphasic release profiles that we observed?**

  Initial instantaneous release has been suggested to be due to transient channels that are formed prior to complete loss by carpet mechanism. It is important to determine if these transient channels are formed due to toroidal pores or due to a transient destabilization of the membrane due to increased lateral pressure by peptide aggregation on the surface. For peptides like GL13 which exhibit very fast action, it might be challenging to differentiate between various mechanisms, particularly if they are not distinct but are all contributing to the release mechanism. Various possible methods that can be used to address this question are listed as follows:

  - The orientation of peptide in lipid membranes that is angle orientation relative to lipid normal. Since in toroidal pores peptides are inserted deep in the membrane as compared to carpet model where peptides are usually located at the solvent membrane interface. Peptide orientation in the lipid molecules studied using either Fourier-Transform infrared (FTIR) spectroscopy in solution and PM-IRRAS using SLBs and oriented CD can be informative.
  - GL13 peptides cause a high level of disordering of DOPG lipid membranes but we do not know how the lipid alignment changes upon interaction with the peptides in particular the bending of lipids. Information about lipids alignment might shed some light on the further mechanistic details about membrane lytic activity of GL13 peptides. Grazing

incidence X-ray diffraction (GIXD) can provide information about the tilt angles of the lipids before and after incubation with GL13 peptides.

- **Role of lipid composition?**

In the current investigations pure DOPG and DOPC were used as models for bacterial and eukaryotic membranes, respectively. Cell membranes are complex mixtures of lipids and consist other lipid molecules with similar charge but different head groups such as phosphatidylserine and phosphatidylethanolamine, combination of lipids also varies among various bacterial strains. It is important to study the effect of the lipid head group size and curvature on the activity of the GL13 peptides. Some studies have already been done using these lipids and GL13K peptide and seems to have significant role in the membrane lysis mechanism. Furthering these studies will help understand the role of various individual lipid components on the activity and selectivity of GL13 peptides. These studies then need to be extended further by using the natural bacterial lipid extracts to relate the activity much closer to the biological perspective. Natural extracts of *E. coli* are commercially available and our preliminary studies (not explained in this thesis) showed that GL13K exhibits strong lytic activity but its release profile lacks the instantaneous release step and takes longer time to achieve the maximum release for a given peptide concentration. Thus it will be good step further to conclude the studies using the membranes of varying lipid composition.

6.6 LONG TERM SUGGESTED FUTURE WORK

The long term aim of this research is focused on more potent GL13 AMPs using the structural activity profile obtained in this thesis or in proposed short term plans. To achieve this aim we need to further optimize the properties of these peptides thus it is essential to do detailed structural property activity relationship studies of these peptides. Gorr *et. al.* have done a systemic alanine scan in which 12 alanine substituted GL13K variants were analyzed showed that lysine at position two was responsible for the loss of bacterial agglutination activity and that the serine residue in position nine is responsible for anti-lipopolysaccharide activity of GL13K [87]. It is also important to study how the particular amino acids alter the activity of the peptide by carrying out biophysical analysis of peptide membrane interactions.

GL13K is the most efficient peptide of all the GL13 peptides characterized by biophysical analysis and *in vivo* cells studies. However, GL13NH2 and GL13D/N can be further improved upon by using the structural activity data obtained, so as to define strategic modifications in their amino acid sequences to improve their antibacterial activity and selectivity while retaining their agglutination activity. A dual mechanism of action by direct bacterial killing and clearance by our immune system due to agglutination or aggregation can make them a novel antibiotic candidate as the chances for bacterial resistance will be minimized.

7 REFERENCES

1. EARSS Management Team, and national representatives of EARSS, *On-going surveillance of S. Pneumoniae, S. aureus, E. coli, E. faecium, E. faecalis, K. pneumoniae, P. aeruginosa*, Europen Centre for Disease Prevention and Control, Bilthoven, The Netherlands, 2008.
2. M.-P. Kieny, *The evolving threat of antimicrobial resistance: options for action*, World Health Organization, Geneva, Switzerland, 2012.
3. G. Cornaglia, *Clinical microbiology and infection : the official publication of the European Society of Clinical Microbiology and Infectious Diseases*, 2009, **15**, 209-211.
4. T. Jones, M. R. Yeaman, G. Sakoulas, S.-J. Yang, R. A. Proctor, H.-G. Sahl, J. Schrenzel, Y. Q. Xiong and A. S. Bayer, *Antimicrobial Agents and Chemotherapy*, 2008, **52**, 269-278.
5. K. K. Kumarasamy, M. A. Toleman, T. R. Walsh, J. Bagaria, F. Butt, R. Balakrishnan, U. Chaudhary, M. Doumith, C. G. Giske, S. Irfan, P. Krishnan, A. V. Kumar, S. Maharjan, S. Mushtaq, T. Noorie, D. L. Paterson, A. Pearson, C. Perry, R. Pike, B. Rao, U. Ray, J. B. Sarma, M. Sharma, E. Sheridan, M. A. Thirunarayan, J. Turton, S. Upadhyay, M. Warner, W. Welfare, D. M. Livermore and N. Woodford, *Lancet Infectious Diseases*, 2010, **10**, 597-602.
6. W. Boucher Helen, H. Talbot George, K. Benjamin Daniel, Jr., J. Bradley, J. Guidos Robert, N. Jones Ronald, E. Murray Barbara, A. Bonomo Robert and D. Gilbert, *Clinical infectious diseases an official publication of the Infectious Diseases Society of America*, 2013, **56**, 1685-1694.
7. B. Spellberg, *Antibiotic Resistance: Promoting Critically Needed Antibiotic Research and Development and Appropriate Use ("Stewardship") of these Precious Drugs*, Infectious Disease Society of America, 2010.
8. L. B. Rice, *Current Opinion in Microbiology*, 2009, **12**, 476-481.
9. l. F.-N. C. de, F. Reffuveille, L. Fernandez and R. E. W. Hancock, *Current Opinion in Microbiology*, 2013, Ahead of Print.
10. N. Hoeiby, T. Bjarnsholt, M. Givskov, S. Molin and O. Ciofu, *International Journal of Antimicrobial Agents*, 2010, **35**, 322-332.

11. T.-F. C. Mah and G. A. O'Toole, *Trends in Microbiology*, 2001, **9**, 34-39.
12. S.-U. Gorr, *Periodontology 2000*, 2009, **51**, 152-180.
13. M. Zasloff, *Nature*, 2002, **415**, 389-395.
14. H. W. Huang, *Biochemistry*, 2000, **39**, 8347-8352.
15. T. Abraham, S. Marwaha, D. M. Kobewka, R. N. A. H. Lewis, E. J. Prenner, R. S. Hodges and R. N. McElhaney, *Biochimica et Biophysica Acta, Biomembranes*, 2007, **1768**, 2089-2098.
16. V. N. Lazarev and V. M. Govorun, *Applied Biochemistry and Microbiology*, 2010, **46**, 803-814.
17. G. P. Page Malcolm and J. Heim, *Current opinion in pharmacology*, 2009, **9**, 558-565.
18. K. Matsuzaki, *Biochimica et. Biophysica. Acta, Biomembranes*, 1999, **1462**, 1-10.
19. J. Davies and D. Davies, *Microbiology and Molecular Biology Reviews*, 2010, **74**, 417-433.
20. M. Adnan, J. Desai, N. Shaikh and S. Mehta, *Asian Journal of Microbiology, Biotechnology and Environment Sciences*, 2013, **15**, 451-455.
21. W. El-Tayab, S. Radwan and A. Al-Sharif, *Egyptian Journal of Biomedical Sciences*, 2004, **15**, 232-242.
22. P. Molan, In *Honey: antimicrobial actions and role in disease management*, Wiley-VCH Verlag GmbH & Co. KGaA: 2009; pp 229-253.
23. Pasteur, *Science*, 1881, **2**, 420-422.
24. R. Emmerich and O. Loew, *Zeit. Hyg.*, 1889, **31**, 1-65.
25. S. A. Waksman and H. B. Woodruff, *Journal of Bacteriology*, 1942, **44**, 373-384.
26. A. Fleming, *J. Pathol. Bacteriol.*, 1932, **35**, 831-841.
27. A. Fleming, H. W. Florey, D. C. Bodenham and E. C. Cutler, *Proceedings of the Royal Society of Medicine*, 1944, **37**, 101-112.
28. H. Yoneyama and R. Katsumata, *Bioscience Biotechnology and Biochemistry*, 2006, **70**, 1060-1075.
29. A. G. Mathew, R. Cissell and S. Liamthong, *Foodborne Pathogens and Diseases*, 2007, **4**, 115-133.
30. P. H. Trnobranski, *Journal of Clinical Nursing*, 1998, **7**, 392-400.
31. A. Marchese and G. C. Schito, *Drugs*, 2001, **61**, 167-173.

32. R. Mueller and J. Wink, *International Journal of Medical Microbiology* **2014**, 304(1), 3-13.
33. G. D. Wright and A. D. Sutherland, *Trends in Molecular Medicine*, 2007, **13**, 260-267.
34. T. Nakatsuji and R. L. Gallo, *Journal of Investigative Dermatology*, 2012, **132**, 887-895.
35. H. Steiner, D. Hultmark, A. Engstrom, H. Bennich and H. G. Boman, *Nature*, 1981, **292**, 246-248.
36. S. K. De and R. Contreras, *Biotechnology Letters*, 2005, **27**, 1337-1347.
37. C. Geetha, S. G. Venkatesh, B. H. F. Dunn and S. U. Gorr, *Biochemical Society Transactions*, 2003, **31**, 815-818.
38. H. Shiba, S. G. Venkatesh, S.-U. Gorr, G. Barbieri, H. Kurihara and D. F. Kinane, *Journal of Periodontal Research*, 2005, **40**, 153-157.
39. K. A. Brogden, *Nature Reviews Microbiolog.*, 2005, **3**, 238-250.
40. A. Giuliani, G. Pirri and S. F. Nicoletto, *Central European Journal of Biology*, 2007, **2**, 1-33.
41. S. E. Blondelle, K. Lohner and M. I. Aguilar, *Biochimica et. Biophysica Acta, Biomembranes*, 1999, **1462**, 89-108.
42. T. J. Cheng John, D. Hale John, M. Elliot, E. W. Hancock Robert and K. Straus Suzana, *Biophysical Journal*, 2009, **96**, 552-565.
43. M. R. Yeaman and N. Y. Yount, *Pharmacological Reviews*, 2003, **55**, 27-55.
44. I. Fernandez David, M.-A. Sani, J. Miles Andrew, B. A. Wallace and F. Separovic, *Biochimica et biophysica acta*, 2013.
45. D. Gidalevitz, Y. Ishitsuka, A. S. Muresan, O. Konovalov, A. J. Waring, R. I. Lehrer and K. Y. C. Lee, *Proceedings of the National Academy of Sciences of the United States of America*, 2003, **100**, 6302-6307.
46. C. Subbalakshmi and N. Sitaram, *FEMS Microbiology Letters*, 1998, **160**, 91-96.
47. P. Fehlbaum, P. Bulet, S. Chernysh, J.-P. Briand, J.-P. Roussel, L. Leitellier, C. Hetru and J. A. Hoffmann, *Proceedings of National Academy of Sciences*, 1996, **93**, 1221-1225.
48. V. V. Andrushchenko, M. H. Aarabi, L. T. Nguyen, E. J. Prenner and H. J. Vogel, *Biochimica et. Biophysica. Acta, Biomembranes.*, 2008, **1778**, 1004-1014.
49. J.-M. Pages, J.-L. Dimarcq, S. Quenin and C. Hetru, *International Journal of Antimicrobial Agents*, 2003, **22**, 265-269.

50. G. Wu, H. Wu, L. Li, X. Fan, J. Ding, X. Li, T. Xi and Z. Shen, *Biochemica et Biophysica Research Communications*, 2010, **395**, 31-35.
51. L. H. Kondejewski, M. Jelokhani-Niaraki, S. W. Farmer, B. Lix, C. M. Kay, B. D. Sykes, R. E. W. Hancock and R. S. Hodges, *Journal of Biological Chemistry*, 1999, **274**, 13181-13192.
52. M. Jelokhani-Niaraki, E. J. Prenner, C. M. Kay, R. N. McElhaney and R. S. Hodges, *Journal of Peptide Research*, 2002, **60**, 23-36.
53. D. L. Lee, J. P. S. Powers, K. Pflegerl, M. L. Vasil, R. E. W. Hancock and R. S. Hodges, *Journal of Peptides Research*, 2004, **63**, 69-84.
54. A. A. Stroemstedt, L. Ringstad, A. Schmidtchen and M. Malmsten, *Current Opinion in Colloid and Interface Sciences*, 2010, **15**, 467-478.
55. G. Laverty, S. P. Gorman and B. F. Gilmore, *International Journal of Mollecular Sciences*, 2011, **12**, 6566-6596.
56. W. C. Wimley and K. Hristova, *Journal of Membrane Biology*, 2011, **239**, 27-34.
57. Y. Shai, *Biochimica et Biophysica Acta, Biomembranes*, 1999, **1462**, 55-70.
58. H. Sato and J. B. Feix, *Biochimica et. Biophysica. Acta, Biomembranes*, 2006, **1758**, 1245-1256.
59. W. C. Wimley, *Advances in Exprimental Medicine and Biology*, 2010, **677**, 14-23.
60. B. H. Honig, W. L. Hubbell and R. F. Flewelling, *Annual Review of Biophysics and Biophysical Chemistry*, 1986, **15**, 163-193.
61. C. D. Fjell, J. A. Hiss, R. E. W. Hancock and G. Schneider, *Nature Reviews Drug Discovery*, 2012, **11**, 37-51.
62. A. Giuliani, G. Pirri, A. Bozzi, A. Giulio, M. Aschi and A. C. Rinaldi, *Cellular and Molecular Life Sciences*, 2008, **65**, 2450-2460.
63. L. T. Nguyen, E. F. Haney and H. J. Vogel, *Trends in Biotechnology*, 2011, **29**, 464-472.
64. Y. Shai, *Biopolymers*, 2002, **66**, 236-248.
65. Z. Oren and Y. Shai, *Biopolymers*, 1998, **47**, 451-463.
66. R. O. Fox, Jr. and F. M. Richards, *Nature*, 1982, **300**, 325-330.
67. M. Mihajlovic and T. Lazaridis, *Biochimica et Biophysica Acta, Biomembranes*, 2010, **1798**, 1485-1493.

68. M. Hanulova, J. Andrae, P. Garidel, C. Olak, J. Howe, S. S. Funari, T. Gutsmann and K. Brandenburg, *Anti-Infective Agents in Medicinal Chemistry*, 2009, **8**, 17-27.
69. J. R. Lai, R. F. Epand, B. Weisblum, R. M. Epand and S. H. Gellman, *Biochemistry*, 2006, **45**, 15718-15730.
70. K. Matsuzaki, O. Murase, N. Fujii and K. Miyajima, *Biochemistry*, 1996, **35**, 11361-11368.
71. S. J. Ludtke, K. He, W. T. Heller, T. A. Harroun, L. Yang and H. W. Huang, *Biochemistry*, 1996, **35**, 13723-13728.
72. H. G. Boman, B. Agerberth and A. Boman, *Infection and Immunity*, 1993, **61**, 2978-2984.
73. C. B. Park, H. S. Kim and S. C. Kim, *Biochemica et Biophysica acta Research Communications*, 1998, **244**, 253-257.
74. A. Carlsson, P. Engstroem, E. T. Palva and H. Bennich, *Infections and Immunity*, 1991, **59**, 3040-3045.
75. J. T. Oh, Y. Cajal, E. M. Skowronska, S. Belkin, J. Chen, D. T. K. Van, M. Sasser and M. K. Jain, *Biochimica et Biophysica Acta, Biomembranes*, 2000, **1463**, 43-54.
76. S. Vannam, P. Juvvadi and R. B. Merrifield, *Journal of Peptide Research*, 1997, **49**, 59-66.
77. B. Skerlavaj, D. Romeo and R. Gennaro, *Infections and Immunity*, 1990, **58**, 3724-3730.
78. A.-B. Hachmann, E. Sevim, A. Gaballa, D. L. Popham, H. Antelmann and J. D. Helmann, *Antimicrobial Agents and Chemotherapy*, 2011, **55**, 4326-4337.
79. T. T. Tran, D. Panesso, N. N. Mishra, E. Mileykovskaya, Z. Guan, J. M. Munita, J. Reyes, L. Diaz, G. M. Weinstock, B. E. Murray, Y. Shamoo, W. Dowhan, A. S. Bayer and C. A. Arias, *mBio*, 2013, **4**, e00281, 00211 pp.
80. V. Nizet, *Current Issues in Molecular Biology*, 2006, **8**, 11-26.
81. A. P. Shelar, MSc, University of Louisville, Louisville, Kentucky, 2009.
82. C. D. Bingle and S. U. Gorr, *The International Journal of Biochemistry & Cell Biology*, 2004, **36**, 2144-2152.
83. T. T. Wheeler, B. J. Haigh, J. Y. McCracken, R. J. Wilkins, C. A. Morris and M. R. Grigor, *Biochimica Biophysica Acta, Gene Structure and Expression*, 2002, **1579**, 92-100.

84. M. Abdolhosseini, J. B. Sotsky, A. P. Shelar, P. B. M. Joyce and S.-U. Gorr, *Molecular and Cellular Biochemistry*, 2012, **359**, 1-8.
85. C. Geetha, S. G. Venkatesh, L. Bingle, C. D. Bingle and S. U. Gorr, *Journal of Dental Research*, 2005, **84**, 149-153.
86. S.-U. Gorr, J. B. Sotsky, A. P. Shelar and D. R. Demuth, *Peptides*, 2008, **29**, 2118-2127.
87. M. Abdolhosseini, S. R. Nandula, J. Song, H. Hirt and S.-U. Gorr, *Peptides*, 2012, **35**, 231-238.
88. V. Balhara, R. Schmidt, S.-U. Gorr and C. Dewolf, *Biochimica et biophysica acta*, 2013, 1829 (9), 2193-2203.
89. Innovagen, *Peptide property calculator*, Accessed 2012 06 22, 2012.
90. E. Lolis and R. Bucala, *Nature Reviews of Drug Discovery*, 2003, **2**, 635-645.
91. M. Zasloff, *Trends in Pharmacological Sciences*, 2000, **21**, 236-238.
92. S. Raffy and J. Teissie, *Biophysical Journal*, 1999, **76**, 2072-2080.
93. H. M. McConnell, T. H. Watts, R. M. Weis and A. A. Brian, *Biochimica et Biophysica Acta*, 1986, **864**, 95-106.
94. L. K. Tamm and H. M. McConnell, *Biophysical Journal*, 1985, **47**, 105-113.
95. S. Nirasay, A. Badia, G. Leclair, J. Claverie and I. Marcotte, *Materials*, 2012, **5**, 2621-2636.
96. D. Gallez, M. Prevost and A. Sanfeld, *Colloids and Surfaces*, 1984, **10**, 123-131.
97. A. Parker, K. Miles, K. H. Cheng and J. Huang, *Biophysical Journal*, 2004, **86**, 1532-1544.
98. J. Huang and G. W. Feigenson, *Biophys. J.*, 1999, **76**, 2142-2157.
99. L. D. Mayer, M. J. Hope and P. R. Cullis, *Biochim Biophys Acta*, 1986, **858**, 161-168.
100. T. M. Domingues, B. Mattei, J. Seelig, K. R. Perez, A. Miranda and K. A. Riske, *Langmuir*, 2013, **29**, 8609-8618.
101. M. W. Freyer and E. A. Lewis, *Methods in Cell Biology*, 2008, **84**, 79-113.
102. A. L. Russell, A. M. Kennedy, A. M. Spuches, D. Venugopal, J. B. Bhonsle and R. P. Hicks, *Chemistry and Physics of Lipids*, 2010, **163**, 488-497.
103. J. Seelig, *Biochimica et Biophysica Acta, Review Biomembranes.*, 1997, **1331**, 103-116.
104. M. Jelokhani-Niaraki, R. S. Hodges, J. E. Meissner, U. E. Hassenstein and L. Wheaton, *Biophysical Journal*, 2008, **95**, 3306-3321.

105. WINTHROP.edu, http://bohr.winthrop.edu/faculty/grossoehme/link_to_webpages/personal/ITC.html, Accessed 24/02/2014, 2014.
106. S. M. Kelly and N. C. Price, *Current protein & peptide science*, 2000, **1**, 349-384.
107. N. Sreerama, S. Y. Venyaminov and R. W. Woody, *Protein Science*, 1999, **8**, 370-380.
108. N. Sreerama, S. Y. Venyaminov and R. W. Woody, *Analytical biochemistry*, 2000, **287**, 243-251.
109. N. Sreerama and R. W. Woody, *Analytical Biochemistry*, 2000, **287**, 252-260.
110. A. S. Ladokhin, W. C. Wimley, K. Hristova and S. H. White, *Methods in enzymology*, 1997, **278**, 474-486.
111. A. S. Ladokhin, W. C. Wimley and S. H. White, *Biophysical Journal*, 1995, **69**, 1964-1971.
112. H. Ostolaza, B. Bartolome, I. O. d. Zarate, F. d. l. Cruz and F. M. Goni, *Biochimica et. Biophysica Acta, Biomembranes*, 1993, **1147**, 81-88.
113. R. A. Parente, S. Nir and F. C. Szoka, Jr., *Biochemistry*, 1990, **29**, 8720-8728.
114. A. I. Sorochkina, S. I. Kovalchuk, E. O. Omarova, A. A. Sobko, E. A. Kotova and Y. N. Antonenko, *Biochimica et. Biophysica Acta, Biomembranes*, 2013, **1828**, 2428-2435.
115. R. Blumenthal, J. N. Weinstein, S. O. Sharrow and P. Henkart, *Proceedings of the National Academy of Sciences of the United States of America*, 1977, **74**, 5603-5607.
116. G. R. Bartlett, *The Journal of Biological Chemistry*, 1959, **234**, 466-468.
117. D. K. Struck, D. Hoekstra and R. E. Pagano, *Biochemistry*, 1981, **20**, 4093-4099.
118. N. Duzgunes, T. M. Allen, J. Fedor and D. Papahadjopoulos, *Biochemistry*, 1987, **26**, 8435-8442.
119. Malvern, *Technical notes*, Accessed 2014/04/29, 2014.
120. J. L. S. Milne, M. J. Borgnia, A. Bartesaghi, E. E. H. Tran, L. A. Earl, D. M. Schauder, J. Lengyel, J. Pierson, A. Patwardhan and S. Subramaniam, *FEBS Journal*, 2013, **280**, 28-45.
121. H. N. Daghestani and B. W. Day, *Sensors*, 2010, **10**, 9630-9646.
122. N. J. Freeman, L. L. Peel, M. J. Swann, G. H. Cross, A. Reeves, S. Brand and J. R. Lu, *Journal of Physics: Condensed Matter*, 2004, **16**, S2493-S2496.
123. R. Horvath and J. J. Ramsden, *Langmuir*, 2007, **23**, 9330-9334.

124. T.-H. Lee, K. Hall, A. Mechler, L. Martin, J. Popplewell, G. Ronan and M.-I. Aguilar, *Advances in Experimental Medicine and Biology*, 2009, **611**, 313-315.
125. A. Mashaghi, M. Swann, J. Popplewell, M. Textor and E. Reimhult, *Analytical Chemistry*, 2008, **80**, 3666-3676.
126. S. Singh, G. Kasetty, A. Schmidtchen and M. Malmsten, *Biochimica et Biophysica Acta, Biomembranes*, 2012, **1818**, 2244-2251.
127. D. J. Hirst, T.-H. Lee, M. J. Swann, S. Unabia, Y. Park, K.-S. Hahm and M. I. Aguilar, *European Biophysical Journal*, 2011, **40**, 503-514.
128. D. I. Fernandez, T.-H. Lee, M.-A. Sani, M.-I. Aguilar and F. Separovic, *Biophysical Journal*, 2013, **104**, 1495-1507.
129. T.-H. Lee, K. N. Hall, M. J. Swann, J. F. Popplewell, S. Unabia, Y. Park, K.-S. Hahm and M.-I. Aguilar, *Biochimica et Biophysica Acta, Biomembranes*, 2010, **1798**, 544-557.
130. T.-H. Lee, C. Heng, M. J. Swann, J. D. Gehman, F. Separovic and M.-I. Aguilar, *Biochimica et Biophysica Acta, Biomembranes*, 2010, **1798**, 1977-1986.
131. S. B. Nielsen and D. E. Otzen, *Journal of Colloid and Interface Science*, 2010, **345**, 248-256.
132. L. Yu, L. Guo, J. L. Ding, B. Ho, S.-s. Feng, J. Popplewell, M. Swann and T. Wohland, *Biochimica et Biophysica Acta, Biomembranes*, 2009, **1788**, 333-344.
133. I. Fernandez David, P. Le Brun Anton, T.-H. Lee, P. Bansal, M.-I. Aguilar, M. James and F. Separovic, *European biophysics journal : EBJ*, 2012.
134. Z. Salamon and G. Tollin, *Biophysics Journal*, 2001, **80**, 1557-1567.
135. K. El Kirat, S. Morandat and Y. F. Dufrene, *Biochimica et Biophysica Acta, Biomembranes.*, 2010, **1798**, 750-765.
136. R. Brasseur, M. Deleu, M.-P. Mingeot-Leclercq, G. Francius and Y. F. Dufrene, *Surface and Interface Analysis*, 2008, **40**, 151-156.
137. T. Abraham, R. N. A. H. Lewis, R. S. Hodges and R. N. McElhaney, *Biochemistry*, 2005, **44**, 11279-11285.
138. V. V. Andrushchenko, H. J. Vogel and E. J. Prenner, *Biochimica et. Biophysica. Acta, Biomembranes.*, 2006, **1758**, 1596-1608.
139. J. L. Fox, *Nature Biotechnology*, 2006, **24**, 1521-1528.
140. D. Davies, *Nature Reviews of Drug Discovery*, 2003, **2**, 114-122.

141. L. Zhang, A. Rozek and R. E. W. Hancock, *Journal of Biological Chemistry*, 2001, **276**, 35714-35722.
142. D. Allende, S. A. Simon and T. J. McIntosh, *Biophysical Journal*, 2005, **88**, 1828-1837.
143. A. S. Ladokhin and S. H. White, *Biochimica et Biophysica Acta, Biomembranes*, 2001, **1514**, 253-260.
144. G. Wiedman, K. Herman, P. Searson, W. C. Wimley and K. Hristova, *Biochimica et Biophysica Acta, Biomembranes*, 2013, **1828**, 1357-1364.
145. S.-U. Gorr, M. Abdolhosseini, A. Shelar and J. Sotsky, *Biochemical Society Transactions*, 2011, **39**, 1028-1032.
146. M. L. Hutchison and J. R. W. Govan, *Microbes and Infection*, 1999, **1**, 1005-1014.
147. M. L. Mangoni and Y. Shai, *Cellular and Molecular Life Sciences*, 2011, **68**, 2267-2280.
148. V. K. Misra, K. A. Sharp, R. A. Friedman and B. Honig, *Journal of Molecular Biology*, 1994, **238**, 245-263.
149. M. Pasupuleti, M. Davoudi, M. Malmsten and A. Schmidtchen, *BMC Research Notes*, 2009, **2**,136.
150. J.-P. S. Powers, A. Rozek and R. E. W. Hancock, *Biochimica et Biophysica Acta, Proteins and Proteomics*, 2004, **1698**, 239-250.
151. C.-C. Lee, Y. Sun and H. W. Huang, *Biophysical Journal.*, 2010, **98**, 2236-2245.
152. L. Hugonin, V. Vukojevic, G. Bakalkin and A. Graeslund, *FEBS Letters*, 2006, **580**, 3201-3205.
153. A. Arbuzova and G. Schwarz, *Biochimica et. Biophyica Acta, Biomembranes*, 1999, **1420**, 139-152.
154. J. M. Rausch, J. R. Marks, R. Rathinakumar and W. C. Wimley, *Biochemistry*, 2007, **46**, 12124-12139.
155. A. Marquette, B. Lorber and B. Bechinger, *Biophysical Journal*, 2010, **98**, 2544-2553.
156. A. Mashaghi, M. Swann, J. Popplewell, M. Textor and E. Reimhult, *Analytical Chemistry*, 2008, **80**, 5276.
157. M. P. Goertz, N. Goyal, B. C. Bunker and G. A. Montano, *Journal of Colloid Interface Sciences*, 2011, **358**, 635-638.
158. E. T. Castellana and P. S. Cremer, *Surface Science Reports*, 2006, **61**, 429-444.

159. J. Murray, L. Cuccia, A. Ianoul, J. J. Cheetham and L. J. Johnston, *ChemBioChem*, 2004, **5**, 1489-1494.
160. K. Mulligan, Z. J. Jakubek and L. J. Johnston, *Langmuir*, 2011, **27**, 14352-14359.
161. M. L. Wagner and L. K. Tamm, *Biophysical Journal*, 2000, **79**, 1400-1414.
162. T. Wang, D. Li, X. Lu, A. Khmaladze, X. Han, S. Ye, P. Yang, G. Xue, N. He and Z. Chen, *Journal of Physical Chemistry*, 2011, **115**, 7613-7620.
163. M. J. Goldman, G. M. Anderson, E. D. Stolzenberg, U. P. Kari, M. Zasloff and J. M. Wilson, *Cell*, 1997, **88**, 553-560.
164. V. S. Balakrishnan, B. S. Vad and D. E. Otzen, *Biochimica et Biophysica Acta, Proteins and Proteomics*, 2013, **1834**, 996-1002.
165. A. Pilotelle-Bunner, P. Beaunier, J. Tandori, P. Maroti, R. J. Clarke and P. Sebban, *Biochimica et Biophysica Acta, Bioenergetics*, 2009, **1787**, 1039-1049.
166. R. N. A. H. Lewis, E. J. Prenner, L. H. Kondejewski, C. R. Flach, R. Mendelsohn, R. S. Hodges and R. N. McElhaney, *Biochemistry*, 1999, **38**, 15193-15203.
167. E. J. Prenner, R. N. A. H. Lewis, M. Jelokhani-Niaraki, R. S. Hodges and R. N. McElhaney, *Biochimica et Biophysica Acta, Biomembranes*, 2001, **1510**, 83-92.
168. T. P. W. McMullen, R. N. A. H. Lewis and R. N. McElhaney, *Biochimica et Biophysica Acta, Biomembranes*, 2009, **1788**, 345-357.
169. A. J. Garcia-Saez, S. Chiantia, J. Salgado and P. Schwille, *Biophysical Journal*, 2007, **93**, 103-112.
170. C. Kim, J. Spano, E.-K. Park and S. Wi, *Biochimica et Biophysica Acta, Biomembranes*, 2009, **1788**, 1482-1496.
171. N. Kucerka, J. Pencer, M. P. Nieh and J. Katsaras, *European Physics Journal*, 2007, **23**, 247-254.
172. P. Wadhwani, J. Reichert, J. Buerck and A. S. Ulrich, *European Biophysical Journal*, 2012, **41**, 177-187.
173. H. Zhao, R. Sood, A. Jutila, S. Bose, G. Fimland, J. Nissen-Meyer and P. K. J. Kinnunen, *Biochimica et Biophysica Acta, Biomembranes*, 2006, **1758**, 1461-1474.
174. M.-L. Jobin, P. Bonnafous, H. Temsamani, F. Dole, A. Grelard, E. J. Dufourc and I. D. Alves, *Biochimica et Biophysica Acta, Biomembranes*, 2013, **1828**, 1457-1470.

175. A. L. Russell, A. M. Spuches, B. C. Williams, D. Venugopal, D. Klapper, A. H. Srouji and R. P. Hicks, *Bioorganic & Medicinal Chemistry*, 2011, **19**, 7008-7022.
176. J. R. Lakowicz, *Principles of Fluorescence Spectroscopy*, Third edn., Kluwer Academic/Plenum Publishers, New York, 1999.
177. T. C. B. Vogt and B. Bechinger, *Journal of Biology and Chemistry*, 1999, **274**, 29115-29121.
178. I. D. Alves, N. Goasdoue, I. Correia, S. Aubry, C. Galanth, S. Sagan, S. Lavielle and G. Chassaing, *Biochimica et Biophysica Acta, General Subjects*, 2008, **1780**, 948-959.
179. J. C. Nickel, I. Ruseska, J. B. Wright and J. W. Costerton, *Antimicrobial Agents and Chemotherapy*, 1985, **27**, 619-624.
180. H. Hirt and S.-U. Gorr, *Antimicrobial Agents and Chemotherapy*, 2013, **57**, 4903-4910.
181. K. V. Holmberg, M. Abdolhosseini, Y. Li, X. Chen, S.-U. Gorr and C. Aparicio, *Acta Biomaterials*, 2013, **9**, 8224-8231.

8 APPENDIX

Steps followed for quantification of phospholipids using calorimetric determination of inorganic phosphate based on Bartlett's method [116].

- 60 µl of desired lipid preparation (approximated based on initial concentration) was incubated with 650 µl of 70% perchloric acid. Concentration was chosen to stay within the linear measurement limits of the method.
- This was then heated at 800°C for 30 minutes using a sand bath heater.
- The mixture was then left to cool for 15-20 minutes.
- To this was added 18MΩ pure freshly obtained water to make a final volume of 3.95 ml
- Added 500 µl of 2% (W/V) of ammonium heptamolybdate.
- Then added 500 µl of 2% (W/V) of ascorbic acid.
- Mix well and measure the absorbance at 812 nm.
- Use the measured absorbance to calculate the moles of phosphate using the equation derived from the standard plot as shown below.